Anker Weidick

The Structure of Dark Flint from Stevns, Denmark

by

HARRY MICHEELSEN

Mineralogical and Geological Institute of the University of Copenhagen

Contents

Abstract ... 286
I. Introduction ... 287
II. Physical properties ... 288
Geology and petrology ... 288
Optical properties ... 290
Density ... 291
Differential thermal analysis ... 291
III. Chemical properties ... 293
Introduction ... 293
Isothermal dehydration ... 293
Thermogravimetric analyses ... 294
Infrared absorption spectra ... 301
Chemical composition ... 307
Internal surface areas ... 310
Thermal behaviour of flint ... 312
Patination of flint artifacts ... 313
IV. Electron microscopy ... 315
Introduction ... 315
A note on electron microscopy and diffraction ... 315
Experimental details ... 316
Polished flint etched by supercritical water ... 316
Polished flint etched by hydrofluoric acid ... 317
The fracture surface of flint ... 320
Flint etched by alkalies ... 321
Conclusions on the observations made with the electron microscope ... 322
V. X-ray diffraction ... 322
Introduction ... 322
Theory ... 323
Experimental details ... 330
Presentation of results ... 331
Results of X-ray diffraction peak analyses ... 334
Particle size determinations based on the assumption that the deformations are small ... 342
The influence of stacking faults on the Fourier coefficients of the peak shape function ... 346
Determination of the lattice faults in dark flint ... 350
The influence of thermal treatment on the lattice faults of flint ... 355

Conclusions on the results obtained by X-ray diffraction 357
The structures of the Dauphiné twin boundaries 357
VI. Conclusions 360
VII. A note on the genesis of dark flint 361
Acknowledgments 362
Dansk resumé 363
Appendix 1. Program in GIER algol III for calculating $|M(t)|$ and $M_S(t)$ for flint 364
Appendix 2. Program in GIER algol III for calculating $|M(t)|$ and $M_S(t)$ for a triplet of twin or stacking faults 365
References 367
14 plates and plate texts

Abstract

The dark flint from the Senonian chalk at Stevns, Denmark, has been investigated by a number of methods including optical microscopy, differential thermal analysis, thermogravimetric analysis, infrared absorption spectroscopy, chemical trace element analysis, surface determination, electron microscopy, and lattice fault determination from X-ray powder diffraction peaks.

As a result it is possible to propose the following structural model for the flint. The dark flint from Stevns consists of anhedral flint grains, 2–30 μ in size with a mean of 7.5 μ. Optically, the flint grains seem to consist of quartz, and they have a random orientation. The flint grains are built up of piles of plates of quartz. The plates are parallel to (0001) and have a mean thickness of 59 nm. The {0001} faces are covered by monolayers of Si-OH groups, and adjacent quartz plates are joined by one *single monolayer* of water molecules. The quartz plates are likely to consist of alternately right-handed and left-handed quartz and to form twins according to the Brazil law.

The quartz plates of the flint grains often consist of subgrains separated by low angle boundaries. The subgrains have a size of 0.2–3 μ and are finely divided by twin faults. The twin faults are parallel to $(\bar{1}2\bar{1}0)$ and occur in threes with a mean distance of 2.2 nm. These triplets are separated by perfect quartz over a mean distance of ca. 16 nm. The twinning corresponds to the Dauphiné law. In right-handed quartz, two $(\bar{1}2\bar{1}0)$ faces are displaced by $0.02\vec{a} + 0.415\vec{b} + 0.37\vec{c}$ from each other, and two $(1\bar{2}10)$ faces are displaced by $0.24\vec{a} + 0.415\vec{b} + 0.37\vec{c}$ from each other. In the twin fault zones, $\frac{2}{3}$ of the oxygen atoms form Si-OH groups and $\frac{1}{3}$ of the oxygen atoms form Si-O-Si bonds from one side of the fault zone to the other. The bulk structure of each quartz plate has hexagonal pseudosymmetry corresponding to the class 622. The Brazil law twinning of the quartz plates gives the flint grains a bulk pseudosymmetry corresponding to the class 6/mmm.

A hypothetical explanation of the genesis of the flint grains is put forward. It seems plausible that the flint grains have been formed by epitaxial replacement of the fine-grained "subsidiary cryptocrystalline silica" found in many Danish flint nodules.

I. Introduction

A very large number of publications have dealt with flint and chert. Most of those who have studied flint and chert have tried to explain the genesis of these rocks from their field relations and petrography, and only a few investigators have tried to describe their detailed structures. However, before ca. 1940 it was difficult to realize that the structures of these important rocks were unknown; only the development of instruments of the last decades has made it possible to detect and to solve the problems involved. Modern instruments, on the other hand, have not prevented some of the modern works being confusing due to use of material from different sources. Today, the two most important facts about the structures of flint, chert, chalcedony etc. are 1) the structures vary considerably even when the fine structure of the cell is that of quartz, and 2) so little is really known about the different varieties that no useful classification can be put forward. The substance described in this paper forms a practically monomineralic rock, and in order to avoid the proposal of a premature classification, the term "flint" is used for the rock as well as for the mineral grains.

At the beginning of this work a few pieces of information about the structures of flint and chert were available in literature. Although much of this information has proved to be more or less irrelevant to the present study, the most important papers will be briefly summarized, as they form the basis of thought for this work.

H. G. MIDGLEY (1951) concluded that chalcedony and flint consist of very fine-grained quartz and that the sub-microscopic cavities found by R. L. FOLK and C. E. WEAVER (1950, 1952) are filled with water. In their study of the Arkansas novaculite by means of electron microscope, R. L. FOLK and C. E. WEAVER (1952) furthermore found two different types of fracture surfaces together with an intermediate type. C. R. PELTO (1956) studied chalcedony and located the water in the angular misfits between radiating quartz fibers. A. TOVBORG JENSEN, C. J. WØHLK, K. DRENCK, and E. KROGH ANDERSEN (1957) investigated a number of Danish flint types by X-ray diffractometry. One of their important results is that the average particle size of the α-quartz in most of the Danish Cretaceous flints ranges from 30 to 80 nm*. The method of particle size determination on the basis of broadened X-ray powder diffraction lines was further elaborated and applied to flint by K. DRENCK (1959). Using DRENCK's method the particle length distributions in the directions of different reflections are measured. In this way it is possible to study the shape of the quartz particles.

H. GRY and B. SØNDERGAARD (1958) gave a petrographic description of the Danish flint types. They state that the optically determined particle size of the Senonian flint is 2–15 μ. This particle size corresponds to that given by R. L. FOLK and C. E. WEAVER (1952), determined by electron microscopy on the Arkansas novaculite, but it differs by a factor of 100 from the particle size determined by X-ray diffraction. This discrepancy between results obtained by two independent, reliable methods, was in fact the starting point for the present work.

*) For the sake of convenience 1 μ = 10^{-6} m and 1 nm = 10^{-9} m have been used as units of length for distances larger than the unit cell edge, whereas 1 Å has been used as the unit of length on atomic scale.

For the above reasons the author has chosen to work out the structure of only one kind of flint from one age and locality: the dark, dense, homogeneous flint from the upper Senonian (Maastrichtian) chalk of the Stevns cliff, eastern Zealand, Denmark. In a few cases other flint types have been investigated for comparison, but results obtained on other flint types have not been used in the investigations of the dark Stevns flint. 20–30 kg. of flint nodules have been used up in this work. They have been collected as loose nodules in the chalk pit east of Sigerslev and are likely to represent various flint layers. The different parts of each nodule are quite different mineralogically, but the samples of dark flint selected from the nodules have been checked by X-ray diffraction and are identical.

The author has tried to use as many independent methods as possible, although results obtained by different methods surprisingly often seemed to contradict each other. This, however, only means that results obtained by one method disproved wrong conclusions based on results obtained by another method, and the author is therefore convinced that for the study of flint it is essential to use many independent methods of observation. This implies that none of the methods used has been fully utilized and there is no doubt that experts can refine the results obtained. The author will therefore not claim to have solved the structure of dark flint definitely, but the structure described here seems to be consistent with all known observations.

Some of the most important of the methods used in this work could not have been applied if a number of laboratories had not placed their instruments at the disposal of the author, the Mineralogical and Geological Institute possessing only some of the equipment used.

The ultimate purpose of this structural study is to give the geological history of flint, it being one of the most common rocks. To make this possible, the structures of a number of more or less mature flints and opals must be known; lacking this, a genetical interpretation of the flint type described in this paper is bound to create a demand for further work instead of being a final solution of a problem.

II. Physical properties

Geology and petrology

The geology of the dark flint from Stevns has not been investigated as part of this work, and the present notes are based mainly on the treatise on Danish flint by H. GRY and B. SØNDERGAARD (1958).

The dark flint occurs in nodules 2 to 100 cm in size in the upper Senonian (Maastrichtian) chalk at Stevns. The nodules occur as discontinuous layers. According to A. ROSENKRANTZ (1938) the flint layers probably represent surfaces of the Senonian sea bottom.

The nodules of flint in the Senonian chalk of Stevns usually consist of three parts. The surface of the nodules is a 0.5 to ca. 5 mm thick, white, porous crust, which has a rather sharp boundary to the interior of the nodule. The dark flint which is the subject of this work is situated inside the white crust. The dark flint occasionally makes up the whole interior part of a nodule, but

in most cases one finds a more or less gradual transition from the dark flint to light grey flint, which usually makes up the central part of the nodule. The light grey flint has not been investigated in detail, but probably it is a mixture of varying proportions of coarse-grained (>50 nm) quartz and the material found in the dark flint.

The dark flint used for the analyses in this work was separated from the grey flint by hand separation of nodules which had been crushed down to a size of of 3–30 mm. This separation was difficult as the dark flint and the light grey flint usually grade into each other. Therefore, one cannot exclude the possibility that a small and varying amount of the coarse-grained grey flint was present in the samples used.

In hand specimen the dark flint from Stevns is bluish black and seems nearly opaque. Thin chips of dark flint – less than ca. 5 mm in thickness – are brownish and translucent, but even a thin section – ca. 30 μ in thickness – will diffuse a light beam strongly. Dark flint has a conchoidal fracture and a subvitreous lustre on fresh surfaces.

In a thin section – ca. 3 μ in thickness – the main component of dark flint appears as small grains, a few microns in size, with optical properties very close to those of quartz (see pl. 1, 1 and p. 290). These grains will be termed "flint grains" in the following to avoid confusion.

Besides the flint grains there are a varying number of spherulites with the same optical properties as chalcedony (pl. 1, 2). Chalcedony is not very different from the flint grains with regard to chemical composition, and as it makes up less than 2% of the samples used it has been neglected in this work.

The dark flint from Stevns contains a little calcite, which is usually found within relatively large (~50 μ) quartz grains. These large quartz grains form a very small part of the flint, and the calcite content is estimated to comprise only a small fraction of one percent. The chemical analysis gives 0.16% of carbonate. In pl. 1, 1 a number (~10^5 per cm^2) of very small (ca. ½ μ) bright grains are seen. Their birefringence has been estimated by means of an elliptic compensator to be 0.16 ± 0.05, i.e. within the limits of accuracy the same as for calcite. As far as it can be seen, these grains are situated outside the flint section and are impurities in the embedding plastic.

A few micaceous grains have been found in the dark flint. They may, however, be due to impurities introduced during the preparation of the sections. In any case they cannot have any detectable influence on bulk measurements.

Stevns flint contains black, rounded bodies 1 to 50 mm in size. Most of these black bodies have no or nearly no detailed structures, but occasionally more or less distinct fibrous structures are visible under the microscope. The flint grains have the same optical properties inside a black body as they have outside. The pigment is thought to be amorphous carbon, (see p. 309). In thin section, only a faint darkening can be seen and no pigment grains are visible. The carbon must therefore be extremely finely dispersed (see also p. 298). The black bodies cross the boundaries between dark and light grey flint without distortions, but they are sharply cut by the crust of the nodules. The black bodies are therefore older than the crust, i.e. older than the shaping of the nodules.

Outside as well as inside the black bodies the dark flint contains a large number of small (2–50 μ), brownish bodies. Most of them are irregularly shaped,

have diffuse boundaries, and look turbid at 1000 times magnification. A few of these brownish bodies are more regularly built and have a definite organic appearance. Neither the black bodies nor the small brown ones have been investigated in detail as they are not parts of the flint grains.

Optical properties

The refractive index of the flint grains in dark flint from Stevns has been measured by the immersion method using wavelength variation and rock crystal as internal standard (H. MICHEELSEN, 1957). The refractive index is 1.5405 ± 0.001. The poor accuracy is due to the fact that the measurements cannot be carried out on a single flint grain but only on small polycrystalline chips. For comparison, the refractive index of flint can be approximately calculated by assuming a linear relation to the volume fractions of water and quartz. The average refractive index of quartz is approximately $\sqrt[3]{n_\omega^2 \cdot n_\varepsilon} = 1.547$. The volume fractions are calculated from the densities of water and quartz and from the thermogravimetric data, which give 1.27% of water. The refractive index becomes

$$n_D = \frac{\frac{1.27 \cdot 1.33}{0.998} + \frac{98.73 \cdot 1.547}{2.648}}{\frac{1.27}{0.998} + \frac{98.73}{2.648}} = 1.540.$$

The refractive index of the flint is thus compatible with the idea that flint consists of quartz with a small amount of water.

In ordinary thin sections (30 μ in thickness) flint seems to be made up of small particles (1–10 μ) with undulatory extinction and very diffuse grain boundaries. The birefringence seems to be very low, 0.001–0.003. The average grain size, however, is smaller than the thickness of the thin section, and the light passes several grains of different orientation. The birefringence measured must therefore be lower than that of the mineral, and even if the extinction of the mineral is perfect, the extinction will be undulatory in such a thin section. Furthermore the grains will appear much too small. In order to avoid these difficulties Mr. P. E. ANDERSEN, of the Danish National Institute of Building Research, skilfully prepared a thin section of the dark flint with a thickness of 3.1 ± 0.2 μ. This is approximately half the size of flint grains, as determined by surface area measurements (see p. 310). A crystal of rutile was placed on (100) beside the flint, and the section was ground until the rutile had a suitable, low interference colour. By use of a Berek compensator the thickness of the section was determined from the path difference in the rutile. The maximum birefringence of the flint grains was then measured to be 0.009 ± 0.001, i.e. identical to that of quartz. In this thin section the grain size seems to be 2–30 μ. The grains still show undulatory extinction although to a much lesser degree than in an ordinary 30 μ thick section of flint, and subjectively, the flint grains have much the same appearance as ordinary quartz grains. The grain boundaries, however, are only visible with crossed nicols as 0.3 to 3 μ wide zones where the direction of extinction changes from one grain to another. It is therefore not possible to

measure the variation in the direction of extinction within a single flint grain.

The boundaries of the flint grains are visible neither by phase contrast nor by dark field microscopy of either a 3 μ or of a 9 μ thick section of dark flint. By phase contrast the section only looks mottled due to the variation of the refractive index with the orientation of the grains. This is surprising as light is supposed to be scattered by grain boundaries. In a freshly made preparation of flint powder in a liquid with $n_D = 1.54$, however, the grain boundaries are really visible as brilliantly white, irregular lines in dark field illumination. The lack of scattering of light in thin section is therefore likely to be due to the mounting plastic which fills the intergranular fissures.

X-ray diffraction shows that the average particle size of the quartz in dark flint from Stevns lies within the range 30–60 nm. The flint grains observed optically must therefore have a very fine structure. From the birefringence of the flint grains it is inferred that the optical axes of the quartz particles are parallel or sub-parallel within each flint grain. The undulatory extinction seems to indicate that the direction of the optical axis varies a little within the single flint grain. These results have been verified by electron microscopy (see p. 319).

Density

The density of the dark flint from Stevns has been determined on a Mettler analytical balance equipped for hydrostatic weighings. Distilled water was cleaned of dissolved air by evacuation, and the vacuum was maintained until the start of the measurements. Four determinations on flint chips of 1.1 to 4.6 grams gave a mean value of 2.594 with a standard deviation of less than 0.001.

For comparison, the density of flint can be approximately calculated by assuming the volumes of water and quartz to be additive. The amount of water is assumed to be 1.27%, (see table 1, p. 298).

$$d \simeq \frac{1.27 + 98.73}{\frac{1.27}{0.998} + \frac{98.73}{2.648}} = 2.594.$$

The density of quartz may vary, and a relative humidity of, for example, 35% will reduce the calculated density to 2.592. The value calculated is therefore so close to the value measured that the difference between the densities of quartz and flint can be explained as being due to the water content of the latter.

Differential thermal analysis

The differential thermal analyses, shown in fig. 1, were kindly carried out by H. L. ANDSAGER, cand. polyt., Den kongelige Porcelainsfabrik, Copenhagen. A Linseis type instrument made by Gebrüdern Netzsch, Germany, was used. The curves have been redrawn with an equidistant temperature scale as abscissa. The oblique background was corrected for by comparing with an inert material.

A comparison between curves (1), dark flint, Stevns, and (2), rock crystal, shows that the endothermic reaction peak of the α–β inversion is very broad in

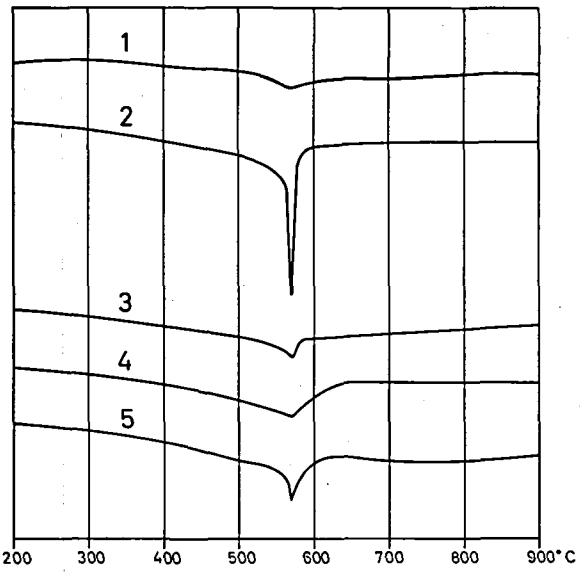

Fig. 1. Differential thermal analyses. 1: Dark flint, Stevns. 2: Rock crystal. 3: Dark flint, Stevns, 800°C for 8 days. 4: Dark flint, Stevns, 540°C, 2200 bars H_2O for 8 days. 5: Light grey flint, Stevns.

the flint. Furthermore, the area of the peak is rather small for a quartz content of ca. 90% which is found by X-ray diffraction (see p. 342).

H. G. MIDGLEY (1951) explains the weak $\alpha - \beta$ reaction as being due to the very small grain size of flint, by analogy with the theories of K. L. MAMPEL (1940). For serpentine, E. MARTINEZ (1961) has shown that the dehydroxylization starts at lower temperatures and becomes less sharp the more finely divided the mineral. P. BAYLISS (1964), however, shows that the particle size has no such effects on calcite and concludes that the decrease in the temperature of reaction found in clays is caused by a lower degree of crystallinity in the smaller particles.

In order to elucidate the $\alpha - \beta$ inversion in flint, a series of high temperature X-ray diffractometer recordings were kindly performed by Dr. TORE DAGERHAMN, Stockholm. The lattice constants of rock crystal and of quartz in the dark flint show the same variation with temperature as found for quartz by F. M. WAHL, R. E. GRIM and R. B. GRAF (1961). The coefficient of thermal expansion decreases discontinuously at the $\alpha \rightarrow \beta$ inversion. This shows that the $\alpha \rightarrow \beta$ inversion does occur and that the lattice of the quartz in the dark flint from Stevns is that of trigonal α-quartz, at least in the main part.

Autoclaving and heating produce an increase in the heat of inversion, as seen in curves 3 and 4 of fig. 1. During these processes numerous lattice faults are annealed, and the flint is altered to an aggregate of quartz grains, ca. 60 nm in size (see p. 355). The fact that grains which are only 60 nm in size, show a conspicuous $\alpha - \beta$ reaction, makes it probable that the grain size cannot account for the low heat of inversion in dark flint. The heat liberated by an-

nealing of the lattice faults probably cannot compensate for the heat of inversion, as the annealing takes a very long time compared with the rate of heating in the thermogravimetric analysis. The lattice faults, however, seem to involve a rotation twinning (see p. 359) which produces an aggregate with hexagonal symmetry, in the same way as the hexagonal symmetry of β-quartz is due to polysynthetic twinning of α-quartz (H. ARNOLD, 1962). Therefore there should be no reason to suppose that the dark flint should give any heat of inversion, and the observed weak α — β reaction probably indicates that the twinning of dark flint is not perfect.

III. Chemical properties

Introduction

K. RØRDAM (1897) and H. GRY and B. SØNDERGAARD (1958) have published chemical analyses of the dark flint. These analyses largely agree but the structural role of the water and the other minor elements was not discussed. The water, however, seems to be closely connected with the surface of SiO_2 minerals, and since the average particle size of flint is very small, the surface area must be very large. A detailed knowledge of the structure of the water in flint is therefore a priori considered to be absolutely necessary when trying to understand the structure of the flint itself. To solve this problem the dark flint from Stevns has been investigated by a number of different chemical methods.

Isothermal dehydration

Fig. 2 gives the isothermal dehydration curve of flint determined at room temperature by the technique – a poor one – described below. The water con-

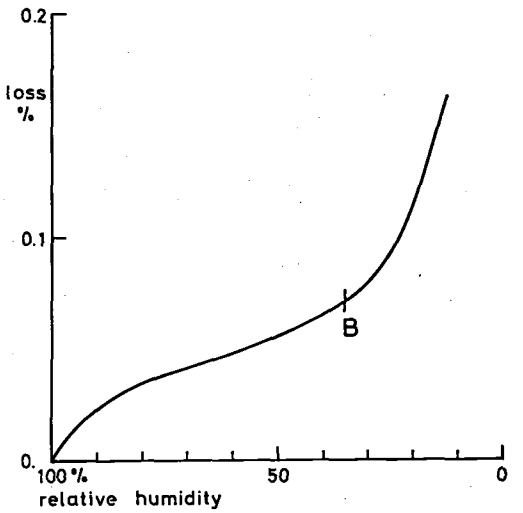

Fig. 2. Isothermal dehydration of dark flint from Stevns at 20°C.

tent of the dark Stevns flint is a continuous function of the relative humidity, and the dehydration is reversible below ca. 100°C (see also p. 296). We can therefore conclude that the water is adsorbed on the internal surfaces of the flint. According to S. BRUNAUER (1943), the s-shape of the isothermal dehydration curve indicates that a unimolecular layer of water is completed at about 35% humidity (point B). At a relative humidity of 100%, 0.07% of water is adsorbed in addition to the monolayer. This additional amount of water is the same at 20°C and at 60°C, and therefore it probably fills the intergranular pores completely forming a phase of "pore condensation".

Experimental details

The isothermal dehydration curve was determined on four plates of flint (about 2 grams each). They were placed for 2–5 days in a container where the humidity of the atmosphere was controlled by mixtures of water and different salts. In one determination the temperature was 60°C; otherwise the runs were made at a room temperature of ca. 20°C. Humidity data were taken from: Handbook of Chemistry and Physics (1949) p. 1951. The plates were then weighed on a semi-micro balance. The relative humidity of air of the laboratory was 25–40%. Therefore the weight of the plates varied in time, and it was necessary to extrapolate the measurements to the moment of opening the container. All experiments were repeated to ensure equilibrium. The reproducibility of the experiments is 0.1 mg or 0.005%.

Thermogravimetric analyses

Experimental details

The thermo-balance used for the analyses given here was constructed by IB SØRENSEN, cand. polyt., lic. techn. The balance is a Mettler analytical balance equipped for hydrostatic weighings (Gehängedurchführung). The sample is placed in a platinum crucible carried by platinum wire about 60 cm below the balance and heated in a Kantal 10/30 laboratory furnace. By good ventilation and shielding it was ensured that the rise in temperature of the support of the balance did not exceed 20°C even after several days of heating at 1300°C. Shifts of the zero point of the balance are easily corrected for since the balance can be unloaded by a special device placed below it. During the experiment the room temperature will rise by ca. 5°C, whereby the buoyancy of the weights corresponding to sample and container will decrease by 0.2 mg. This correction, and the correction due to change in the buoyancy of the sample, as well as the correction due to convection currents in the furnace, are all given by one curve. The curve depends on the rate of heating and the size of the load (here 10 g). The reproducibility of the correction curve is ± 0.2 mg. The crucible always sways a little, and the balance can therefore only be read with an accuracy of ± 0.2 mg. This gives an uncertainty of ± 0.003% for a 10 g load at temperatures below 1200°C. Above this temperature vaporization of platinum will cause small errors. The constant rate of heating of the furnace is obtained by making the Watt-input a special, nearly linear function of time. The power consumption is regulated by manual adjustment of a variable transformer and is controlled by a Watt-meter. The rate of heating used here is 4°C/min. The maximum deviation from linear heating is 10°C within the range 40°–1300°C. The temperature is measured by a Pt/Pt-10% Rh thermocouple with a reproducibility of 2°C. The temperature of the furnace can be kept constant within 5°C by electronic control. The atmosphere of the furnace can be renewed by means of a gas inlet at the bottom.

The samples were first crushed to a grain size of ca. 2 mm in a steel mortar and the steel dust was removed by a strong electromagnet and in most cases also by 5% HCl. Unless otherwise stated, the samples were then finely crushed in an agate mortar and the fraction between 140 and 270 mesh (ca. 0.1–0.05 mm) was used for the analysis. In all cases 10.0 g were analysed in order to ensure the validity of the corrections.

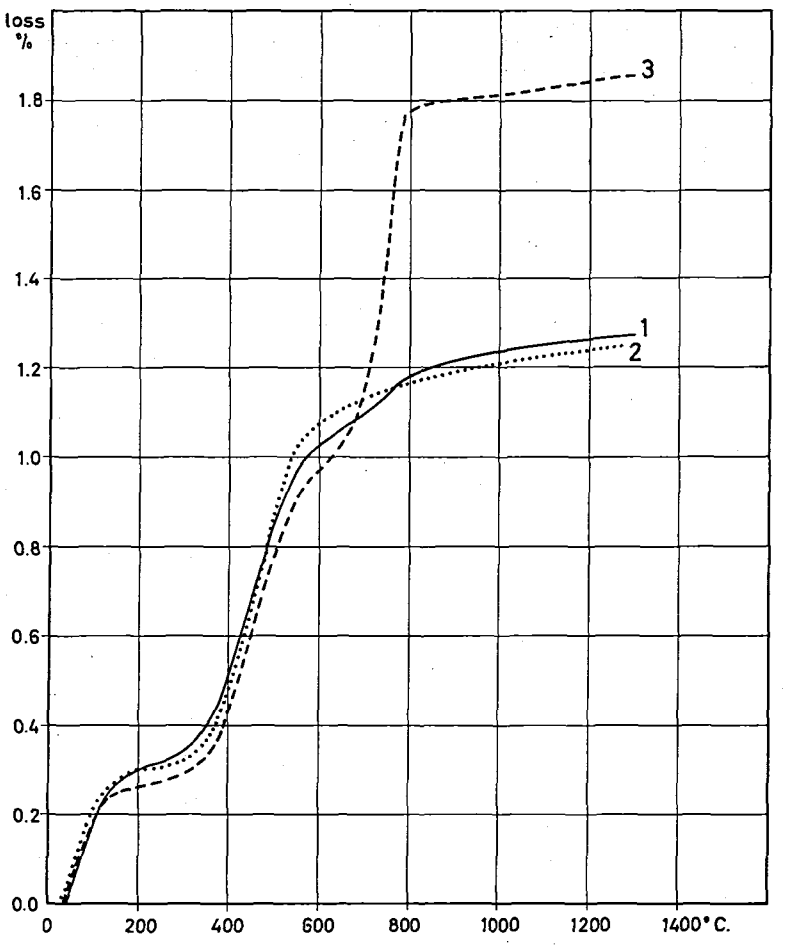

Fig. 3. Thermogravimetric analyses, rate of heating 4°C per minute. Curve 1: Dark flint, Stevns. Curve 2: Dark flint, Møens Klint. Curve 3: Light grey flint, Kagstrup.

Results

The thermogravimetric analyses shown in figs. 3, 5, and 6 were carried out at a rate of heating of 4°C per min.

Curve 4 of fig. 4 is an equilibrium curve determined by keeping the sample at fixed temperatures until further losses were negligible (for 2–5 days). The curve was drawn by analogy with curve 1, fig. 3, through the points measured. When the sample had been weighed at a chosen temperature, the furnace was allowed to cool, and, after a few days, the amount of matter readsorbed at room temperature was weighed (curve 5, fig. 4). It should be noted that the reactions in fig. 3 occur at somewhat higher temperatures (50–150°C) than those in curve

4. The reason is probably the sluggishness of the diffusion which delays the escape of vapour from the sample. The temperature of reaction obtained by rapid heating will therefore approximately be equal to the temperature at which the internal vapour pressure exceeds one atmosphere.

Four different reactions can be distinguished on the thermogravimetric curves for the dark flint from Stevns (fig. 4, curves 1, 4, and 5):

Reaction I

A low-temperature reaction – I – occurs in the interval 20–250°C (20–200°C at equilibrium conditions). The readsorption curve (curve 5 of fig. 4) shows that reaction I is reversible. The weight loss of this reaction is determined as the maximum on curve 5, being 0.23%. The humidity of the laboratory air was ca. 60%. According to the isothermal dehydration curve of fig. 4, the full weight loss of reaction I should then be 0.23 + 0.04 = 0.27%. The dependence on the humidity (see p. 293) shows reaction I to be due to water molecules. Curve 1 on fig. 3 gives a somewhat higher weight loss due to reaction I; the reason is that reaction II has started before reaction I has come to an end.

Reaction II

Reaction II occurs from 200 to ca. 700°C (150–600°C at equilibrium conditions). The range of temperature of reaction II indicates that it may be due to decomposition of Si-OH groups. This theory is verified by the infrared spectrograms, p. 304, but also the oxidation of carbon, which gives an increase in weight of 0.10%, occurs in the same temperature interval (see p. 307). Reaction II ends rather gradually in contrast with the chemical reaction involving liberation of carbon dioxide from calcite, (see curve 3, fig. 3). This fading out of reaction II suggests that in the main it is a degassing of a surface monolayer (S. BRUNAUER, 1943). The weight loss due to decomposition of Si-OH groups can only be determined after having discussed reactions III and IV. The result comes out to 1.00%.

Reaction III

Reaction III occurs at 650–800°C when heating at a rate of 4°C per minute. The reaction is strong in the light grey flint from Kagstrup (curve 3, fig. 3) and it is absent in dark flint from Møens Klint (curve 2, fig. 3) and on the curve 6, fig. 5. If the atmosphere of the furnace is carbon dioxide, reaction III does not start until ca. 720°C and it is then more sharp. Reaction III disappears after washing with HCl (curve 4, fig. 4). It is concluded that reaction III is due to the decomposition of a carbonate. A comparison between curves 1 and 6 shows that the weight loss due to reaction III is close to 0.07%. This result corresponds to 0.17% calcite in agreement with the calcium content given by the chemical analysis, (table No. 3, p. 308). The calcite content of the light grey flint from Kagstrup is 1.6%.

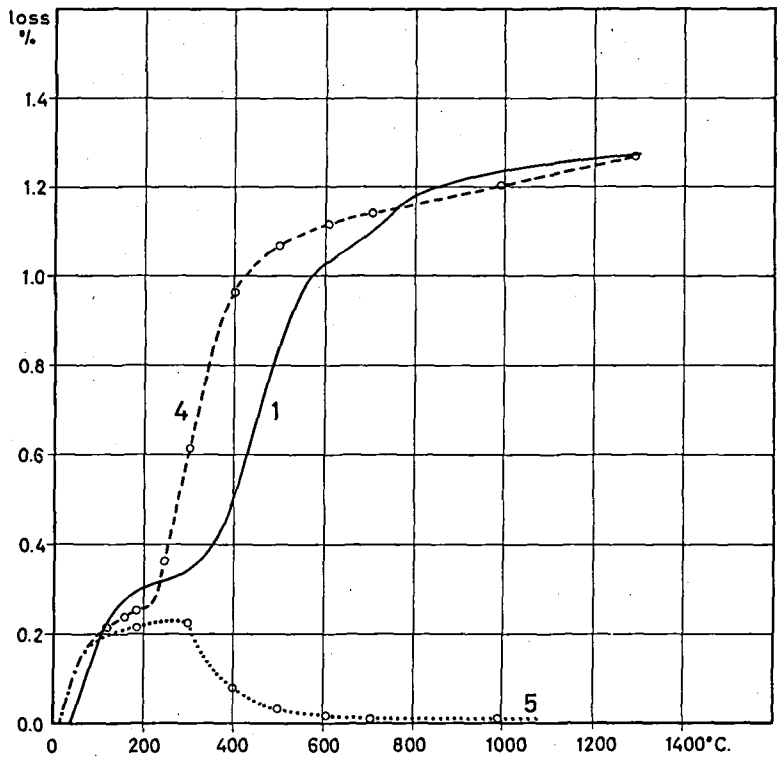

Fig. 4. Thermogravimetric analyses. Curve 1: Dark flint, Stevns, rate of heating 4°C per minute. Curve 4: Dark flint, Stevns, washed with 5% HCl, equilibrium determinations. Curve 5: Dark flint, Stevns, washed with 5% HCl, readsorption at room temperature after heating to the temperature indicated by the abcissa values.

Reaction IV

Reaction IV is shown by the slope of the thermogravimetric curve at high temperatures. The plot here becomes a straight line, and the weight loss due to reaction IV is thus a linear function of temperature. Reaction IV gives a weight loss of 0.14% in the interval 650°–1300°C at equilibrium conditions, but the reaction has perhaps not come to an end at 1300°C. All flint types investigated show this reaction, and even silica gel (for gas chromatography, Merck, Germany) shows a high temperature reaction like reaction IV. According to R. S. McDonald (1958), silica gel contains a certain amount of strongly bonded Si-OH groups even after degassing at 940°C in vacuum for 8.5 hours. The reason is supposed to be that Si-OH groups, which are not in contact because of low concentrations, are unable to react with each other and to move along the surface. The author has therefore tried to explain reaction IV as due to decomposition of Si-OH groups. The assumption, however, was made improbable by the infrared spectrograms (table No. 2), and by the fact that the

Table No. 1

Results of thermogravimetric analyses of dark flint from Stevns

Reaction number	Temperature range	Weight loss	Reason for the reaction
I*)	20–200°C	0.27%	Reversible loss of water molecules**)
II*)	150–650°C	0.90%	Decomposition of Si-OH groups and oxidation of carbon. The weight loss due to the Si-OH groups is 1.00%
III***)	650–800°C	0.07%	Decomposition of 0.17% calcite
IV*)	650–1300°C	0.14%	Release of CO_2 produced by oxidation of carbon

*) Temperatures and weight losses have been obtained by the equilibrium curves 4 and 5, fig. 4.

**) The weight loss of reaction I includes all water present at 20°C and 100% humidity. The monolayer of water molecules makes up 0.20%.

***) Temperature and weight loss of reaction III have been obtained from curve 1, fig. 3.

shape of the thermogravimetric curve shows that reaction II is a complete degassing of a monolayer of Si-OH groups, and that no Si-OH groups therefore are available for reaction IV. To check this point it was decided to undertake a vacuum distillation at high temperatures.

A sample of 10 grams of dark flint from Stevns, 140 to 270 mesh in size, was pre-heated at 650°C for 5 days, and mixed with 10 grams of $CaWO_4$ flux. The mixture was heated at 200°C and 0.2 mm Hg pressure for two hours, and the system was closed. Heating to 500°C caused a slight rise in pressure. Heating to 1100°C produced a strong increase in pressure – in total ca. 20 mm Hg. A small part of the gas in the system, 0.3 ± 0.1 mg, condensed at −80°C. The condensate has a freezing point of $0° \pm 2°C$ and is therefore assumed to be water. The gas which did not condense at −80°C was not analysed, but it is probably carbon dioxide as this gas has been found by infrared spectroscopy, (see p. 307). From the pressure observed and from a relative density of 44/29, the content of carbon dioxide in the heated flint is calculated to be ca. 0.14%, in agreement with the weight loss due to reaction IV.

The carbon dioxide liberated in reaction IV must be trapped much more efficiently than the carbon dioxide liberated from calcite in reaction III. The calcite occurs as small separate grains and the carbon dioxide derived from the calcite can probably escape through the fissures between the flint grains. The better trapping of the carbon dioxide of reaction IV can probably only occur inside the flint grains. Possibly the linear relation between weight loss and temperature reflects the mechanical work of liberation and may correspond to the linear relation between temperature and gas pressure.

The carbon dioxide of reaction IV is assumed to have been created by oxidation of the 0.033% carbon found in the unheated flint. This would yield 0.12% of carbon dioxide, an amount which agrees sufficiently well with the 0.14% weight loss of reaction IV. An attempt was made to remove the carbon

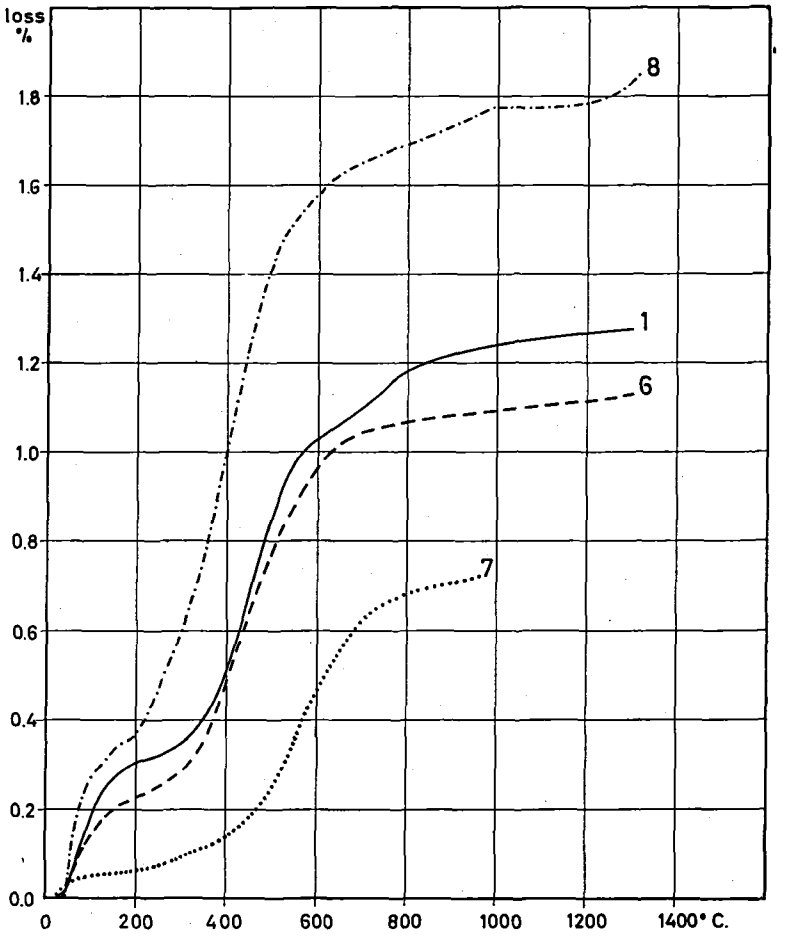

Fig. 5. Thermogravimetric analyses, rate of heating 4°C per minute. Curve 1: Dark flint, Stevns. Curve 6: Dark flint, Stevns, washed in 5% HCl and heated to 100°C for 12 hours in a 5% solution of sodium carbonate. Curve 7: Dark flint, Stevns, washed in 5% HCl and autoclaved at 540°C and 2500 bars H_2O pressure for 20 days. Curve 8: White, leached crust of flint flake.

from flint chips by means of 40% H_2O_2 at ca. 80°C and by $K_2Cr_2O_4$ in concentrated H_2SO_4. The dark colour of the flint chips, however, did not change. This also makes it probable that the carbon is situated inside the flint grains.

Discussion of reaction II

The weight loss due to reaction II is to be determined from the equilibrium curve (No. 4, fig. 4) where reaction III is absent as the sample has been treated with HCl. This curve gives a weight loss of 1.04% due to reactions II and IV

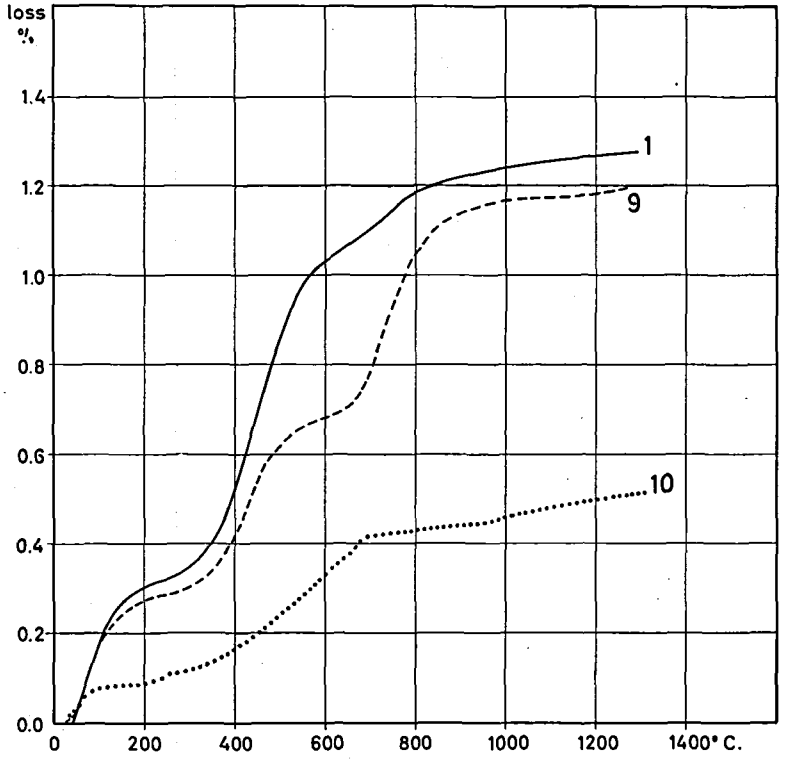

Fig. 6. Thermogravimetric analyses, rate of heating 4° C per minute. Curve 1: Dark flint, Stevns, grain size 0.05–0.1 mm. Curve 9: Dark flint, Stevns, grain size 1–2 mm. Curve 10: Light grey flint from cores of nodules of dark flint, Stevns, grain size 0.05–0.1 mm.

together. Reaction IV is the loss of 0.14% carbon dioxide, produced by an oxidation of carbon, which gives an increase in weight of $0.14 \cdot 32.00/44.01 = 0.10\%$ in the interval 200–600°C. The weight loss due to the decomposition of Si-OH groups is thus $1.04 - 0.14 + 0.10 = 1.00 \pm 0.02\%$.

Other thermogravimetric analyses

Curve 10, fig. 6 shows a thermogravimetric analysis of the light grey flint from Stevns. This type of flint is found in the central parts of the nodules of dark flint from Stevns. It has a larger average grain size than the dark flint, and has possibly been formed by recrystallization of the dark flint. Without entering further into a discussion on this flint type, the author wishes to stress that reaction IV gives the same loss in the light grey flint as in the dark flint, whereas reactions I and II are strongly reduced. This observation also shows the lack of consistency between reaction IV and the OH content. The ratio between the losses in reaction I and reaction II is similar to the ratio found in the dark flint

from Stevns, i.e. ca. 1:3. The sample may therefore be a simple mixture of crystalline quartz and dark flint.

Curve 7, fig. 5, gives the thermogravimetric analysis of flint which has been autoclaved at 540°C and 2500 bars H_2O pressure for 20 days. The curve stops at 960°C due to an instrumental defect. Reaction I has been reduced to 0.07% at ca. 30% humidity. Reaction II has been reduced to 0.63%; it starts more gently and occurs at higher temperatures than usual. The structures which contain the OH groups change during the autoclaving from twin faults into grain boundaries. The average grain size is increased, and the OH groups probably cover the surface of quartz grains as a monolayer (see p. 355). Such a surface monolayer would probably decompose at lower temperatures than the Si-OH groups of the twin boundary zones found in natural flint. The higher temperature of reaction II may be due to a destruction of the {0001} interface structures, a process which is made likely by the small loss in reaction I.

Curve No. 6, fig. 5 shows the thermogravimetric analysis of dark flint from Stevns which has been treated with a 5% solution of sodium carbonate in water at 100°C for 12 hours. The purpose of the treatment was to determine amount and composition of "soluble silica" in flint (W. F. HILLEBRAND and G. E. F. LUNDELL, 1944). 1.6% SiO_2 was dissolved. Curve 6 was determined at ca. 30% humidity and the H_2O content is therefore lowered by ca. 0.08% compared with curve 1. Apart from this parallel displacement and from the absence of reaction III – the carbonate has been removed by HCl – curve 6 follows curve 1 rather closely. The same result was also obtained after 3 hours treatment with 5% Na_2CO_3 at 100°C and after 24 hours treatment with 40% NaOH at 56°C. Within the limits of accuracy, these analyses show that the alkaline solutions have not selectively attacked those parts of the flint structure which contain H_2O or OH. The material dissolved is thus likely to be a representative part of the flint grains. (It should be noted that the H_2O determination is not very accurate as the atmosphere of the furnace cannot be controlled effectively).

Infrared absorption spectra

The structural role of water in flint has also been investigated by infrared absorption spectra. DANIEL HØJGAARD CHRISTENSEN, cand. polyt. et lic. techn., Chemical Laboratory V of the University of Copenhagen, kindly recorded the spectra and offered valuable advice on the interpretation.

In the first part of this investigation a thin section of flint, 56 ± 5 μ in thickness, was used. The mount was removed and the Lakeside cement dissolved. The flint slice was placed in a metal holder to fit the spectrometer (Perkin-Elmer, model 21 Infrared Spectrophotometer). A thin section of quartz parallel to $(10\bar{1}1)$, 93 ± 5 μ in thickness, and cleavage flakes of muscovite and gypsum were analysed for comparison. The positions of the absorption bands were compared with the data for silica gel (H. A. BENESI and A. C. JONES, 1959), and for quartz crystals (G. O. BRUNNER, H. WONDRATSCHEK, and F. LAVES, 1961).

The thin sections used were rather too thick, and, in order to get suitable resolution of the spectrograms, the 100% adjustment of the spectrophotometer was left out. The values for the absorbance should therefore be considered as semi-quantitative only, although they are quite reliable as relative measurements. The peak absorbances have been determined by the base line method according to

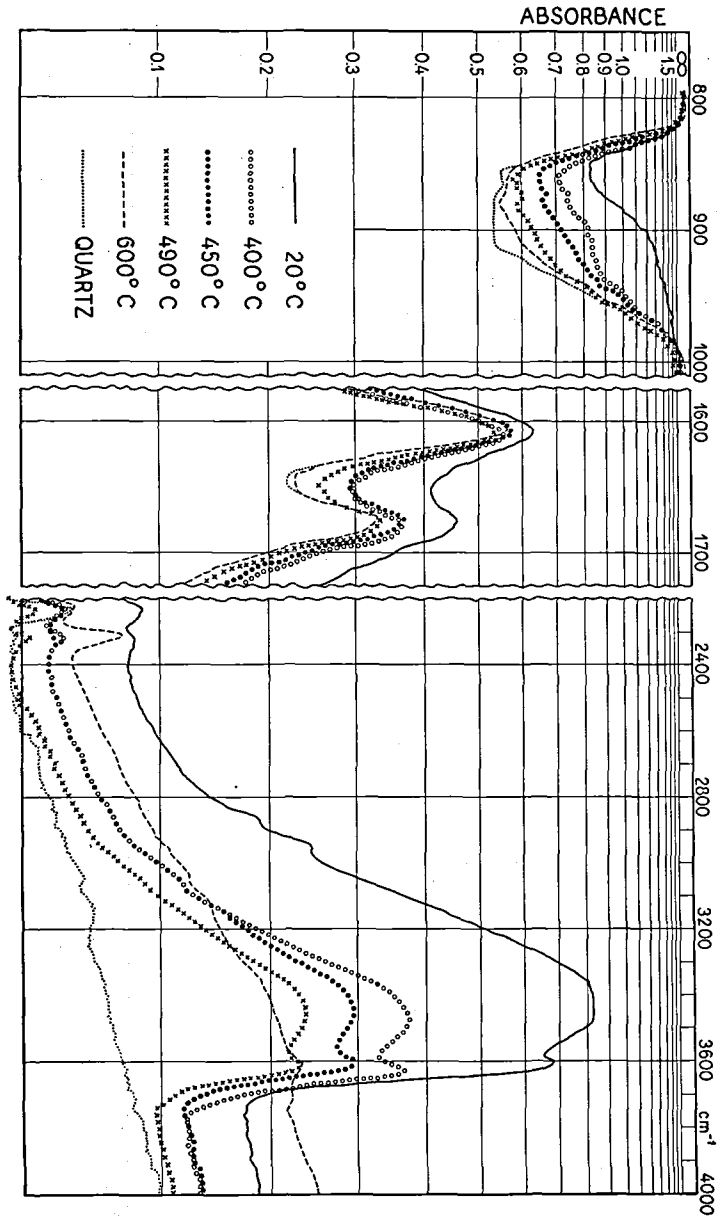

Fig.7. Infrared absorption spectra of flint, which has been heated to various temperatures.

W. J. POTTS, Jr. (1963). For the 900 cm^{-1} and the 1635 cm^{-1} absorption bands, the base lines are highly dependent on the wavelength. The base line used is therefore the absorption spectrum of quartz, recalculated in such a manner that the intensity of the SiO bands corresponds to the spectra of the flint specimen. The absorption curve of quartz is nearly a straight line in the 2400 to 4000 cm^{-1} region. For the absorption band at ca. 3450 cm^{-1}, a tangent is therefore used as base line – according to W. J. POTTS, Jr. (1963). The 3600 cm^{-1} line is situated on the slope of the broad 3450 cm^{-1} band. The base line of the 3600 cm^{-1} line, i.e. the shape of the 3450 cm^{-1} band, was therefore chosen so as to make the 3600 cm^{-1} peak roughly symmetrical. In a few instances the integrated absorbance has been determined by numerical integration of the difference in absorbance between the curve and the base line.

The flint plate was heated for a few days to the temperatures shown in table 2. The infrared spectra were then recorded at room temperature, the specimen having the opportunity to readsorb water from the air. The amount of volatile materials present in the flint under these conditions can be calculated from the thermogravimetric curves Nos. 4 and 5 of fig. 4. The results are given in table 2.

A few years after the first measurements, new infrared absorption curves were measured on a thin section of flint, 38 $\pm$ 5 μ in thickness. The new measurements were taken with a Perkin-Elmer Infrared Spectrophotometer model 125, at room temperature and at 158°C in dry air. The curves have been redrawn with an equidistant absorbance axis as ordinate – fig. 8. An attempt was made to replace the hydrogen of the water and of the Si-OH groups by deuterium, but after boiling in D_2O at ca. 101°C for 3 weeks the ca. 2600 cm^{-1} band showed that only some of the water molecules had been replaced by D_2O.

Table No. 2

Infrared spectroscopy and thermogravimetry of dark flint from Stevns

Structural unit	Position of absorption band cm^{-1}	Peak intensity*) of the absorption bands after heating to temperatures given				
		20°C	400°C	450°C	490°C	600°C
Si-OH	ca. 900	ca. 0.7	0.3	0.2	0.1	ca. 0.04
H_2O	1635	ca. 0.17	0.10	0.08	0.04	ca. 0.01
OH-H	ca. 3450	ca. 0.68	0.28	0.20	0.16	ca. 0.04
OH	3600	ca. 0.3	ca. 0.15	ca. 0.10	ca. 0.05	ca. 0.02
Remainder of reaction I plus readsorbed water in weight %, i.e. the content of water molecules**)		0.27	0.08	0.05	0.03	0.02
Remainder of reaction II in weight %, i.e. 18/34 of the weight content of OH groups after correction for the oxidation of carbon**)		1.00	0.26	0.20	0.14	0.01

*) The peak intensity is the difference in absorbance between the peak and the background, which has been established by means of an infrared spectrogram of quartz (see text).

**) These figures have been calculated from curves 4 and 5 of fig. 4. It is assumed here that the carbon of flint is oxidized between 490°C and 600°C.

Results

The infrared SiO absorption bands have the same positions in flint and quartz. Besides the SiO bands, however, flint gives four absorption bands or lines at ca. 900, 1635, 3450, and 3600 cm^{-1}. According to the literature, and in agreement with the absorption spectra of muscovite and gypsum, these bands are due to the following groups: The band at 900 cm^{-1} is due to Si-OH groups. The band at 1635 cm^{-1} is due to water molecules. The very broad band at ca. 3450 cm^{-1} is due to OH groups which are more or less bonded to hydrogen, i.e. water molecules as well as OH groups which are close neighbours. The 3600 cm^{-1} absorption is due to OH groups which are not hydrogen bonded.

The absorption bands at 1635 cm^{-1} and at 900 cm^{-1} show water molecules as well as Si-OH groups to be present in flint. According to curves 4 and 5 of fig. 4, however, the readsorption at room temperature implies that the amount of H_2O is roughly proportional to that of Si-OH in the heated flint plates. In the spectrograms of the heated plates, therefore, the peak intensities of these two absorption bands have been changed by roughly the same factor. This means that the infrared spectrograms prove the existence of water molecules as well as of Si-OH groups, but the spectrograms cannot tell which of reactions I and II is due to water molecules and which is due to Si-OH groups. However, the low temperature and the reversibility indicate that reaction I is the desorption of water molecules. Likewise, reaction II is assumed to be the decomposition of the Si-OH groups present, since the chemical analysis (p. 308) does not show any other compounds that can give this reaction.

The absorption bands at 3600 cm^{-1} and at ca. 3450 cm^{-1} show two kinds of OH groups to be present, i.e. OH groups without hydrogen bonding and OH groups with hydrogen bonding. Water molecules will absorb in the broad 3450 cm^{-1} band, but an infrared absorption spectrogram carried out at 158°C in dry air (fig. 8) shows that the major part of this band is due not to water molecules but to Si-OH groups.

It will be shown later (p. 357) that the surface area of $\{\bar{1}2\bar{1}0\}$ of the grains in

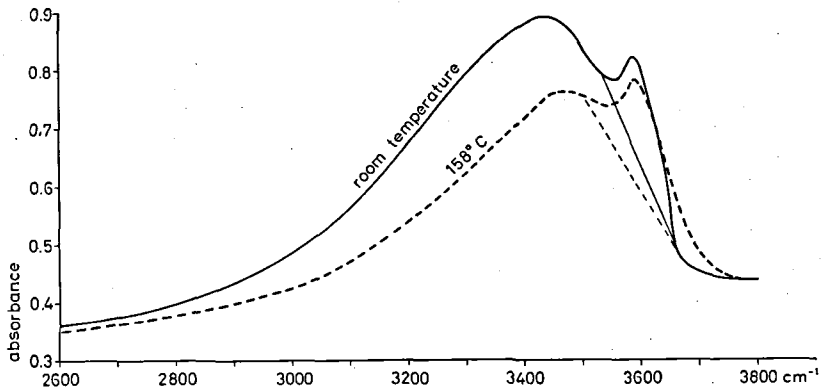

Fig. 8. Infrared absorption spectra of flint at room temperature and at 158°C. The thin lines are used as base lines for the 3600 cm^{-1} absorption peak.

flint – as determined by X-ray diffraction – is so large compared with the amount of Si-OH groups – as determined by thermogravimetry – that the Si-OH groups cannot form a full monolayer, but two neighbouring surfaces must have one monolayer in common. One monolayer of Si-OH groups, however, can balance only one half of the electric charges on two neighbouring quartz surfaces. Impurities are nearly absent in flint, and the remaining half of the charges must be balanced by Si^{4+}. Four $(OH)^-$ groups will probably occur together to balance the electrical charges. Also the contribution of the OH groups to the ca. 3450 cm^{-1} band makes it likely that they are very close to the neighbouring groups. A more detailed picture of the boundary relations is shown in fig. 31.

The OH groups which are not hydrogen bonded, i.e. the OH groups that absorb at 3600 cm^{-1}, cannot be explained by the structure shown in fig. 31, and must have another structural role. This absorption line has been described by G. O. BRUNNER, H. WONDRATSCHEK, and F. LAVES (1961) from twinned amethyst (Brazil law), which gives an infrared absorption spectrum similar to that of flint. These workers conclude that the 3600 cm^{-1} line cannot be due to the AlH and LiOH defects, usually found in untwinned quartz, and that this line is only found in crystals where water molecules are also present, namely in crystals consisting of polysynthetic twin lamellae according to the Brazil law.

In the flint, the water molecules probably form a monolayer on the {0001} faces of the plates of quartz (see p. 311). When the results of G. O. BRUNNER, H. WONDRATSCHEK, and F. LAVES are applied to flint, it must therefore be assumed that the OH groups which are not hydrogen bonded are found on these basal faces. Two different structural models may be suggested for the arrangement of Si-OH groups and water molecules on {0001} of quartz, viz. figs. 9, a and 9, b. According to S. GREENBERG (1956) the surfaces of quartz are covered by monolayers of Si-OH groups. In fig. 9, a, drawn according to this theory, it is supposed that the water molecules form complete monolayers on both neighbouring surfaces. Such a structure corresponds to the commonly accepted idea of a monolayer of water molecules on quartz (see also p. 310). However, all the OH groups in the surface are hydrogen bonded to water molecules, and as the water molecules are close enough to interact, such a structure cannot explain the existence of the 3600 cm^{-1} band. On the other hand the nitrogen adsorption measurement makes it probable that the water cannot build up two monolayers, but only one (see p. 311). Fig. 9, b schematically shows a structure where only one monolayer of water molecules occurs between two surfaces covered by Si-OH groups. One half of the OH groups is not likely to hydrogen bond to the oxygen of water molecules. According to this structure, the OH groups, which possess no hydrogen bonds, will decompose as $\frac{1}{2} \cdot 0.19\% = 0.095\%$ water in the thermogravimetric analysis, i.e. ca. $7\frac{1}{2}\%$ of the 1.27% water released from flint. The integrated absorbance of the 3600 cm^{-1} band is only ca. 5% of the integrated absorbance of the 3450 cm^{-1} band plus the 3600 cm^{-1} band, but the integrated absorbances per molecule are not necessarily identical in the two bands. Another consequence of this hypothesis is that the integrated absorbance of the 3600 cm^{-1} band should increase when the water molecules are removed. If the absorbance is proportional to the concentration, the increase should be by a factor of two. Fig. 8 shows infrared spectrograms

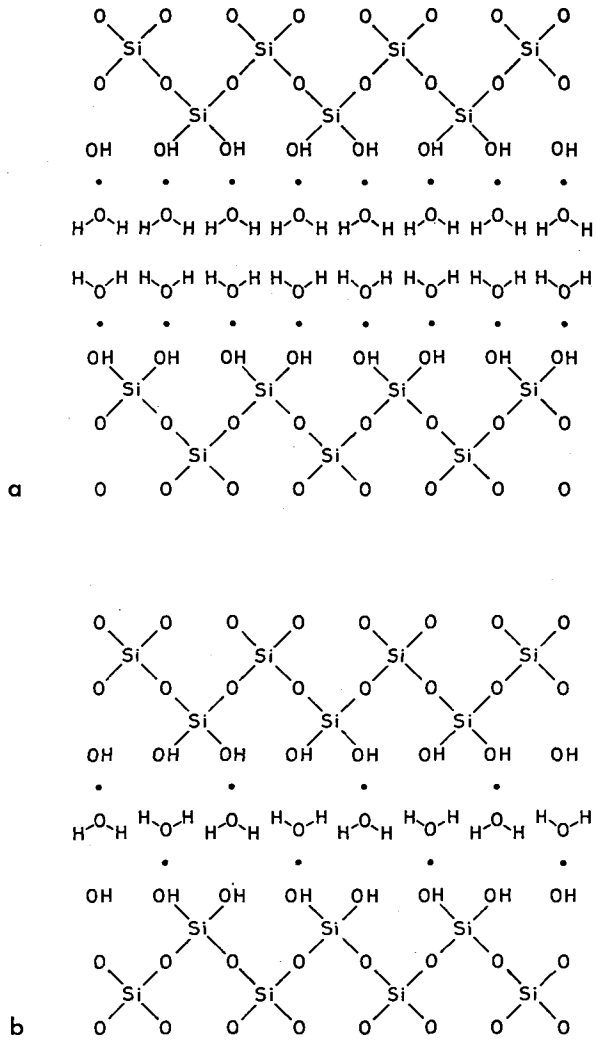

Fig. 9. Hypothetical structural schemes for the arrangement of OH groups and water molecules on {0001} of quartz in flint. The dots indicate hydrogen bonding between the OH groups and the H_2O molecules.

of flint at room temperature (ca. 30% humidity) and under conditions where practically no water molecules are left, i.e. at 158°C in dry air. The peak absorbance of the 3600 cm^{-1} band has decreased a little corresponding to the decrease of the background, but the absorbance has risen at ca. 3700 cm^{-1}. If it is assumed that the 3600 cm^{-1} band is symmetrical and that its background has not been increased by removal of the water molecules, then the background of this peak can be approximated by the straight, thin lines in fig. 8.

The integrated absorbances at room temperature and at 158°C can then be determined as 11 cm^{-1} and 20 cm^{-1} respectively, i.e. in agreement with the hypothesis illustrated in fig. 9, b.

G. O. BRUNNER, H. WONDRATSCHEK, and F. LAVES (1961) found water molecules and free OH groups only in quartz crystals which consist of polysynthetic twin lamellae according to the Brazil law. The water molecules and the OH groups on the {0001} faces of the quartz plates in flint therefore seem to indicate that pairs of quartz plates form twins according to the Brazil law, i.e. the plates are likely to consist of right-handed and of left-handed quartz alternately. No direct proof has been found for this hypothesis, but it is compatible with the genetical hypothesis discussed on p. 361.

The spectrum of flint that has been heated to 600°C shows an absorption peak at 2325 cm^{-1}. This position corresponds to carbon dioxide retained in the flint at high pressure. This carbon dioxide has probably been produced by oxidation of the 0.033% carbon present in the dark flint before heating (see p. 309).

Conclusions

The conclusions of the investigation by infrared spectroscopy are: 1) The 0.27% released below ca. 200°C in the thermogravimetric analysis, i.e. reaction I, is due to water molecules. 2) Reaction II of the thermogravimetric analysis is due to decomposition of Si-OH groups, but the weight loss is diminished by the oxidation of carbon. 3) Some of the Si-OH groups – corresponding to a weight loss of 0.095% – have no hydrogen bonding and are found together with water molecules, probably on twin boundaries between right- and left-handed quartz. 4) Reaction IV of the thermogravimetric analysis is probably due to carbon dioxide produced by oxidation of carbon.

Chemical composition

In order to determine the impurities in flint, a spectrographic analysis was first undertaken by HALDIS BOLLINGBERG, cand. real. The result indicated that the dark flint from Stevns is a rather pure variety of SiO_2, containing roughly the same amounts of trace elements as the "spectrally pure quartz", used for comparison. With this in mind, MARIE LOUISE MOURITZEN, cand polyt., carried out a wet trace element analysis. The material for analysis was selected by hand, crushed and sieved to 1–2 mm size. It was cleaned with a magnet and washed at room temperature with 5% HCl to remove dust and iron. It was then dried at 105°C and saturated with water vapour at room temperature. The sample then weighed 127.1421 g. After a few weeks of boiling with HF, a greyish black, hygroscopic residue of 0.539 g – at 100% humidity – was obtained. This residue was investigated by spectral analysis, by analysis by combustion, by X-ray powder diffractometry, as well as by wet chemical analysis; the results appear in table No. 3.

The spectral analysis of the residue was very difficult to carry out as the sample exploded in the arc. This is probably due to the high content of volatiles, which gives a loss of ignition of 50.9%. One out of the several spectral analyses

Table No. 3

Results of the chemical investigations of dark flint from Stevns

	Analyses of the residue after volatilization of Si by HF. Percentages of the residue saturated with water			Analyses of the complete rock. Percentages of the rock saturated with water		Data from column No.
	1 Wet analysis	2 Semiquantitative spectral analysis	3 Microanalysis by combustion	4 Thermogravimetric analysis	5* Dark flint, Stevns	
	%	%	%	%	%	
P_2O_5	6.6				0.028	1
V_2O_5		0.05			0.0002	2
C**)			7.9	0.04	0.033	3
CO_2**)				0.07	0.07	4
TiO_2	0.4	0.2			0.002	1
ZrO_2		0.04			0.0002	2
SiO_2	0.2					
Al_2O_3	7.6	15			0.032	1
Sc_2O_3		0.002			0.00001	2
Cr_2O_3		0.02			0.0001	2
Y_2O_3		0.03			0.0001	2
La_2O_3		0.04			0.0001	2
MgO	0.6	0.8			0.002	1
CaO	21	5			0.088	1
MnO	tr.	<0.0006			<0.000003	2
FeO†	1.7	1			0.007	1
NiO		0.01			0.00006	2
SrO		0.5			0.002	2
BaO		0.03			0.0001	2
H_2O^-	5.2			0.27	0.27	4
H_2O^+			14.6	1.00	1.00	4
Na_2O		0.0007			0.000003	2
loss of ignition	51					
Total	94	0.7		1.38	1.53	
Not determined	6				0.022	1
SiO_2††					98.44	††

1) Analyst: MARIE LOUISE MOURITZEN, cand. polyt., Mineralogical and Geological Institute, Copenhagen.

2) Analyst: HALDIS BOLLINGBERG, cand. real., Mineralogical and Geological Institute, Copenhagen.

3) Analyst: PREBEN HANSEN, mag. scient., Chemical Laboratory II, University of Copenhagen.

4) Analyst: the author.

*) The results in column No. 5 are derived from columns Nos. 1–4, as described in text. The sources of the results are indicated in column No. 6.

**) *C* as free carbon, CO_2 from carbonate.

†) FeO has been determined as total iron.

††) SiO_2 has been calculated by subtraction of the determined wt. % of the minor elements (1.53 % + 0.022 %) from 100 %.

seems to agree sufficiently well with the wet chemical analysis and is listed in table 3, column No. 2. The results are semi-quantitative and are subject to a factor of uncertainty of 2.

The analysis by combustion was made by PREBEN HANSEN, mag. scient., at Chemical Laboratory II of the University of Copenhagen. Two determinations gave C = 8.03% and H = 1.48%, and C = 8.03% and H = 1.45%. The analyses were carried out at a relative humidity of 55%. When the results are converted to 100% humidity and H calculated as H_2O, we get C = 7.90% and H_2O = 14.6% in the water saturated residue. These values are listed in table No. 3, column No. 3.

An X-ray powder diffractogram showed that the carbon was neither graphite nor diamond. The chemical compounds in the residue are very fine-grained and have not been identified.

The wet chemical analysis was carried out on only 0.3 g of the residue. Furthermore, the loss of ignition was 50.9% and the results are therefore not very accurate. Accordingly, the analysis of the residue is given to a maximum of two significant figures (column No. 1 of table No. 3). The iron was determined as total iron.

The results obtained by the analyses of the residue after volatilization with HF (after evaporation of SiF_4) are muliplied by 0.539/127.1421 in order to give the weight percentages of these elements found in the dark flint from Stevns (column No. 5 of table No. 3). For each element the most accurate of the various sources of information has been used to obtain this analysis, the source being indicated in column No. 6. SiO_2 has been calculated as the difference between 100% and the total amount of other constituents found by the various analyses.

Within the limits of accuracy, the contents of Ca, Mg, Sr, and Ba are equivalent to the amount of CO_2, giving 0.16% of carbonate in the flint, which is in good agreement with the optical observation, see p. 289.

Pyrite is common in flint, and it is therefore assumed that the iron is found in FeS_2, which makes up 0.012%.

The phosphorus might be supposed to occur in apatite, but the calcium content would then be too low. The author supposes that P replaces Si in the quartz structure, possibly as a coupled substitution of P-O-Al for Si-O-Si. This implies that ca. one Si out of 2000 should be substituted by P or Al. The remaining part of the aluminium – and the other trivalent metals – may be present in some clay mineral poor in alkalies, e.g. kaolinite. Such small amounts of a clay mineral would hardly be detectable under the microscope. Another possibility is that these metals are found in AlH defects, which are common in quartz according to G. O. BRUNNER, H. WONDRATSCHEK, and F. LAVES (1961). In that case one Si out of ca. 7000 should have been replaced by AlH.

The 0.033% of free carbon probably contributes to the dark colour of the Stevns flint analysed. Most of the carbon, however, is likely to be found inside the black, oblong bodies which are common in flint. O. WETZEL (1960) has described some of these black parts as being organic remains. Some of the dark colour is probably due to a weak scattering of light, which will occur at each of the numerous grain boundaries in flint. Unfortunately it has not been possible to evaluate the effects of scattering and of optical absorption separately.

Conclusions

The conclusions from the chemical analyses are: 1) The major part of the impurities found in the bulk analysis of the dark flint from Stevns probably consists of carbonates. 2) The flint grains are rather pure silica, apart from their water content. 3) The amount of water present as OH groups is more than 100 times too large to be accounted for by AlH and FeH defects in the quartz structure.

Internal surface areas

The specific internal surface area of the dark flint from Stevns was measured by the nitrogen adsorption method of S. BRUNAUER, P. H. EMMETT and E. TELLER (1938) – the BET surface.

The measurement was kindly performed by HANS BOHLBRO, cand. polyt., at Haldor Topsøe, Consulting Engineers, Hellerup, Denmark. The specimen, weighing 26.03 grams, was crushed to a grain size of 1–2 mm. It was evacuated at 200°C for 5 hours and then exposed to nitrogen. The specimen had a total surface area of 8.0 m^2, corresponding to a specific surface area of 0.31 m^2/g or 0.80 m^2/cm^3.

H. G. MIDGLEY (1951) gives a BET surface of 0.57 m^2/cm^3 for a variety of flint from England. MIDGLEY assumes that the BET surface is the surface of rounded micropores and that the water of the flint fills these pores. A little earlier, in 1950, rounded micropores had been found in the Arkansas novaculite by R. L. FOLK and C. E. WEAVER (published in 1952). Electron microscopy of the Stevns flint, however, does not point to the existence of any such round micropores. The nitrogen is therefore most likely to be adsorbed on the surface of the flint grains. A free surface of 0.80 m^2/cm^3 would correspond to a grain size of 6/8000 cm = 7.5 μ if the grains were cubes of equal size. The grain size of the Stevns flint, determined optically and by electron microscope, is 2–30 μ, and the grains are anhedral. It is therefore fair to conclude that the BET surface is identical with the surface of the flint particles.

N. HACKERMAN and A. C. HALL (1958) record that the area per water molecule on quartz is approximately 11.73 $Å^2$. One percent of water will therefore be able to form a monolayer with an area of 39.2 m^2/g or 101.7 m^2/cm^3 of flint. At high vapour pressures they found fine-grained quartz to adsorb nearly five times as much water as the equivalent of one monolayer. According to S. GREENBERG (1956) the surface of quartz particles is covered by a monolayer of Si-OH groups. This agrees with the shape of the thermogravimetric curve (fig. 4) and with the infrared spectrum (p. 304). S. GREENBERG also indicates that the surface β-cristobalite adsorbs two hydroxyl groups per silicon atom on a free surface (see R. S. MCDONALD (1958), p. 1178). Applied to quartz, this corresponds to an area per Si-OH group of 10.44, 13.26, and 11.49 $Å^2$ on (0001), $(10\bar{1}0)$, and $(\bar{1}2\bar{1}0)$ respectively. The figure 11.73 $Å^2$, used for H_2O, thus seems to be an appropriate average value for calculating the area occupied by Si-OH groups, and in the following a one to one correspondence between H_2O and Si-OH is assumed. The figures used for the areas occupied by 1% of water derived from H_2O and from Si-OH are listed in table No. 4.

Table No. 4

Face	Area per group	Area of monolayer formed by 1 % of water derived from	
		H_2O	Si-OH
	Å²	m²/cm³	m²/cm³
Average	11.73	102	203
(0001)	10.44	90	181
$(10\bar{1}0)$	13.26	115	229
$(\bar{1}2\bar{1}0)$	11.49	100	199

The BET surface of flint should be able to adsorb a monolayer of only 0.31/39.2 = 0.008% H_2O.

The thermogravimetric analysis and the isothermal dehydration curve gave a water content of 0.27% at 100% relative humidity. 0.07% forms a pore condensate and 0.20% forms a monolayer (see p. 294). Of this monolayer only 0.008% can be accommodated on the BET surface, and the remaining 0.19% must be adsorbed on a surface within the flint grains.

It is shown by electron microscopy that the flint grains consist of plates of quartz crystals (see p. 318). The plates, which are parallel to (0001), can be separated by hydrofluoric acid, and must be tied together by some structure which is sensitive to HF. The plates have a thickness of 30–100 nm.

During the BET surface determination the water molecules are removed before the exposure to nitrogen, but the nitrogen molecules do not condense on the large surface left by the water molecules. The reason for this is probably that the entrance to this surface is narrow compared with the large nitrogen molecules. R. A. SVEHLA (1962) gives the following values for σ (L. J. 6–12 potential): H_2O 2.641 Å, and N_2 3.798 Å. The σ values will be used as approximate, effective diameters for the molecules. The width of the fissure between the adsorbing {0001} faces is therefore larger than ca. 2.6 Å and less than ca. 3.8 Å. Complete monolayers on both neighbouring surfaces would require a minimum space width of 4.7 Å in all. Actually H. OTSU and T. YASUDA (1964) have shown that adsorption of one monolayer of hexagonally arranged water molecules expands the c-axis of stevensite by 3.0 Å, and that one pair of monolayers expands the c-axis by 5.9 Å. Therefore it seems most likely that water cannot form a monolayer on both neighbouring surfaces, but the two surfaces have one monolayer in common. Each water molecule is probably hydrogen bonded to one of the two neighbouring Si-OH groups alternately (see fig. 9, b) leaving the other Si-OH group without hydrogen bonding. In this way, 0.19% H_2O will occupy an {0001} interface area of $0.19 \cdot 90 = 17$ m²/cm³. The corresponding thickness of the quartz plates is 59 ± 5 nm. This is in agreement with the thickness determined by electron microscopy. It has not been possible to prove this hypothesis, but it is compatible with the infrared spectroscopy (see p. 305 and fig. 9, b) and with the directional sensitivity to HF (see p. 318). This hypothesis will therefore be accepted in the following.

0.07% H_2O fills the intergranular pores at a relative humidity of 100%.

According to the electron microscopy these pores are intergranular fissures. Their surface is 0.31 m^2/g as mentioned above. The mean width of the intergranular fissures is therefore

$$\frac{0.07 \cdot 10^{-2}\ cm^3/g}{\frac{1}{2} \cdot 0.31 \cdot 10^4\ cm^2/g} = 4.5\ nm.$$

There is very little uncertainty concerning the location of the 1.00% water produced from Si-OH groups. As mentioned above, the area of the surface covered by water molecules is $0.8 + 2 \cdot 17\ m^2/cm^3$, and most of the surface is assumed to be {0001}. Below the water molecules a layer of Si-OH groups will be present, according to S. GREENBERG (1956). The structure of the Si-OH layer on {0001} has been discussed on p. 305, and a hypothetical scheme is given in fig. 9, b. The Si-OH groups in this monolayer and in the monolayer situated under the BET surface correspond to 0.20% water.

Fig. 22, a shows the shape of the single quartz domains which constitute the quartz plates. The picture is a rather approximate one obtained by means of electron microscopy (see p. 322). Perpendicular to $(10\bar{1}0)$ the length of the quartz domains ranges from 60 to 170 nm. The termination is unknown, but if we suppose a $(10\bar{1}0)$ face to be present, the area will be 12–32 m^2/cm^3 and it will adsorb Si-OH groups corresponding to a weight loss of 0.03 to 0.07%, i.e. ca. 0.05% in the thermogravimetric analysis.

The Si-OH groups which have still not been accounted for correspond to a weight loss of $1.00 - 0.20 - 0.05 = 0.75\%$ in the thermogravimetric analysis. These must be located on $\{\bar{1}2\bar{1}0\}$, being the only surface left. A monolayer on this face will have an area of 149 m^2/cm^3. To account for this area the average thickness of quartz domains must be 13.4 nm perpendicular to $(\bar{1}2\bar{1}0)$. Electron microscopy gives a mean thickness of ca. 20 nm (see p. 319), but X-ray determinations show that a length of ca. 20 nm should be subdivided into three parts, being ca. 2.2, 2.2, and 15.8 nm in thickness, giving an average thickness of 6.7 nm. This means that the surface density of the Si-OH groups is very close to one half of a full monolayer on $\{\bar{1}2\bar{1}0\}$.

One half of a monolayer on the surfaces – i.e. one monolayer in common between two adjacent surfaces – can only neutralize one half of the electrostatic charges. Impurity atoms will probably to a large extent be located on such an interface, but the impurities in the dark flint from Stevns can satisfy only 3% of the remaining charges (see p. 309). Therefore, approximately one half of the interface charges must be neutralized by Si^{4+}. A discussion on the detailed structure of the crystalline interface is given on p. 359 (see fig. 31).

Thermal behaviour of flint

When chips of the dark flint from Stevns are heated to temperatures between 300°C and 400°C, the flint turns faintly greyish. When the dark flint is heated to temperatures above 400°C, the dark colour will gradually disappear, until finally the flint turns brilliantly white above 1000°C. A thin dark crust – 0.1 to 1 mm in thickness – is formed on the flint chips during the first part of

this change. Later the chips crack or explode, and the thin dark crust will often form on the fresh surfaces.

Plate 2, 1 illustrates how the interior of a heated flint chip has expanded during formation of cracks. The walls of the cracks have to some extent the dark surface crusts which look clear in thin section. The white part of the heated flint looks dark brown and turbid in thin section due to scattering of light. This change can be explained by the disappearance of water, which was shown to take place by the thermogravimetric analysis. The crusts look like the unheated flint, but they seem to lack the faint but characteristic brownish tinge due to scattering of light. This difference can be explained by assuming that the interstitial water has been replaced by silica.

A thermogravimetric analysis of coarse flint pieces (1–2 mm) is shown on curve 9, fig. 6. The water released above 400°C by destruction of Si-OH groups is trapped inside the coarse flint grains until higher temperatures are reached. This prevention of the release of water vapour shows that the interstitial pores of the flint have been closed by deposition of silica, as is also indicated by the optical clearness of the dark crust. The decomposition of the Si-OH groups is therefore not a mere release of H_2O, but some of the silicon atoms are mobilized and transported by the steam to the external parts of the flint pieces. When the pieces are large enough, the pores will be closed by deposited silica, and the interstitial vapour pressure will rise on further heating. This explains the internal expansion, the cracking, and the exploding of the flint. The fact that a certain volume of drainage is necessary to close the pores near the surface is also shown by a thin section which did not explode and only turned light grey when gently heated to 600°C.

Most Danish flint types behave in the same manner. An exception is the light grey flint from Stevns, which is found as cores within the nodules of dark flint. The reason is probably that the Si-OH content of the light grey flint is much smaller than that of the dark flint (see curve 10, fig. 6).

F. M. WAHL, R. E. GRIM, and R. B. GRAF (1961) state that cristobalite is formed from silica gel at 900°C. Rock crystal gives cristobalite at 1200°C. The dark flint from Stevns partly changed to cristobalite after two days at 1030°C, but at 908°C there was no phase transformation.

Patination of flint artifacts

The nature of the patination of flint artifacts in sea water has been discussed by a number of authors, the main point of controversy being whether or not the patination is a removal of a marginal layer of opal on quartz grains (J. W. JUDD, 1887, H. VINCIENNE, 1938, and K. P. OAKLEY, 1939). The most important argument for the presence of an opal surface layer comes from thin section microscopy, where it is seen that sea water readily dissolves the marginal part of the single flint grains. On the other hand, R. F. SCHMALZ (1960) gives strong evidence against the presence of any opal in flint; neither staining tests, density, refractive indices, nor density separation combined with X-ray diffractometry reveal any opal. Flint, however, may vary considerably in mineral composition. A. TOVBORG JENSEN, C. J. WØHLK, K. DRENCK, and E. KROGH ANDERSEN (1957), who made an investigation of Danish flint types by X-ray powder

diffractometry, did actually find opal in several samples, but not in the dark flint type used for Stone Age tools. The same authors state that weathered and bleached dark Senonian flint has the same mineral composition as the fresh, unweathered flint (sample 4–13–Bognæs). This disproves the hypothesis of an opaline surface layer on the flint grains. On the other hand, "petrographic opal" has been found by thin section studies of the same sample by G. M. IDORN (see A. TOVBORG JENSEN et al. (1957), appendix by G. M. IDORN) and by H. GRY and B. SØNDERGAARD (1958). However, a correlation between the amount of "petrographic opal" and the amount of opal determined by X-ray diffraction can hardly be expected, as the term "petrographic opal" only means a substance which scatters light strongly. "Petrographic opal" may therefore very well be quartz rich in pores, cracks, or inclusions.

The problem of an opaline surface layer on the flint grains is of primary importance to an understanding of the structure of dark flint from Stevns. The author has therefore investigated some flint flakes from the Danish Mesolithic which have been found below shallow sea water at Gyllingnæs in Jutland. The original flint was rather dark as can be seen in small unaltered cores. Most of the flint has been altered and forms a hard, 2–5 mm thick, white, porous crust. In the microscope it is seen that the sea water has dissolved the the marginal parts of the flint grains in the white crust; total reflection from numerous surfaces is the reason for the white colour. However, the original shape and the smooth surface of the Stone Age flakes were preserved. This shows that the chemical attack has progressed much more rapidly (roughly 1000 times) along the grain boundaries than into flint grains. X-ray powder diffractograms showed that the leached crust and the unleached core are identical with regard to mineral composition, and apart from a somewhat smaller average grain size, both are identical to the dark flint from Stevns. A thermogravimetric analysis of the leached crust is shown by curve 8, fig. 5. Reaction II is here the strongest hitherto observed in flint, as one would suspect from the small average particle size. Unfortunately it was not possible to get sufficient material from the dark core for a thermogravimetric analysis.

In order to determine the amount of "soluble" silica in the dark flint from Stevns, a sample (140–270 mesh) was treated by a 5% solution of Na_2CO_3 at 100°C for 1½ hours. The sample was then washed, and the process was repeated. MARIE LOUISE MOURITZEN, cand. polyt., kindly analysed the dissolved material from each treatment and found the solutions nearly identical. This means that the silica present after the first treatment with Na_2CO_3, was no less soluble than the silica present in the outer part of the flint grains (see also p. 301 and p. 321).

Conclusion

The hypothesis that flint grains should have an opaline surface layer has been disproved by X-ray diffractometry, thermogravimetry, and by wet chemical analysis. The fact that the chemical attack of sea water progresses much more rapidly along the grain boundaries than into the grains is therefore not due to a soluble surface layer, but to a high velocity of diffusion in the intergranular fissures, which are 4.5 nm wide on average (see p. 312).

IV. Electron microscopy

Introduction

The purpose of the electron microscopic investigation was to obtain a picture of the external shape and the internal geometry of the flint grains.

Observations made with electron microscope are strongly dependent on the preparation technique used. It was therefore considered necessary to search for techniques which would give information that could prove, disprove, or improve the conclusions below, which have been drawn from other methods of observation:

1) The dark flint consists of grains ("flint grains") 2–30 μ in size. This result is based on the optical properties.
2) The flint grains are built up of α-quartz in such a way that the mean size of the coherent lattice is 8–40 nm. This result is based on the broadening of X-ray diffraction peaks.
3) The different parts of one flint particle have nearly the same orientation of the [001] axis of the quartz. This result is based on the birefringence and the undulating extinction of the flint grains.

Furthermore the electron microscope is the only one of the instruments used that can give direct information on the following problems:

1) Shape and surface of the flint particles.
2) Orientation of the quartz within the flint grains.
3) Shape and size of the single quartz crystals and the pattern of lattice faults.

The third problem has not been solved definitely here, as the results obtained with the electron microscope have yielded only an approximate picture of the detailed structures. This picture, however, made it possible to interpret the X-ray diffraction data and was thereby verified indirectly.

A note on electron microscopy and diffraction

A general note on electron diffraction and electron microscopy will serve to explain the following pages to the crystallographer and mineralogist familiar with X-ray diffraction but not acquainted with the electron microscope.

The electron diffraction photographs given here are all selected area Laue photographs taken, however, with a monochromatic electron beam. The high voltage – 75 kV – makes the wavelength very short, 0.0432 Å (e.g., Z. G. PINSKER, 1953). The sphere of reflection of P. P. EWALD (1921) can therefore – with sufficient accuracy – be replaced by a "plane of reflection", which is perpendicular to the primary electron beam. When a zone axis is parallel to the primary beam, the reciprocal lattice plane of the zone coincides with the "plane of reflection" and a Laue photograph, which looks like an X-ray precession photograph, is obtained. Due to the magnetic lenses of the microscope the optical length used in the diffraction work varies by a few percent. The accelerating voltage and hence the wavelength of the electron beam also vary to some extent. The d-value corresponding to a measured reciprocal vector is therefore not accurate, and the selected area electron diffraction patterns are not suited for mineral identification. The observed axial ratios and reciprocal lattice angles, however, are reliable and the diffraction patterns are excellent for orientation purposes. All the crystalline material within the field of view contributes to the diffraction pattern if the orientation satisfies Bragg's law. With the high resolution microscope a small area (2 μ) can be selected

for the diffraction work. But even then, more than one crystal may often be present inside the field of view and some of the reflections will therefore often be foreign to the main diffraction pattern. Electron diffraction furthermore differs from X-ray diffraction by the very high intensity of the diffracted beams and by the presence of diffraction spots not allowed by the space group theory.

The common "light field" electron micrograph is made by enlargement of the primary electron beam. The intensity seen in the light field picture is influenced by diffuse scattering in the specimen and by diffraction in the crystals. Due to the high intensity of the diffracted beams, diffraction often blackens the crystals severely, and a diffracted beam can be used to produce a "dark field picture". In such a dark field picture, the only bright grains are those which contribute to the diffracted beam used for the dark field picture. The dark field picture can therefore be used to find those particles which have reciprocal lattices of the same orientation.

Experimental details

The electron microscopic work on flint was carried out on two different microscopes. Most of the pictures were taken on a Phillips EM 75 electron microscope by E. LANGER, cand. polyt., Laboratory of Metallurgy, the Technical University of Denmark. A number of the pictures were taken by Dr. G. W. HORNE, The Cavendish Laboratory, Cambridge, England, on a high resolution Siemens Elmiskop I.

The plastic replica technique of D. E. BRADLEY (1954) was used for the investigation of the fracture surface of flint. A solution of collodion is allowed to dry on the fracture surface and is then stripped off. A carbon film is deposited on the collodion replica by sublimation of carbon in vacuum from an arc. In order to make the relief visible, carbon or palladium is deposited in the same way but at an oblique angle producing a shadow effect. The collodion is dissolved, and the shadowed carbon film is placed on a copper grid. Replicas produced in this way give a negative relief, where grooves stand out as ridges. These replicas have a rather low resolution owing to the structure of the collodion.

For the the investigation of polished and etched flint specimens the direct carbon replica technique of E. SMITH and J. NUTTING (1956) was used. The shadow and the carbon film are deposited directly on the specimen under vacuum. The carbon film is loosened by gentle lowering of the specimen into 4% hydrofluoric acid. It is necessary to immerse the carbon coated surface several times in the acid since a period of etching precedes the loosening. The carbon film is washed in water and placed on a copper grid. Unfortunately, polishing of flint is very difficult, and no satisfactory method has been found so far. Small areas, however, are sometimes neatly polished and may therefore be used in spite of numerous large scratches.

Polished flint etched by supercritical water

C. R. PELTO (1956) states that supercritical water is suitable for structural etching of chalcedony.

In the first experiment, polished specimens of dark Stevns flint were subjected to water vapour at 500°C, 300 bars vapour pressure for 48 hours in a small autoclave. Under these conditions the average particle size of the quartz will be increased by a factor of about 2, see p. 355. In this experiment, the boundaries of the flint grains were poorly visible, and silica condensed as small crystals on the polished surface of the specimen. The crystals have a rectangular outline and are therefore assumed to be keatite.

In order to improve the etching and to remove the condensed silica, a quartz crystal was placed in the autoclave during the next treatment, the other conditions being unchanged. Pl. 2, 2 illustrates that after this treatment the grain boundaries have become 0.1–0.3 μ wide fissures. The size of the grains,

10–20 μ, is in accordance with the grain size of the flint particles determined by adsorption (p. 310). The boundaries of the flint particles are irregular in detail, and the texture is allotriomorphic.

The volume of the intergranular fissures can be estimated from pl. 2, 2 by measuring their length and width. The width seen in the micrograph, however, is strongly dependent on the orientation of the fissure, but if the width is measured where the fissure seems to be perpendicular to the polished surface, a volume of ca. 3% is obtained. This corresponds well to the content of water present in the dark flint – 3.3% by volume – and it probably reflects an increase in density due to release of water, see p. 291.

The polished cross sections of the flint grains are only weakly attacked by the vapour, but locally a regular block structure is revealed (see pl. 3, 1 and 3, 2). The size of the blocks is 200–400 nm; but they seem to consist of minor blocks of the size 50–100 nm. The average particle size of the quartz in a flint sample treated in the same way has been determined by the approximation method of K. DRENCK (1959), see fig. 30. The result is 67 nm when measured by the $\{10\bar{1}0\}$ reflection and 82 nm when using $\{10\bar{1}1\}$. The minor blocks are therefore considered to be single crystals of quartz.

Pl. 3, 2, upper right part, shows a plate structure where the dip of the plates can be seen in the NNE trending scratch in the surface. If it is assumed that the depth of the scratch is $\frac{1}{3}$–$\frac{2}{3}$ of its width, it will be possible to calculate the inclination of the plates, and the thickness of the plates can then be estimated to 40–80 nm. Electron microscopy (p. 319), infrared spectroscopy, and thermogravimetric analyses of flint, which has not been autoclaved, have revealed a plate structure with a mean thickness of 59 nm. The plates are parallel to {0001} of the quartz particles. The fact that the plates in the autoclaved specimen seem to have the same thickness renders it probable that the crystal growth which accompanies the autoclaving is not an amalgamation of the plates but occurs within the single plate. This is in agreement with the assumption that the plates alternately consist of right-handed and left-handed quartz (see p. 307). The structural difference between these two kinds of quartz is so large that the transition from the one to the other cannot occur unless the lattice is completely destroyed.

Polished flint etched by hydrofluoric acid

Polished specimens of dark flint from Stevns were etched by 4% HF at room temperature for 5 to 20 seconds. For these preparations the carbon replica technique was used. The carbon film is scratched in order to form small squares and then released from the flint surface by 4% HF. The time of release varies from 10 seconds to one hour, but only those parts of the film which are released within 30 seconds derive from areas of the specimen where the polishing is good and the etching adequate.

The replicas contain a large number of pieces of flint which are suited for electron diffraction. Many pieces are quite irregular in shape and of random orientation, but the conditions of diffraction can be fulfilled as the grid can be tilted a few degrees. Pl. 4 shows such an irregularly shaped particle where a reciprocal $h0\bar{h}l$-plane is parallel to the plane of the picture. Another diffraction

pattern from an irregularly shaped grain has been indexed having the zone axis $[\bar{2}\bar{3}2]$ parallel to the electron beam.

Many of the flint pieces in the replicas are thin plates which according to the diffraction patterns are parallel to (0001) (see pl. 5 to 10). The plates are often polygonal. In most cases the outlines are ⟨100⟩, but also ⟨210⟩ is common. These edges correspond to some forms $\{10\bar{1}l\}$ and $\{11\bar{2}l\}$ respectively. The size of l is unknown and in order to simplify, the forms will be called $\{10\bar{1}0\}$ and $\{11\bar{2}0\}$ in the following. This means that they are assumed to be perpendicular to the base of the plates. The borders of the plates are not straight lines; especially $\{10\bar{1}0\}$ is rather hackly in detail, whereas $\{11\bar{2}0\}$ is smooth (pl. 5). The structural defects in the plates are therefore likely to be parallel to a $\{11\bar{2}0\}$ face. The degree of blackening of the plates varies strongly in detail, but on the whole the average degree of blackening is rather constant over large areas (1–3 μ). The flint pieces seen on pl. 5 to 8 have therefore a rather constant average thickness in different parts – justifying the term "plates" – although the thickness seems to vary strongly in detail. In some cases plates overlap and the darkness of the grain is thereby suddenly increased at a sharp boundary (pl. 8). The overlying plates have the same orientation of the reciprocal lattices, and the real lattices of the plates have therefore either the same orientation or the plates are twinned. Plates up to 4 μ wide have been observed, and the plates probably continue across a whole flint particle (2–30 μ). The strong tendency for the HF molecules to separate the quartz plates directly shows that the plates are joined by a special {0001} structure – very different from that of quartz. The small size of the HF molecule makes it likely to replace adsorbed H_2O rapidly, and therefore, the chemical attack on a silicate is likely to start from the site of the H_2O molecules. The special {0001} structure is thus likely to contain the water molecules of the flint as suggested on the basis of thermogravimetric analyses and infrared spectroscopy (see p. 305 and fig. 9).

The diffraction patterns consistently show that the c-axis of the quartz is perpendicular to the plates, but additional details of the internal structure of the plates can only be determined with some uncertainty. The a*-axis of the quartz within each plate shows a few different orientations, which in most cases are turned a few degrees about the c-axis with respect to each other. In a single case (pl. 9) the a*-direction varies by 25°. The edges of the quartz plate shown on pl. 5 have the same variation in direction as the diffraction pattern, and the quartz plates therefore seem to consist of subgrains 0.2–3 μ in size separated by low angle boundaries.

After the carbon film has come loose from the flint surface, it takes a few minutes to transfer the film to water. In this interval the quartz plates in the replica are exposed to the hydrofluoric acid, and hereby numerous small rounded excavations and holes are produced in the plates (pl. 5 to 7). The midpoints of the holes have an average separation of ca. 20 nm, and these points of chemical attack probably reflect the distance between lattice faults in some way. As mentioned above, these lattice faults seem to be parallel to $\{11\bar{2}0\}$, but otherwise most of the strongly etched plates do not reveal any internal structure. Only one quartz plate gave a dark field micrograph (pl. 7) which

seems to indicate the presence of particles which are a little oblong, roughly parallel to a $\{11\bar{2}0\}$ face.

Some weakly etched grains (pl. 8, 9 and 10), which in most cases are somewhat irregularly shaped, have the c-axes parallel to the electron beam, and they are thus parallel to the above mentioned plates. These grains show diffuse bands that appear as light bands in dark field micrographs. Their spacings range from 16 to 25 nm and their lengths from 60 to 160 nm with average values of ca. 20 nm and ca. 100 nm. The bands are roughly parallel to a $\langle 210\rangle$-direction. The dark field pictures show that the blackening of these bands in the light field micrographs is due to a strong diffraction of the primary electron beam. In the light field micrographs the dark bands are broader than the light bands which separate them, and they are too irregular to be a periodic diffraction phenomena like moiré patterns. It might be supposed that the black bands are separated by parts which have been etched thin by the hydrofluoric acid. The light, thin parts would then probably indicate the site of lattice faults. On the other hand pl. 5 shows that hydrofluoric acid produces rather sharp and irregular holes in the quartz plates and not bands. Structural defects – stacking faults as well as dislocations – produce strong variations in the intensity of the diffracted beams (M. J. WHELAN and P. B. HIRSCH, 1957) and may account for the dark bands. Unfortunately, the preparations used are not true thin foils, and they are too poor for a detailed description of the lattice faults. It can therefore only be concluded that the banding is due to lattice faults, which are roughly parallel to a $\langle 210\rangle$-direction, i.e. parallel to a crystal face that is called $(\bar{1}2\bar{1}0)$, and that they have an average spacing of ca. 20 nm. In other words, lattice faults separate quartz domains which have the same orientation of the reciprocal lattices. The domains are irregularly oblong and measure roughly 100 nm in the long direction, which is parallel to $(\bar{1}2\bar{1}0)$. The X-ray diffraction data (p. 357) show that the lattice faults are likely to be twin faults and that they occur at distances which are compatible with the electron microscopical observations.

The regular quartz plates (shown on pl. 5 to pl. 9) indicate that the flint grains are built up of a pile of thin plates which are parallel to (0001). In pl. 4 the orientation of the grain should make it possible to see the plates edgewise, and actually – in spite of the considerable thickness of the grain – plates with a thickness of 30–100 nm can be discerned.

Because of poor polishing, the surface seen in the replica does not usually give information on parallel structures. In a few areas of a single specimen, however, the polishing was good enough for the etching to reveal parallel, gently bent structures (pl. 11 and pl. 12). The structures seen on pl. 11 have spacings of 50–100 nm, and they probably correspond to {0001} of the quartz plates, the true thickness of plates being close to the smallest of the observed spacings in a polished specimen. The {0001} faces are etched more rapidly by HF than any of the other faces of quartz (A. C. GILL, 1894, see also E. S. DANA/W. E. FORD, 1932, fig. 529). Furthermore the {0001} faces are covered by water molecules (see p. 306), and they are thus likely to become the most important site of attack of the HF. Surface determination by water desorption gives an average thickness of the plates of 59 nm (see p. 311). Pl. 11 also shows

that the plates are not plane but gently curved. On pl. 12, 1 two sets of parallel structures are seen. The one set consists of rows of etched holes. The rows are separated by ca. 85 nm and are likely to correspond to {0001} of the quartz plates, as mentioned above. The other set consists of subparallel furrows which have a spacing of only 26 ± 5 nm (see also pl. 12, 2). The spacing of these furrows indicates that they have been formed on the lattice faults which occur inside the quartz plates. The lattice fault pattern is evidently more regular than indicated by the dark bands seen in the above-cited pictures of irregularly shaped grains, but the spacings of the faults do vary and one lattice fault ends at a dislocation within the micrograph. Pl. 12, 2 shows that some of the etched furrows are doublets and that some are accompanied by faint satellite furrows. The lattice faults are thus not simple stacking faults but they are composite. The X-ray investigation indicates that the faults are triplets of twin faults. In the twin fault zones alternately two $(\bar{1}2\bar{1}0)$ faces and two $(1\bar{2}10)$ faces will be in contact. A. C. GILL (1894) showed that in HF the etching velocities of $(\bar{1}2\bar{1}0)$ and $(1\bar{2}10)$ are very different. The alternating twin faults will thus be excavated by HF as alternating heavy and faint furrows. Under optimum conditions it should be possible to discern two alternating kinds of triplet in the etched pattern: at one triplet a heavy central furrow will be accompanied by two faint satellite furrows, which will be difficult to detect. At the neighbouring triplets the two marginal furrows will be heavy, but the central furrow will be faint and is likely to disappear. The interpretative drawing of the furrows (pl. 12, 2) shows that the composite nature of the etched furrows can be explained on the basis of the theory of triplets of twin faults.

The fracture surface of flint

Dark Stevns flint shows three kinds of fracture surface in the electron microscope. Most frequent is the occurrence of a rough, spongy-looking surface (pl. 13, 1 and 13, 2). It corresponds to the spongy surface of R. L. FOLK and C. E. WEAVER (1952). Less frequent is a more smooth, curved fracture surface (pl. 13, 1 and 13, 2) which looks much like the novaculite type of surface described by the same authors. The rough and the smooth surfaces cover areas with an average diameter of 5–15 μ. The rough surface is interpreted as a fracture through the flint grains. The rough surface contains faint, parallel structures which are probably due to the quartz plates building up the flint grains (pl. 13, 1).

In areas with a smooth, curved fracture several outstanding ridges were seen. The plastic replica technique was used, and the ridges therefore show the presence of fissures in the fracture surface. The occurrence of fissures in areas with a smooth, curved surface makes it likely that these areas derive from the unbroken surface of the flint grains with their intergranular fissures. At their crests the ridges often have a width of only 10–30 nm.

The collodion replica has limited resolving power, and very thin fissures can hardly be accessible to the plastic. Therefore, a width of 10–30 nm does not contradict an average width of 4.5 nm, which was determined by water adsorption (see p. 312).

A third, less common type of fracture surface is smooth, nearly plane, and has small, subparallel steps (pl. 14, 1). The angle of shadow-casting is not well known, and from the width of the shadow zone the height of the steps can only be estimated roughly as 40–120 nm. In a single case faint, parallel structures with spacings of ca. 18–22 nm can be discerned (pl. 14, 1). These structures are parallel to the above-mentioned steps and probably reflect the lattice faults between domains of perfect quartz. This type of surface is best explained as a fracture through a flint grain and parallel to the quartz plates, the height of the steps corresponding to the thickness of a quartz plate.

R. L. FOLK and C. E. WEAVER (1952), J. S. PITTMAN, Jr. (1959), and E. A. MONROE (1964) studied the fracture surface of chert by electron microscope. The rocks examined by these authors are unfortunately quite different from the Stevns flint. FOLK and WEAVER studied the Arkansas novaculite and other cherts with density close to that of quartz, i.e. cherts which contain very little water. For the Arkansas novaculite an average particle size of 75–200 nm has been determined by means of X-ray diffraction by professor, dr. phil. A. TOVBORG JENSEN, Copenhagen (personal communication). The chert investigated by J. S. PITTMAN, Jr. (1959), contains a large amount of spherulitic, fibrous chalcedony, which is subordinate in the Stevns flint. The flint samples investigated by E. A. MONROE (1964) show no broadening of the X-ray diffraction lines. These authors describe the presence of round micropores from observations made on replicas of fracture surfaces of silica rocks. The fracture surface of the dark flint from Stevns shows numerous small irregularities similar to those described as pores, but the polished specimens show that no such pores are present, only fissures in the grain boundaries. Furthermore, the amount of water in the Stevns flint is far below the volume of such pores. In the case of the Stevns flint the "pores" must be due to the preparation technique used.

Flint etched by alkalies

When a piece of dark flint is treated with a boiling solution of NaOH in water, the surface turns milk-white. Under the optical microscope it can be seen that in a zone next to the surface the flint has become an aggregate of small (5–10 μ), brilliantly white, rounded grains.

A fracture surface of flint was treated for one minute with a boiling solution of 20% NaOH in water and then washed. The surface of the flint had turned faintly greyish but it was possible to strip off the collodion replica. Compared with the fresh fracture surface, the etched one shows a general smoothing of the details and some widening of the intergranular fissures.

In another experiment, two polished specimens of flint were treated for 5 and 15 minutes respectively by a hot solution (ca. 90°C) of 5% sodium carbonate in water. The direct carbon replica technique was used. The electron micrographs are rather astonishing since the grain boundaries have not been hollowed out but, on the contrary, protrude as ridges (pl. 14, 2). Furthermore, the grain boundaries are accompanied by "blisters", which have evidently been deposited on the surface after the polishing. On the specimen which was treated for 15 minutes, the blisters are larger and rounded polygonal or even definitely crystalline in outline. The blisters probably consist of a hydrous sodium silicate.

The course of the ridges and the size of the areas enclosed by them show that the ridges have arisen on the grain boundaries. Sodium carbonate has probably formed water-glass by reaction with the flint. During the evacuation that precedes the deposition of the carbon film, the water-glass has boiled over from the fissures and has formed the blisters by splashing. The micrograph (pl. 14, 2) gives the impression that the margins of the flint grains are much more affected than are the interior parts. The thermogravimetric analysis (curve 6, fig. 5), however, shows that the sodium carbonate does not change the composition of the flint, i.e. it attacks the single flint grain as a whole. The seemingly strong attack on the intergranular fissures may therefore be attributed to the fissures being the way of diffusion in flint as well as the way of escape for reaction products during evacuation.

Conclusions on the observations made with the electron microscope

The dark flint from Stevns consists of flint grains 2–30 μ in size. The flint grains are anhedral and have smooth, curved surfaces. Their internal fracture is very rough although no round pores are present.

The flint grains are built up of regular, plane or gently bent plates of quartz, roughly 60 nm in thickness. This means that ca. 200 plates make up one flint grain. The plates are parallel to (0001), and quartz crystals of adjacent plates have the same orientation of their reciprocal lattices. Hydrofluoric acid readily splits the plates from each other.

The quartz plates consist of subgrains, which are 0.2–3 μ in size and separated by low angle boundaries. Inside the subgrains, the quartz contains lattice faults which are parallel to $(\bar{1}2\bar{1}0)$ and occur with a spacing of ca. 20 nm. The lattice faults are composite, in agreement with the theory of triplets of twin faults. The quartz between the lattice faults has been found to be coherent for distances of ca. 100 nm, after which the coherence is likely to be destroyed by dislocations at the ends of twin faults. The quartz plates break parallel to $\{10\bar{1}0\}$ and $\{\bar{1}2\bar{1}0\}$. $\{10\bar{1}0\}$ is rough but an $\{\bar{1}2\bar{1}0\}$ face called $(\bar{1}2\bar{1}0)$ is smooth, corresponding to the orientation of the lattice faults.

V. X-ray diffraction

Introduction

The electron microscope has supplied important information on the shape and the orientation of the quartz crystals which build up the flint grains. This information, however, is not very detailed and it does not agree with the surface determination based on the content of Si-OH groups.

The purpose of the X-ray investigation was to explain the contradiction between the two surface determinations as well as to supply detailed, quantitative data on crystal sizes. The X-ray data themselves give mean values and can be understood only when applied to the picture of the particles obtained by electron microscopy.

For this purpose the shapes of a number of X-ray powder diffraction peaks were investigated in detail by Fourier transformation. This investigation concerned

the fresh, dark flint from Stevns, as well as a number of samples which had been heated or autoclaved under various conditions to promote crystal growth.

In the dark flint from Stevns only α-quartz has been found by this method, the calcite content being below the limit of detection.

Orientation photographs have been taken on three mutually perpendicular thin sections – one cut parallel to the surface of the nodule – but no preferred orientation was detected. Cu-Kα radiation and a stationary Buerger precession camera was used. The precession camera has been placed at the disposal of the Mineralogical and Geological Institute by the Carlsberg foundation.

Theory

The theory for the broadening of X-ray powder diffraction lines has been fully worked out by several authors (B. E. WARREN, 1955; B. E. WARREN and E. P. WAREKOIS, 1955; K. DRENCK, 1959, and others). The theory will be reviewed very shortly here in order to indicate the methods used. Only the use of the sine terms of the Fourier transform will be given in full as the author has not found this described in the literature.

The Laue conditions are derived on the assumptions that the crystals are infinitely large (1 μ or larger) and that all unit cells have the same lattice constants. If these are fulfilled the diffracted X-ray beams are very narrow, and the profile of a peak in the powder diffractogram – i.e. the observed intensity as a function of the angle of diffraction 2θ – is only due to instrumental broadening and to the fact that the X-rays used are not strictly monochromatic. This peak profile can be measured on a coarse-grained standard and will be called the "standard profile" or g(θ) in the following. When the particles are small or deformed, the observed diffraction peak h(θ) is broader than the standard peak due to the "broadening function of the particles" f(θ). f(θ) is to be calculated from the observed line profile and the standard profile.

When λ is the wavelength of the radiation used and d is the spacing of the reflecting lattice planes, the angle θ_0 is given by Bragg's law:

$$\lambda = 2d \sin\theta_0.$$

The three peak profiles can be expressed as functions of a distance in the reciprocal lattice. The standard profile is written g(w), where

$$w = \frac{2d}{\lambda}[\sin\theta - \sin\theta_0] = \frac{\sin\theta - \sin\theta_0}{\sin\theta_0} \simeq \frac{\theta - \theta_0}{\tan\theta_0}. \qquad (1)$$

The shape of the observed peak for flint is h(x), and the particle broadening function of the particles is f(y). When w, x, and y are measured in the same units and from the same θ_0, the three functions g(w), h(x), and f(y) are related by the convolution integral (A. R. STOKES, 1948).

$$h(x) = \frac{1}{\int_{-\infty}^{+\infty} g(w)dw} \int_{-\infty}^{+\infty} f(y)g(x - y)dy = \frac{1}{A}\int_{-\infty}^{+\infty} f(y)g(x - y)dy,$$

where A is the area below the standard profile.

The convolution integral can be solved for f(y) by using the Fourier transforms of the two observed peaks.

In order to do this, the three functions are written as Fourier series, e.g.

$$h(x) = \sum_{n=-\infty}^{n=+\infty} H(n)\exp(-2\pi i x n).$$

The Fourier transforms – e.g. H(n) – of the two observed peaks can be calculated approximately by numerical integration, i.e. the continuous functions g(w) and h(x) are replaced by discontinuous functions, e.g. h(t), where t are integers, h(t) being zero for $|t| \geq T/4$.

$$H(n) = \frac{1}{T}\sum_{t=-T/2}^{t=+T/2} h(t)\exp\left(i\frac{2\pi}{T}nt\right) = H_c(n) + iH_s(n) \tag{2}$$

$$= |H(n)|\exp(i\varphi_H(n)),$$

where

$$|H(n)| = \sqrt{H_c(n)^2 + H_s(n)^2}, \quad \tan\varphi_H(n) = \frac{H_s(n)}{H_c(n)}.$$

The coefficients of the Fourier transform of the particle broadening function can be calculated from the Fourier transforms of h(x) and g(w) according to A. R. STOKES (1948).

$$F(n) = \frac{A}{T}\cdot\frac{H(n)}{G(n)} = \frac{A}{T}\frac{|H(n)|}{|G(n)|}\exp(i\varphi_H(n) - i\varphi_G(n))$$

$$= |F(n)|\exp(i\varphi_F(n)) = F_c(n) + iF_s(n). \tag{3}$$

I.e.

$$|F(n)| = \frac{A}{T}\frac{|H(n)|}{|G(n)|}, \quad \text{and } \varphi_F(n) = \varphi_H(n) - \varphi_G(n). \tag{4}$$

$$F_c(n) = |F(n)|\cos\varphi_F(n), \quad \text{and } F_s(n) = |F(n)|\sin\varphi_F(n). \tag{5}$$

The broadening function of the particles is thus

$$f(y) = \sum_{n=-\infty}^{n=+\infty} |F(n)|\exp(i\varphi_F(n))\exp(-2\pi i y n). \tag{6}$$

It has been shown by B. E. WARREN (1955), and B. E. WARREN and E. P. WAREKOIS (1955) that the particle broadening function can be approximated by

$$f(y) = k\sum_{n=-\infty}^{n=+\infty} N(n)\langle\exp(-2\pi i Z(n))\rangle\exp(-2\pi i y n). \tag{7}$$

N(n) is the number of unit cells which have an n'th neighbour in the direction perpendicular to the reflecting lattice plane. k is a constant for each peak.

Z(n) is a measure of the degree of deformation and will be fully explained below. $\langle\rangle$ denotes the mean value.

From equations (6) and (7),

$$kN(n)\langle\exp(-2\pi iZ(n))\rangle = F(n) = |F(n)|\exp(i\varphi_F(n)), \quad (8)$$

$$kN(n)\langle\cos(2\pi Z(n))\rangle = F_c(n) = |F(n)|\cos\varphi_F(n), \quad (9)$$

$$-kN(n)\langle\sin(2\pi Z(n))\rangle = F_s(n) = |F(n)|\sin\varphi_F(n). \quad (10)$$

As a first approximation, we will assume that the deformations are sufficiently small to allow the approximation

$$N(n) = \frac{|F(n)|\cos\varphi_F(n)}{k\langle\cos 2\pi Z(n)\rangle} \simeq \frac{1}{k}|F(n)|. \quad (9A)^*$$

This, however, is to be modified later.

Interpretation of N(n)

N(n) is the number of unit cells which have an n'th neighbour. For instance, for a single column p cells in length, N(n) becomes [p − n] when measured in the direction of the column. The number of columns of unit cells which have a length of p cells in the direction perpendicular to the reflecting lattice plane is P(p). In these terms, for example, N(3) becomes

$$N(3) = 1P(4) + 2P(5) + 3P(6) + \ldots + [p-3]P(p) + \ldots.$$

In general

$$N(n) = \sum_{p=n+1}^{p=\infty} [p-n]P(p). \quad (11)$$

An important value is

$$N(0) = \sum_{p=1}^{p=\infty} pP(p).$$

N(0) is thus the number of unit cells in the powder specimen investigated.

When N(n) is plotted against n and a smooth curve drawn through the points (fig. 10), the slope of the curve becomes

$$N'(n) \simeq N'(n-\tfrac{1}{2}) \simeq \frac{N(n) - N(n-1)}{1} = -\sum_{p=n}^{p=\infty} P(p). \quad (12)$$

The slope of the curve thus gives the number of columns which are longer than or equal to n cells. The change of N'(n) from n_1 to n_2 gives the number of columns longer than or equal to n_1 but shorter than n_2 cells:

$$N'(n_2) - N'(n_1) \simeq N'(n_2-\tfrac{1}{2}) - N'(n_1-\tfrac{1}{2}) \simeq \sum_{p=n_1}^{p=n_2-1} P(p). \quad (13)$$

*) "A" indicates that the equation is valid only when the deformations are small.

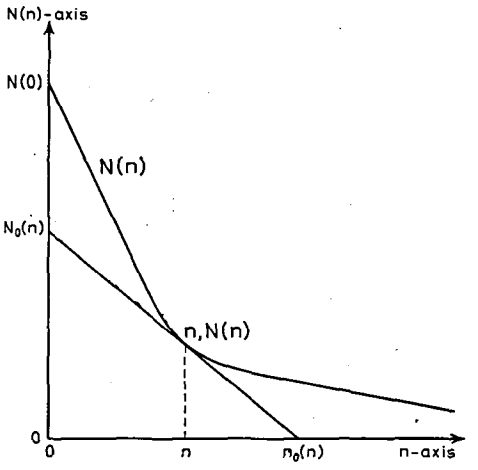

Fig. 10.

Let the tangent to the curve at n,N(n) cut the abscissa axis at $n_0(n)$ and the ordinate axis at $N_0(n)$. From the triangle $n_0(n),0 - n,0 - n,N(n)$,

$$N(n) = [n - n_0(n)]N'(n),$$

$$n_0(n) = \frac{nN'(n) - N(n)}{N'(n)} \simeq \frac{-n\sum_{p=n}^{p=\infty} P(p) - \sum_{p=n}^{p=\infty} [p - n]P(p)}{-\sum_{p=n}^{p=\infty} P(p)}$$

$$= \frac{\sum_{p=n}^{p=\infty} pP(p)}{\sum_{p=n}^{p=\infty} P(p)}. \qquad (14)$$

$n_0(n)$ is thus the ratio between the number of unit cells found in columns of minimum length n and the number of these columns. $n_0(n)$ is therefore the mean length of the columns with a minimum length of n cells. $n_0(0)$ is the mean length of all the columns in the powder.

In fig. 10 the triangle $n_0(n),0 - 0,0 - 0,N_0(n)$ gives

$$N_0(n) = -n_0(n)N'(n) \simeq \sum_{p=n}^{p=\infty} pP(p), \qquad (15)$$

according to (14) and (12). $N_0(n)$ is thus the number of unit cells found in columns of minimum length n. The change of $N_0(n)$ from n_1 to n_2 thus gives the number of unit cells found in columns with lengths between n_1 and n_2 unit cells.

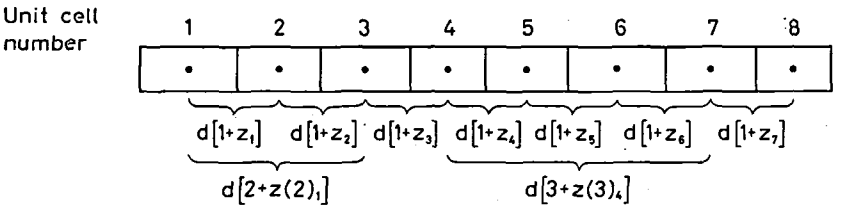

Fig. 11.

Interpretation of $F_s(n)$

The X-ray diffraction peaks of flint have asymmetric f(y) functions, and the sine terms of the Fourier transforms are therefore important. In order to get an interpretation of $F_s(n)$ we will study F(n) in detail.

$$kN(n)\langle\exp(-2\pi iZ(n))\rangle = F(n) = |F(n)|\exp(i\varphi_F(n)). \tag{8}$$

When d is the ideal lattice spacing, d[n + Z(n)] is the distance between two identical lattice points which are separated by n unit cells in a column of cells perpendicular to the reflecting lattice plane. We will now consider one column of p cells. Let the degree of deformation "z" vary with the position in the column (see fig. 11). The distance from the first cell to the second one is $d[1 + z_1]$. The distance from the second cell to the third one is $d[1 + z_2]$, etc. The mean value of $\exp(-2\pi iZ(1))$ can then be calculated for the column as the mean of the $N(1) = p - 1$ different z_j values:

$$\begin{aligned} N(1)\langle\exp(-2\pi iZ(1))\rangle &= [p-1]\langle\exp(-2\pi iZ(1))\rangle = \exp(-2\pi iz_1) \\ &+ \exp(-2\pi iz_2) + \exp(-2\pi iz_3) + \ldots + \exp(-2\pi iz_{p-1}) \\ &= \sum_{j=1}^{j=p-1} \exp(-2\pi iz_j). \end{aligned}$$

For n = 2:

$$\begin{aligned} N(2)\langle\exp(-2\pi iZ(2))\rangle &= \exp(-2\pi i[z_1 + z_2]) + \exp(-2\pi i[z_2 + z_3]) + \ldots \\ &+ \exp(-2\pi i[z_{p-2} + z_{p-1}]) = \sum_{j=1}^{j=p-2} \exp(-2\pi i[z_j + z_{j+1}]). \end{aligned}$$

Z(n) will depend on the position in the column. When the position is given by cell number m, we will define

$$Z(n)_m = \sum_{j=m}^{j=m+n-1} z_j, \quad 1 \le m \le p - n. \tag{16}$$

Still for one column,

$$N(n)\langle\exp(-2\pi iZ(n))\rangle = [p-n]\langle\exp(-2\pi iZ(n))\rangle = \sum_{m=1}^{m=p-n} \exp(-2\pi iZ(n)_m)$$

$$= \sum_{m=1}^{m=p-n} \exp\left(-2\pi i \sum_{j=m}^{j=m+n-1} z_j\right). \tag{17}$$

For P(p) columns, which have the same length, but which may differ in respect of deformations, (17) becomes

$$N(n)\langle\exp(-2\pi i Z(n))\rangle_p = [p-n]P(p)\langle\exp(-2\pi i Z(n))\rangle_p$$
$$= P(p)\sum_{m=1}^{m=p-n}\langle\exp\left(-2\pi i\sum_{j=m}^{j=m+n-1} z_j\right)\rangle_p, \tag{18}$$

for P(p) columns of length $p > n$.

For each value of m, $\langle\rangle_p$ is the mean value for all columns of the length p cells. (18) can be made valid for a powder with varying columnar lengths by summation over all possible values of p, $p > n$, using $\langle\rangle$ without subscript for the mean of all possible values as hitherto.

$$N(n)\langle\exp(-2\pi i Z(n))\rangle = \sum_{p=n+1}^{p=\infty} P(p)\sum_{m=1}^{m=p-n}\langle\exp\left(-2\pi i\sum_{j=m}^{j=m+n-1} z_j\right)\rangle_p, \tag{19}$$

for all columns.

When the z_j values are zero or very small, the following approximations are allowed in (9) and (10), when combined with (19):

$$|F(n)| = \frac{F_c(n)}{\cos\varphi_F(n)} = \frac{kN(n)\langle\cos 2\pi Z(n)\rangle}{\cos\varphi_F(n)} \simeq kN(n) = k\sum_{p=n}^{p=\infty}[p-n]P(p). \tag{9A}$$

$$F_s(n) = |F(n)|\sin\varphi_F(n) = -kN(n)\langle\sin 2\pi Z(n)\rangle \simeq -2\pi kN(n)\langle Z(n)\rangle$$
$$= -2\pi k\sum_{p=n+1}^{p=\infty} P(p)\sum_{m=1}^{m=p-n}\langle\sum_{j=m}^{j=m+n-1} z_j\rangle_p$$
$$= -2\pi k\sum_{p=n+1}^{p=\infty} P(p)\sum_{m=1}^{m=p-n}\sum_{j=m}^{j=m+n-1}\langle z_j\rangle_p. \tag{10A}$$

In the investigation of flint, we will at first make the assumption that the deformations are small enough to allow these approximations. The results obtained by different reflections will, however, to some extent be contradictory, and it will therefore be necessary to assume the existence of stacking faults at certain places in the crystals. (19) will then be used without approximations. The reason for using (9A) and (10A) at first is that these equations make it possible to get an approximate picture of the distribution of the stacking faults, a picture which seems to be indispensable for the practical use of (19).

We will now introduce the approximation (10A) in (18). That is, we will consider P(p) columns of p cells, the deformations of which are small enough to allow the use of (10A). (18) becomes

Unit cell number	1	2	3	4	5	6	7	8	9	10	11

$$z_j = z_1 \quad z_2 \quad z_3 \quad z_4 \quad z_5 \quad z_6 \quad z_7 \quad z_8 \quad z_9 \quad z_{10}$$

$$\begin{aligned}
\langle Z(4)\rangle N(4) = {} & z_1 + z_2 + z_3 + z_4 \\
& + z_2 + z_3 + z_4 + z_5 \\
& + z_3 + z_4 + z_5 + z_6 \\
& + z_4 + z_5 + z_6 + z_7 \\
& + z_5 + z_6 + z_7 + z_8 \\
& + z_6 + z_7 + z_8 + z_9 \\
& + z_7 + z_8 + z_9 + z_{10} \\
= {} & 1z_1 + 2z_2 + 3z_3 + 4z_4 + 4z_5 + 4z_6 + 4z_7 + 3z_8 + 2z_9 + 1z_{10}
\end{aligned}$$

$$\begin{aligned}
\langle Z(7)\rangle N(7) = {} & z_1 + z_2 + z_3 + z_4 + z_5 + z_6 + z_7 \\
& + z_2 + z_3 + z_4 + z_5 + z_6 + z_7 + z_8 \\
& + z_3 + z_4 + z_5 + z_6 + z_7 + z_8 + z_9 \\
& + z_4 + z_5 + z_6 + z_7 + z_8 + z_9 + z_{10} \\
= {} & 1z_1 + 2z_2 + 3z_3 + 4z_4 + 4z_5 + 4z_6 + 4z_7 + 3z_8 + 2z_9 + 1z_{10}
\end{aligned}$$

Fig. 12.

$$F_s(n) \simeq -2\pi k P(p) \sum_{m=1}^{m=p-n} \sum_{j=m}^{j=m+n-1} \langle z_j\rangle_p \text{, for P(p) columns, p cells long.} \qquad (20A)$$

$F_s(n)$ is symmetrical about p/2. This is illustrated in fig. 12 which gives $N(4)\langle Z(4)\rangle$ and $N(11-4)\langle Z(11-4)\rangle$ for one column of 11 cells. z_j and z_{p-j} will always occur in pairs, and the two ends of the column cannot be distinguished by this method.

$F_s(n)$ is plotted against n and a smooth curve is drawn through the points. When $p > n+1$, the slope of the curve can be calculated from (20A), for P(p) columns, p cells long:

$$F_s'(n+\tfrac{1}{2}) \simeq F_s(n+1) - F_s(n) \simeq -2\pi k P(p) \sum_{j=n+1}^{j=p-n-1} \langle z_j\rangle_p ,$$

for $p > n+1$.

By analogy

$$F_s'(n-\tfrac{1}{2}) \simeq -2\pi k P(p) \sum_{j=n}^{j=p-n} \langle z_j\rangle_p , \quad \text{for } p > n.$$

The second derivative to the $F_s(n)$ curve is

$$\begin{aligned}
F_s''(n) &\simeq F_s'(n+\tfrac{1}{2}) - F_s'(n-\tfrac{1}{2}) \simeq 2\pi k P(p)[\langle z_n\rangle_p + \langle z_{p-n}\rangle_p] \\
&= 4\pi k P(p)\langle z_n\rangle_p, \quad \text{for } p > n+1, \qquad (21A)
\end{aligned}$$

since z_n and z_{p-n} are measured at the same distances from the ends of the columns. Their mean values therefore cannot be distinguished.

This way of calculating the average degree of deformation at various places in the columns can only be applied to a polydisperse specimen inside an interval of n where P(n) is zero. Inside such an interval we have $p > n + 1$, and (21A) is therefore valid for those kinds of columns which have a minimum length of $n + 1$. By summation of $F_s''(n)$ over all possible kinds of columns we get for a powder specimen:

$$F_s''(n) \simeq 4\pi k \sum_{p=n+1}^{p=\infty} P(p)\langle z_n\rangle_p = 4\pi k\langle z_n\rangle \sum_{p=n+1}^{p=\infty} P(p).$$

By use of (12) and (9A), p. 325,

$$F_s''(n) \simeq 4\pi k\langle z_n\rangle N'(n) \simeq 4\pi\langle z_n\rangle |F(n)|', \quad \text{for } N''(n) = 0. \qquad (22A)$$

As mentioned above, $F_s(n)$ is symmetrical about p/2 for the columns which are p cells long. Therefore, if only a few types of columns are present, it may be possible to separate the contributions of each kind of column to the $F_s(n)$ curve of the powder, and it should then be possible to calculate $\langle z_n\rangle_p$ for each type of column. In most cases, however, it will only be possible to calculate the average degree of deformation for all unit cells irrespective of their position in the columns.

For this purpose (10A) is rearranged by use of (9A):

$$\langle z_1\rangle = \langle Z(1)\rangle \cong \frac{-F_s(1)}{2\pi k N(1)} \cong \frac{-\sin\varphi_F(1)}{2\pi} \cong -\frac{\varphi_F(1)}{2\pi}. \qquad (23A)$$

Experimental details

The quartz standard that gives the instrumental broadening is rock crystal from Nûgssuaq, Greenland. The crystals were ground and a fraction 1–5 μ in size was separated by an elutriator (E. JENSEN and H. MØLLER HANSEN, 1961).

The dark flint was selected manually from nodules containing light grey, rather coarse-grained flint in the central parts. The contamination of grey flint is difficult to estimate, but it probably does not exceed 10 percent.

The recordings of the line profiles used in this investigation were made with a Philips X-ray diffractometer. Filtered copper radiation was used. The recordings were made by means of a Geiger counter with a dead time of ca. 210 μsec. Low voltage (17–20 kV, 36 mA) and helium-filling of the diffraction camera ensured a low background and rather strong peaks. The recordings have been repeated with a scintillation counter, with a dead time of 2.5 μsec., combined with a pulse height discriminator. The rapid counter gave better accuracy but also a higher background and extra peaks due to the discriminator. The extra peaks do not seem to influence the F(n) values noticeably, but the high background is a serious drawback and the Geiger counter was preferred.

The peak shapes were determined by counting point for point as well as by recording at the lowest scanning speed ($\frac{1}{8}$° per minute, time constant 8 seconds). To ensure instrumental stability the continuous recording was preferred, and the curves for flint and for quartz were recorded alternately.

In the beginning the calculations were made with 3° Beevers and Lipson strips. Later the calculations were repeated on the GIER electronic computer of the Mathematical Institute of the University of Copenhagen. Mr. B. SVEJGAARD, mag. scient., kindly made the program, which corresponds to the use of 1° strips, i.e. T = 360 in (2) p. 324, see appendix 1. The points determined by electronic computation fit the curves much more accurately than do the points determined by Fourier strips, but the resulting curves are virtually identical. The time of calculation is ca. three minutes.

According to equation (2) the summation should be made from $x = -\frac{1}{2}$ to $x = +\frac{1}{2}$. In most cases, however, the h(x) and the g(w) function would then become zero in the large majority of the points to be read, and significant values are only read in rather few points. H(n) and G(n) would then be rather inaccurate. In most cases we will therefore use a smaller interval of summation, say from Θ_1 to Θ_2, which are placed symmetrically around θ_0. The independent variable x is given by

$$\mathbf{x} = \frac{\theta - \theta_0}{\Theta_2 - \Theta_1} = \frac{\tan\theta_0}{\Theta_2 - \Theta_1} \cdot \frac{\theta - \theta_0}{\tan\theta_0} \simeq \mathrm{rx},$$

where

$$\mathrm{r} = \frac{\tan\theta_0}{\Theta_2 - \Theta_1} > 1.$$

In this way we determine Fourier coefficients **H(n)**, which are related to H(n) by

$$\mathbf{H(n)} = \mathrm{rH(n)}, \quad \text{for } \mathrm{n} = \mathrm{rn}. \tag{24}$$

According to K. DRENCK (1959) the interval of summation must be chosen so large that the values of g(w) and h(x) are negligible for |w| and |x| > 1/6. In the program used this corresponds to a t interval of ±60. A smaller interval of summation can be chosen for the quartz peak than for the flint peak. The intervals, however, are not very different in size, and as the **G(n)** values always are more accurate than the **H(n)** values, the same interval was actually chosen for both h(x) and g(w) in the GIER program.

Presentation of results

For practical reasons we will now define a new set of Fourier coefficients for f(y):

$$\mathrm{M(t)} = \frac{\mathrm{F(n)}}{\mathrm{G(0)}}, \text{ for } \mathrm{t} = \mathrm{nd} = \mathrm{rnd}. \tag{25}$$

G(0) can be determined from (3), p. 324, as well as from (9), p. 325, when these equations are applied to the quartz standard:

$$\mathrm{G(0)} = \frac{\mathrm{A}}{\mathrm{T}} = \mathrm{kN(0)} = \mathrm{kN_q},$$

where N(0) is the number of unit cells in the quartz standard and will be termed N_q in the following. (25) can now be modified by use of (3), p. 324, and (24):

$$M(t) = \frac{F(n)}{G(0)} = \frac{A}{T} \cdot \frac{H(n)}{G(n)} \cdot \frac{T}{A} = \frac{H(n)}{G(n)} = \frac{H(n)}{G(n)},$$

$$\text{for } t = nd = rnd. \tag{26}$$

The physical meaning of M(t) becomes clear when (9A) is written

$$|M(t)| = \frac{|F(n)|}{kN_q} \simeq \frac{N(n)}{N_q}. \tag{9B}*$$

M(t) are thus the Fourier coefficients of the flint which have been normalized, M(0) being the volume fraction of quartz in the flint sample. |M(t)| varies from nearly one for $t = 0$ to nearly zero for $t \to \infty$. The fact that M(0) is less than one for flint is partly due to the water which occupies about 5 % of the volume (see p. 343). Another reason is that part of the peak area will be counted as background, an error which is largely eliminated by linear extrapolation of the M(t)-curve to $t = 0$. This is justified because $N''(n) \geq 0$, according to (13), p. 325. The M(0) value determined in this way is therefore likely to be a minimum value.

The equations on the preceding pages are changed as follows (for $t = nd = rnd$):

$$M_S(t) = |M(t)| \sin \varphi_F(n). \tag{5B}, \text{ see p. 324.}$$

When |M(t)| is plotted against t and a smooth curve drawn through the points, the slope of the curve – |M(t)|′ – is derived from (9B)

$$|M(t)|' \simeq \frac{1}{d} \cdot \frac{N'(n)}{N_q}. \tag{27B}$$

When V is the volume of the unit cell, $\sigma = V/d$ is the cross-section area of a column of unit cells, and VN(0) is the volume of quartz in the flint sample. In these terms (27B) becomes

$$|M(t)|' \simeq \frac{V}{d} \cdot \frac{N'(n)}{VN(0)} \cdot \frac{N(0)}{N_q} \simeq \frac{\sigma N'(n)}{VN(0)} M(0). \tag{28B}$$

$-N'(n)$ is the number of columns of minimum length n. $-\sigma N'(n)$ is therefore the cross-section area of all such columns. The ratio $-\sigma N'(n)/VN(0)$ is

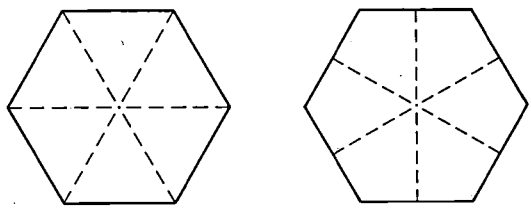

Fig. 13. (0001)-section of $\{10\bar{1}0\}$. Dotted lines indicate the cross-sections corresponding to a $\{h0\bar{h}0\}$ reflection (left) and to a $\{h, h, \overline{2h}, 0\}$ reflection (right).

*) "B" indicates that the equation is valid for $t = nd$.

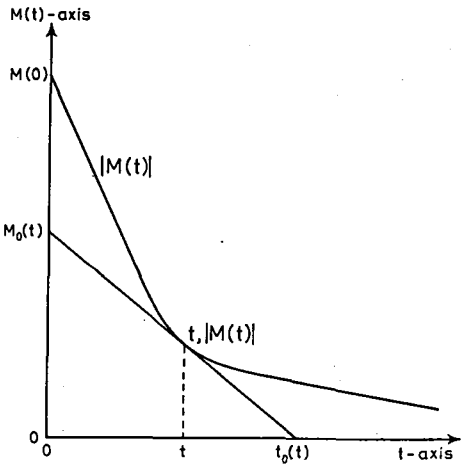

Fig. 14.

thus the cross-section area of the columns of minimum length $t = nd$ per unit volume of quartz in the flint sample. When this ratio is multiplied by the relative volume of quartz in the flint sample – i.e. by M(0) – we obtain the cross-section area per unit volume of flint. For $t = 0$, $-|M(t)|'$ is the total cross-section area of the columns in a volume unit of flint. When t is given in nm, the cross-section area is given in nm^2/nm^3. For the sake of convenience this is changed into m^2/cm^3 by a factor of 1000. The cross-section area of columns with lengths between t_1 and t_2 is thus

$$[|M(t_2)|' - |M(t_1)|'] \cdot 1000\ m^2/cm^3.$$

The ratio between cross-section area and particle surface area will depend on the shape of the particles and the orientation of the normals to the reflecting lattice planes. Fig. 13 shows that the minimum and the maximum values of this ratio are 3.00 and 3.46 respectively for *{hki0}* reflections from a hexagonal prism. Crystals which are infinitely long in one direction ∥ (0001) give the same extremes for *{hki0}* reflections due to the hexagonal symmetry. In the following a value of π, corresponding to a cylinder, will be used for the ratio between the area of surfaces parallel to [001] and the cross-section area determined by *{hki0}* reflections. For reflections from faces oblique to the [001]-axis we will use the ratio between the surface and the cross-section of a sphere, i.e. 4.

The tangent to the |M(t)| curve will cut the coordinate axes at $t_0(t)$ and $M_0(t)$ (see fig. 14). From (14), p. 326,

$$t_0(t) = dn_0(n) = rdn_0(n), \tag{14B}$$

is the mean length of the columns with a minimum length of $t = nd$.

From (15), p. 326,

$$M_0(t) = -t_0(t)|M(t)|' \simeq -n_0(n)d\frac{N'(n)}{dN_q} = \frac{N_0(n)}{N_q}.$$

$M_0(t)$ is thus the number of unit cells found in columns of minimum length $t = nd$, divided by the number of unit cells found in the rock crystal specimen. In other words, $M_0(t)$ is the relative volume of the columns of minimum length t.

From (26), p. 332,

$$|F(n)|' = kdN_q|M(t)|'.$$
$$F_s''(n) = kd^2N_qM_s''(t).$$

When these expressions are used in (22A), p. 330, the average degree of deformation $\langle z_t \rangle$ at a distance of t from the ends of the columns becomes

$$\langle z_t \rangle \simeq \frac{1}{4\pi} \cdot \frac{F_s''(n)}{|F(n)|'} = \frac{d}{4\pi} \cdot \frac{M_s''(t)}{|M(t)|'}, \quad \text{for } |M(t)|'' = 0. \tag{22B}$$

The average degree of deformation now becomes

$$\langle Z(d) \rangle \simeq \frac{-1}{2\pi} \varphi_F(d). \tag{23B}$$

Results of X-ray diffraction peak analyses

The shapes of the following reflections were analysed to obtain the particle size distributions: $\{10\bar{1}0\}$, $\{10\bar{1}1\}$, $\{11\bar{2}0\}$, $\{20\bar{2}0\}$, $\{20\bar{2}1\}$, $\{11\bar{2}2\}$, and $\{12\bar{3}1\}$. The shapes of these reflections – h(x) and g(w) – are given in figs. 15, a to 21, a. The Fourier transforms $|M(t)|$ and $M_s(t)$ are given in figs. 15, b to 21, b. Of these reflections only $\{10\bar{1}0\}$ and $\{10\bar{1}1\}$ are really suited for particle size determination, the results obtained by the other five reflections being of rather limited use. Notably the information on the very short columns is unreliable. On the other hand, each reflection has its own way of being influenced by particle shape, deformations, stacking faults, and twinning. Poor reflections may therefore give some important information.

At first, an attempt was made to interpret the results on the assumption that the approximations (9A) and (10A) were valid, i.e. on the assumption that the deformations were small and that the grains were separated by low angle boundaries. As shown by K. DRENCK (1959) it is not possible to obtain a picture of the quartz crystals solely on the basis of X-ray data. It was therefore attempted to interpret the X-ray data in the light of the semi-quantitative picture of the particle shape which was obtained by electron microscopy (see figs. 22, a and 23, a).

The results obtained by the different reflections, however, did not agree with each other or with fig. 22, a, and the integral deformations determined in this way reached $1/4\vec{a}$. Therefore, it was finally attempted to interpret the M(t) curves in terms of a quartz lattice with numerous lattice faults, a possibility which was already suggested by K. DRENCK (1959). The electron microscope study of flint showed that the quartz plates contain lattice faults, which imply a parallel displacement of the Bravais lattice, a displacement which may or may not be accompanied by a twinning operation, i.e. the lattice faults are either stacking faults or twin faults.

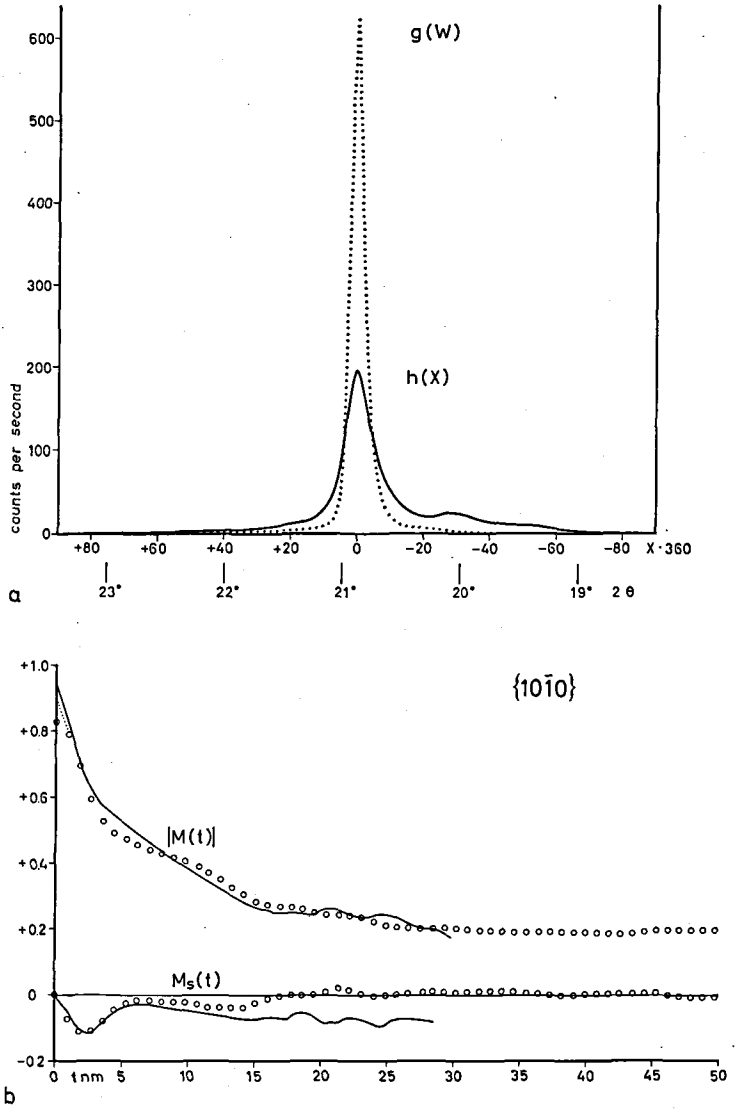

Fig. 15. X-ray diffraction results obtained with {10$\bar{1}$0}. a) The experimental curves for flint – h(x) – and quartz – g(w). b) The circles give the Fourier transformed to f(y) for the dark flint. The full lines are calculated on the assumption of triplets of twin faults (see p. 351).

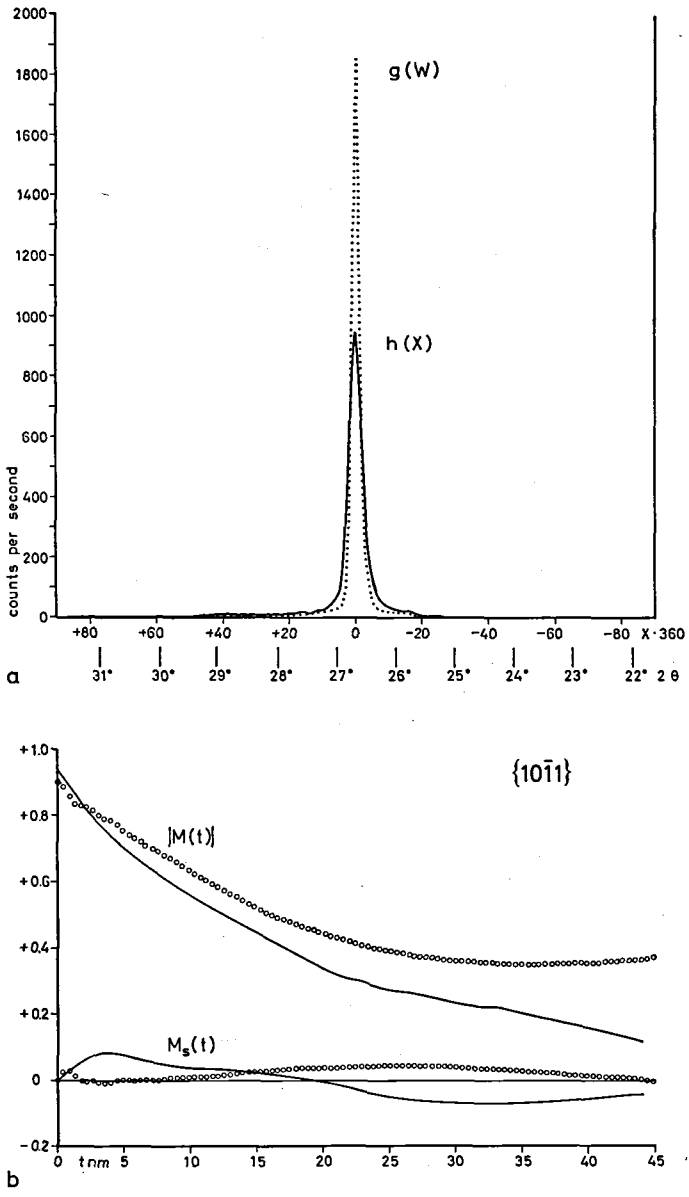

Fig. 16. X-ray diffraction results obtained with {10$\bar{1}$1}. a) The experimental curves for flint – h(x) – and quartz – g(w). b) The circles give the Fourier transformed to f(y) for the dark flint. The full lines are calculated on the assumption of triplets of twin faults (see p. 351).

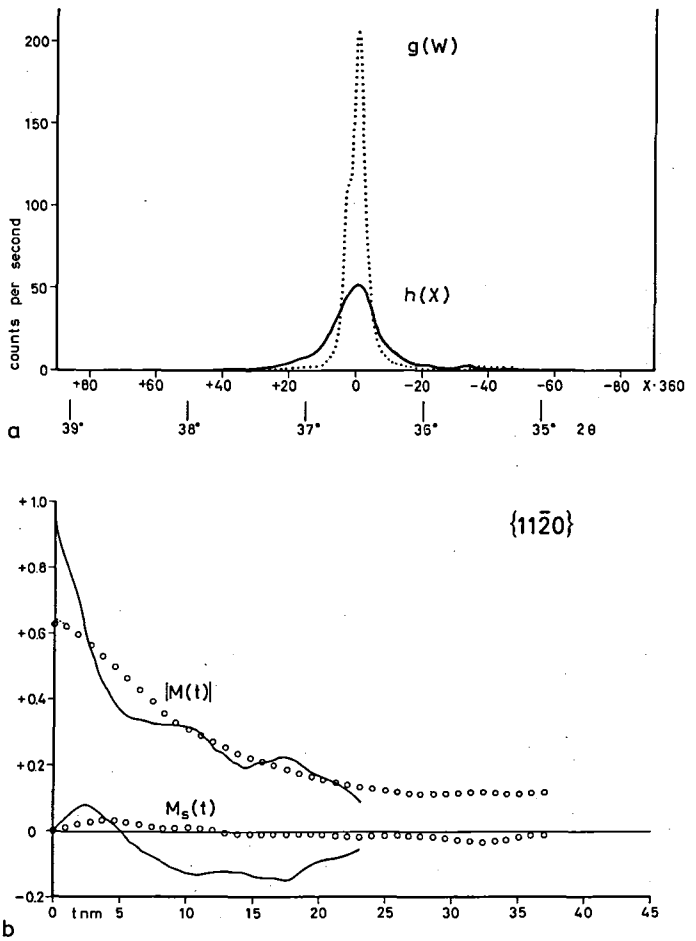

Fig. 17. X-ray diffraction results obtained with {11$\bar{2}$0}. a) The experimental curves for flint – h(x) – and quartz – g(w). b) The circles give the Fourier transformed to f(y) for the dark flint. The full lines are calculated on the assumption of triplets of twin faults (see p. 351).

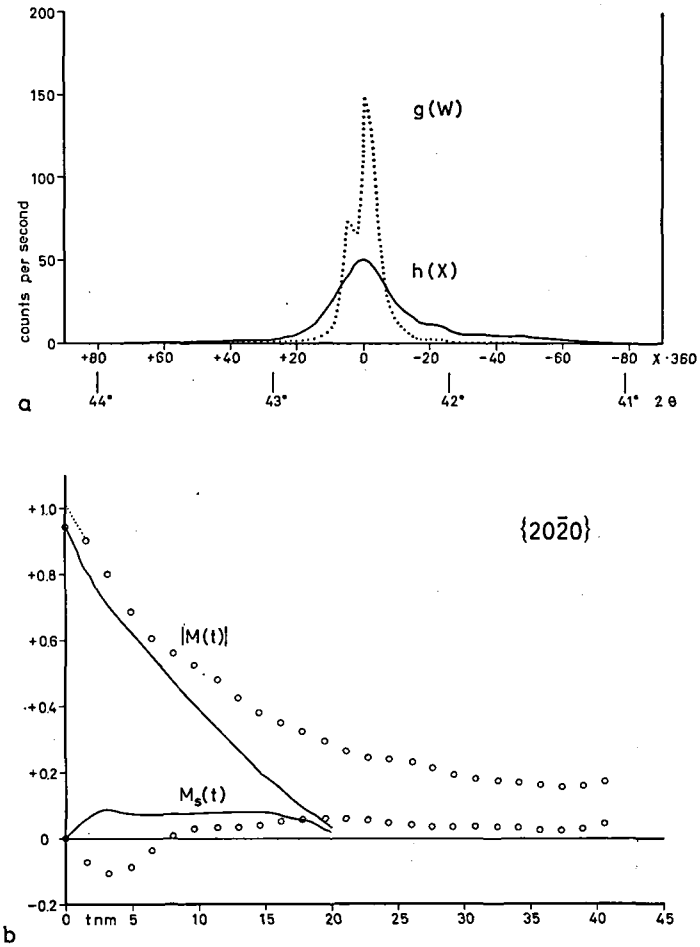

Fig. 18. X-ray diffraction results obtained with {20$\bar{2}$0}. a) The experimental curves for flint – h(x) – and quartz – g(w). b) The circles give the Fourier transformed to f(y) for the dark flint. The full lines are calculated on the assumption of triplets of twin faults (see p. 351).

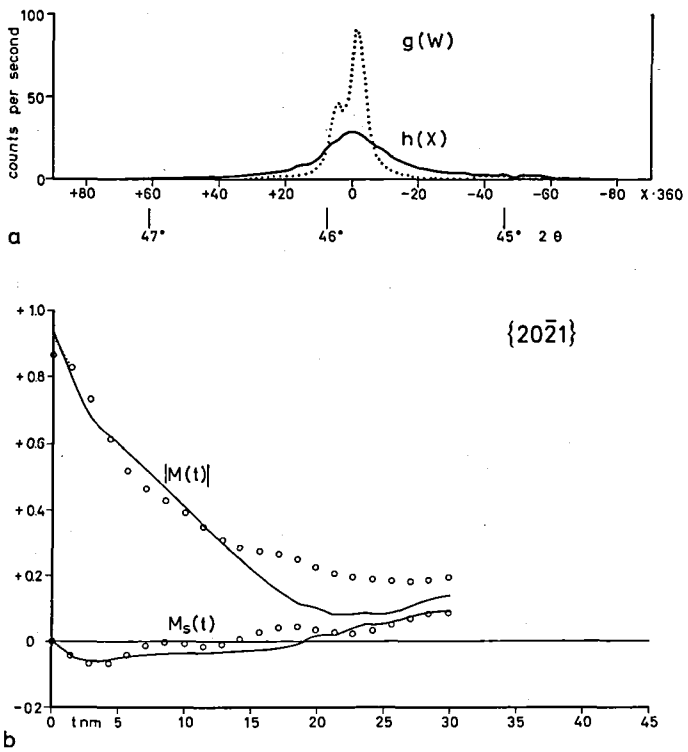

Fig. 19. X-ray diffraction results obtained with {20$\bar{2}$1}. a) The experimental curves for flint – h(x) – and quartz – g(w). b) The circles give the Fourier transformed to f(y) for the dark flint. The full lines are calculated on the assumption of triplets of twin faults (see p. 351).

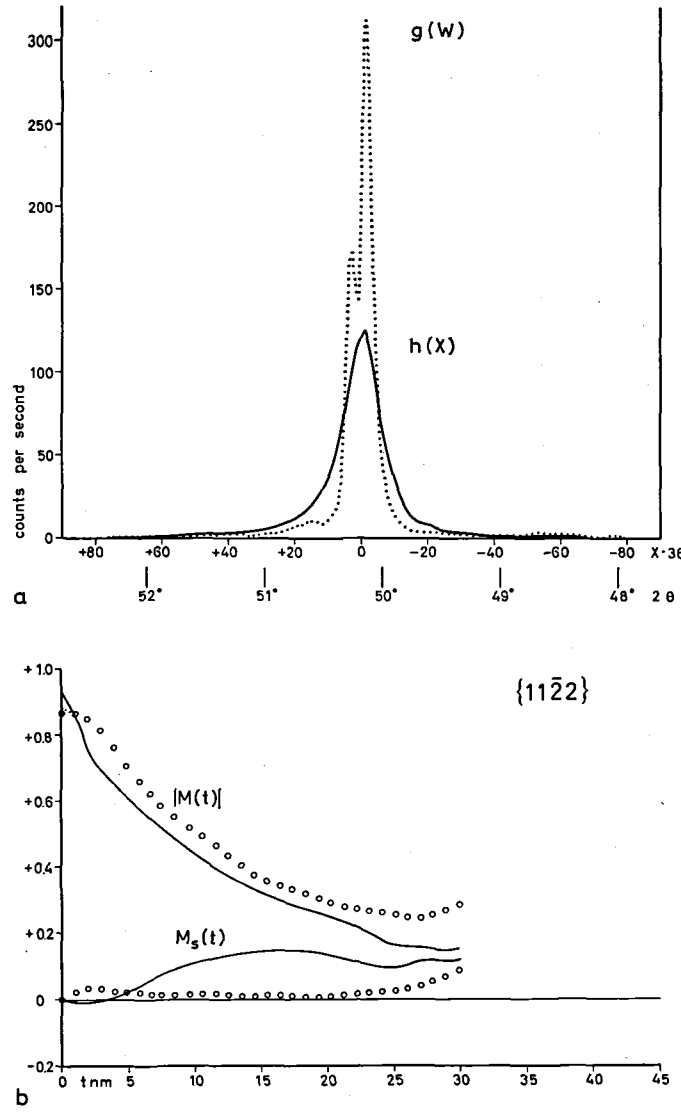

Fig. 20. X-ray diffraction results obtained with {11$\bar{2}$2}. a) The experimental curves for flint – h(x) – and quartz – g(w). b) The circles give the Fourier transformed to f(y) for the dark flint. The full lines are calculated on the assumption of triplets of twin faults (see p. 351).

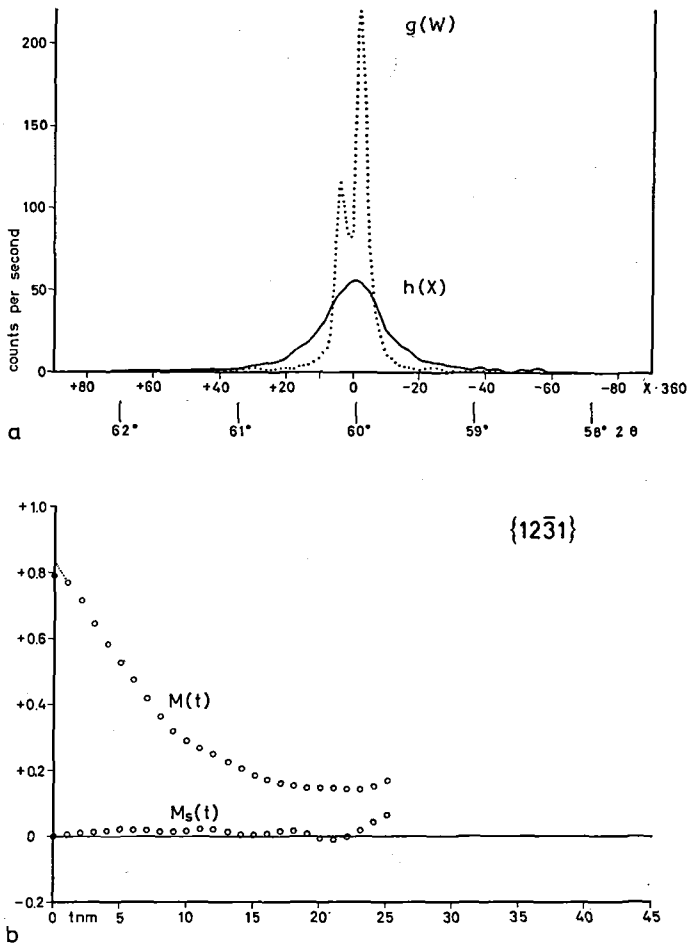

Fig. 21. X-ray diffraction results obtained with {12$\bar{3}$1}. a) The experimental curves for flint – h(x) – and quartz – g(w). b) The circles give the Fourier transformed to f(y) for the dark flint.

Table

Particle size and average degree of deformation of dark flint from Stevns. The de-

Reflection	Treatment	Relative volume of quartz	Mean length	Total surface area	Different types			
					A		B	
					Length	Relative volume	Length	Relative volume
		%	nm	m^2/cm^3	nm	%	nm	%
$\{10\bar{1}0\}$	natural	89	8	338	3–4	30		0
$\{10\bar{1}1\}$**	–	88	36	96		0		0
$\{11\bar{2}0\}$	–	67	18	121		?	8——	———
$\{20\bar{2}0\}$	–	100	15	206		?	5–7	22
$\{20\bar{2}1\}$	–	95	12	319		?	4–8	29
$\{11\bar{2}2\}$	–	97	18	222		?	4–9	16
$\{12\bar{3}1\}$	–	84	13	253	3–5	5	8–11	29
$\{10\bar{1}0\}$	2200 bars H_2O pressure at 510° C for 20 days	88	42	67	3–5	2		0
$\{10\bar{1}0\}$	650°C in air for 48 hours	82	20	131	3–5	11		0
$\{10\bar{1}0\}$	Heated 80 times to 650°C in air	88	45	61	3–5	3		0
$\{10\bar{1}1\}$**	–	86	52	66		0		0
$\{11\bar{2}0\}$	–	81	26	98		?	7——	———

*) The different types of columns have been discerned according to the following rules, taking into regard the dependence of the columnar length on the orientation of the reflecting lattice planes: Length of B $\sim$ 2 $\times$ length of A. Length of D $\sim$ length of C + length of A or B. Length of E $\sim$ 2 $\times$ length of C + 0 to 6 $\times$ length of A. Type F includes the columns which can only be classified as long columns, the lower limit being poorly defined.

Particle size determinations based on the assumption that the deformations are small

It is now assumed that the lattice deformations are small and that the crystals are separated by tilt or twist boundaries. The approximations (9A) and (10A) are then valid, and applied to the $|M(t)|$ and $M_s(t)$ curves of figs. 15, b – 21, b they yield the results given in table No. 5. It is possible to distinguish between various types of columns according to their lengths and this distinction has been used in the table.

The best of the reflections – $\{10\bar{1}0\}$ and $\{10\bar{1}1\}$ – show a content of 89 vol.% and 88 vol.% of quartz respectively. This may seem to be too low, but besides SiO_2 the dark flint from Stevns contains 1.00 wt.% water present as Si-OH groups and 0.27 wt.% water present as water molecules. These two components comprise 3.26 atom% and 0.44 atom% respectively of the oxygen present in the flint. It will later be shown that the Si-OH groups probably enter into

No. 5

terminations are based on the approximations specified by equations (9A) and (10A)

of columns*								Average degree of deformation
C		D		E		F		
Length	Relative volume	Length	Relative volume	Length	Relative volume	Length	Relative volume	
nm	%	nm	%	nm	%	nm	%	%
15–16	20	25–28	16			>35	23	+0.7
13——	———	——34	53			>35	35	−0.02
——16	26	19–22	15	26–30	13	>30	12	−0.06
14——	———	——26	36			>30	42	+0.2
13–20	21	>20——	———	———	———	———	45	+0.1
14–16	24	19–22	19	>25——	———	———	38	−0.1
14–20	33	>20——	———	———	———	———	17	−0.02
13–17	4	23–26	17			>35	65	0.0
14–16	13			28–37	22	>37	36	+0.3
13–17	5	24–26	15			>35	65	−0.1
14——	———	——26	23	29–35	14	>36	49	−0.03
—13	18	18–26	20	>26——	———	———	40	−0.08

**) The M(t) curves seem to indicate the presence of a few percent of strongly deformed columns only 1 nm in length. This information is not regarded as reliable and is disregarded here.

?) This indicates that the reflection can give no reliable information about very short columns.

special interface structures comprising another 1.30 atom% of the oxygen. Therefore, 5.0% of the oxygen atoms are not found in the quartz structure. If it is assumed that the volume percentage of quartz has the same value as the atomic percentage of oxygen then only 95 vol.% of quartz can be expected to be present in the flint. Furthermore, the structure of the quartz in the unit cells next to the interfaces is probably slightly deformed (see also p. 359), and these unit cells make up ca. 11% of the quartz. In total, the experimental results of ca. 89% seem to be reasonable.

The results obtained should be compared with that shape of the quartz crystals which was found by electron microscopy, see fig. 22, a. Perpendicular to $(\bar{1}2\bar{1}0)$, i.e. parallel to the [010] axis, the flint shows a period of repeat of ca. 20 nm in the electron microscope. The termination of the crystals in the direction of the a*-axis is unknown but for the sake of simplicity $(10\bar{1}0)$ has been drawn on fig. 22, a.

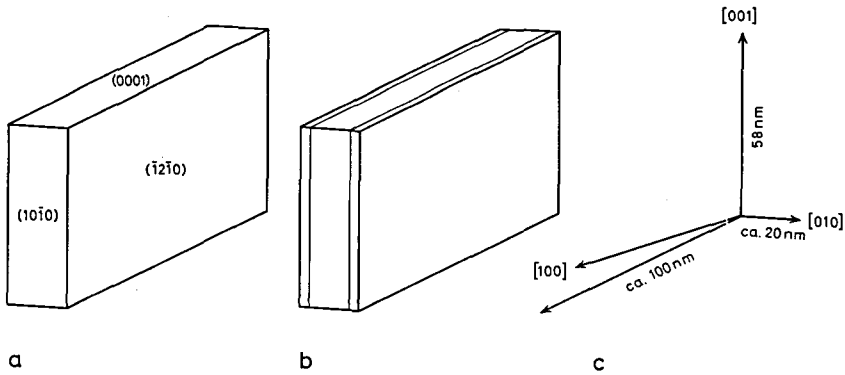

Fig. 22. a) Quartz crystal in flint, habit and size determined by electron microscopy. b) Quartz crystals in flint, habit and size determined from the peak profile of $\{10\bar{1}0\}$ on the assumption that the deformations are small. c) Coordinate axes for the two models.

At first sight, the results obtained by different reflections seem to contradict each other and to disagree entirely with the model of the quartz grains in fig. 22, a. However, only a few different types of columns predominate and therefore the crystals are bound to be rather regular in size and shape. Also, the volume of the long columns is roughly 30% when measured by means of a $\{h0\bar{h}l\}$ reflection, but low when measured by $\{1\bar{2}10\}$. This corresponds well to figs. 22, a and 23, a. One of the three $\{h0\bar{h}0\}$ normals, namely that of $(h0\bar{h}0)$, runs lengthwise in the crystal, and one third of the volume will therefore appear as long columns. The two other sets of lattice planes, $(0h\bar{h}0)$ and $(\bar{h}h00)$, will give rise to short columns in the analysis. By analogy, none of the $\{1\bar{2}10\}$ normals runs lengthwise in the crystal, and the volume of the long columns therefore ought to be low.

The experimental results are as would be expected from crystals which are long perpendicular to $(10\bar{1}0)$, but the model cannot account for the short columns. For instance, a thickness of 20 nm ∥ [010] would imply that two thirds of the volume found by the {1010} reflection should occur as columns $20/\cos 30° = 23$ nm in length, see fig. 23, a. Columns of this length, however, are rare, whereas columns with lengths of ca. $3\frac{1}{2}$ and ca. $15\frac{1}{2}$ nm are very common although not predicted by the model. The great abundance of columns $3\frac{1}{2}$ nm and $15\frac{1}{2}$ nm in length can only be explained if the model is modified by assuming some kind of alternation of crystals with thicknesses of ca. $3\frac{1}{2} \cdot \cos 30° = 3$ and ca. $15\frac{1}{2} \cdot \cos 30° = 13\frac{1}{2}$ nm ∥ [010]. After a number of trials with different models an aggregate like the one shown in figs. 22, b and 23, b was accepted. The 3 nm crystals were supposed to form a kind of surface layer on the thick 13 nm crystals, or put in another way, the thick crystals were supposed to be separated by two thin crystals. In the main, the model can account for the results obtained by $\{10\bar{1}0\}$, and it is also in accordance with the electron micrographs. The period of repeat of the triplet of grain boundaries is ca.

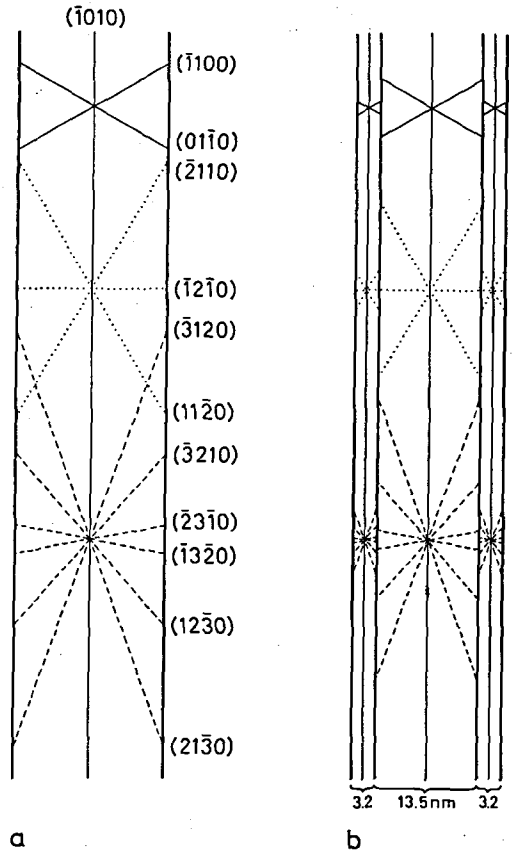

Fig. 23. a) Face normals projected on (0001) of a quartz crystal in flint. Habit and size determined by electron microscopy. b) Face normals projected on (0001) of a group of quartz crystals in flint. Habit and size determined from the peak profile of $\{10\bar{1}0\}$ on the assumption that the deformations are small.

$(3.5 + 3.5 + 15.5) \cdot \cos 30° \simeq 20$ nm. $\parallel$ [010] the mean length becomes ca. 7 nm. The model with the thin surface layer, however, fails to explain the results obtained by other reflections than $\{10\bar{1}0\}$. For reflections with $l \neq 0$ some allowance must be made for the effects of the unknown termination of the crystals in the direction of the c-axis, but even then the model cannot explain the experimental results. The disagreement between experimental and theoretical results, however, is not complete. All reflections show that columns, 13–20 nm in length, are common – type C. Five reflections show the presence of columns ca. 6 nm in length, i.e. short columns with a length of roughly twice the length found by $\{10\bar{1}0\}$ – type B. Only $\{10\bar{1}0\}$ and $\{10\bar{1}1\}$ can give reliable information on columns shorter than ca. 5 nm, and the lack of such very short columns in the results obtained by the other reflections has no

significance. $\{11\bar{2}0\}$ shows the presence of columns ca. 14 nm and ca. $14/\cos 60° = 28$ nm in length – types C and E respectively – as predicted from the shape of the grain in fig. 23, b. In total, there seems to be some kind of qualitative relationship between the model and the flint, but the model cannot explain the experimental results quantitatively. The most evident discrepancy between the theoretical and experimental results is certainly the lack of the very short columns in the results obtained by $\{10\bar{1}1\}$. On the other hand this discrepancy cannot be explained by any particle shape and it therefore shows that the grain boundaries have very little influence on some of the reflections. This is not possible when grain boundaries involve a tilt or a twist, and therefore the neighbouring crystal lattices seem to be parallel and their separation must then be a displacement with or without a twinning operation. The displacement is not necessarily a simple fraction of a unit cell, as in the classical treatment of stacking faults by H. D. MEGAW (1961). Nevertheless, the term stacking fault will be employed here since the phenomena are closely related geometrically.

A stacking fault will introduce a phase difference in the X-ray waves. The phase difference will depend on the displacement vector as well as on the reciprocal vector of the reflecting lattice plane. *A priori* it seems possible that a stacking fault or a sequence of stacking faults may influence only some of the reflections.

The influence of stacking faults on the Fourier coefficients of the peak shape function

The influence of stacking faults on the diffraction phenomena has been treated thoroughly by H. D. MEGAW (1961). MEGAW's treatment is mainly based on the positions and intensities of extra, non-Bragg reflections which can be found on single crystal photographs. Actually, MEGAW's method is not suited for a detailed investigation of peak shape functions of fine-grained powders. The use of the Fourier coefficients will therefore be continued here, equations (18) and (19), p. 328, being suited for the purpose.

In accordance with the semi-quantitative models of the quartz grains (fig. 22) it will be assumed in the following that stacking faults occur on (1210). Each stacking fault implies a perfect parallel displacement, which in the terminology of H. D. MEGAW (1961) is given by a vector called $\vec{\mu}_2$, formally using $(\bar{1}2\bar{1}0)$ as a b-pinacoid.

$$\vec{\mu}_2 = \mu_{21}\vec{a} + \mu_{22}\vec{b} + \mu_{23}\vec{c}. \tag{30}$$

Such a stacking fault will create a phase difference in the waves of an *hkl* reflection given by:

$$\Delta\varphi = 2\pi(\mu_{21}h + \mu_{22}k + \mu_{23}l) = 2\pi z, \tag{31}$$

where z is used in the same sense as on p. 327.

The effect of stacking faults will furthermore depend upon their distribution in the columns. Provisionally, it will be assumed that the stacking faults have the same displacement vector and that they occur in a perfectly regular distribution with a distance of w cells. When P(p) identical columns of length p are considered, equation (18), p. 328, can be modified, and by use of (8), p. 325:

$$F(n) = kN(n)\langle \exp(-2\pi i Z(n))\rangle = kP(p)[p-n]\langle \exp\left(-2\pi i \sum_{j=m}^{j=m+n-1} z_j\right)\rangle_m .$$

$\langle\rangle_m$ denotes the mean value for all possible values of m, viz. from $m = 1$ to $m = p - n$.

By means of (26), this becomes for $t = nd$:

$$M(t) = \frac{F(n)}{kN_q} = \frac{P(p)[p-n]}{N_q}\langle \exp\left(-2\pi i \sum_{j=m}^{j=m+n-1} z_j\right)\rangle_m . \qquad (32B)$$

When the stacking faults occur with a distance of w cells, the sum of the lattice spacing errors will depend on n. Thus for $n \leq w$:

$$\sum_{j=m}^{j=m+n-1} z_j = \begin{cases} z, & \text{with a frequency of } \frac{n}{w}, \text{ and} \\ 0, & \text{with a frequency of } \frac{w-n}{w}. \end{cases}$$

(32B) is therefore for $n \leq w$:

$$M(t) = \frac{P(p)[p-n]}{N_q}\left[\left(\frac{w-n}{w}\right) + \frac{n}{w}\exp(-2\pi i z)\right].$$

By analogy for $w \leq n \leq 2w$:

$$M(t) = \frac{P(p)[p-n]}{N_q}\left[\left[\frac{2w-n}{w}\right]\exp(-2\pi i z) + \left[\frac{n-w}{w}\right]\exp(-4\pi i z)\right],$$

and for $2w \leq n \leq 3w$:

$$M(t) = \frac{P(p)[p-n]}{N_q}\left[\left[\frac{3w-n}{w}\right]\exp(-4\pi i z) + \left[\frac{n-2w}{w}\right]\exp(-6\pi i z)\right],$$

etc.

Fig. 24 shows $M_c(n)$ and $M_s(n)$ for a powder consisting of infinitely long columns where 5 unit cells separate stacking faults each of which gives a phase difference of +130°. The curves calculated in this way show no resemblance to the experimental results. The calculations have been repeated with other values of z, but the model is wrong. The model, however, shows that the slopes of the curves change – often by sign – when n passes a multiple of w. Such strong changes of slopes are seen in some of the experimental M(t) curves, and thus the theory of stacking faults in the flint seems to be reasonable. However, the distribution of the stacking faults is not the simple, perfectly regular distribution used for the calculations above.

The simple, perfectly regular model makes it easy to obtain a general idea of the effects of variations in w and z on the M(t) curves for a powder consisting of different columns. If w varies, the positions of the maxima and minima of $M_c(t)$ and $M_s(t)$ for the single columns will vary, and when these curves are

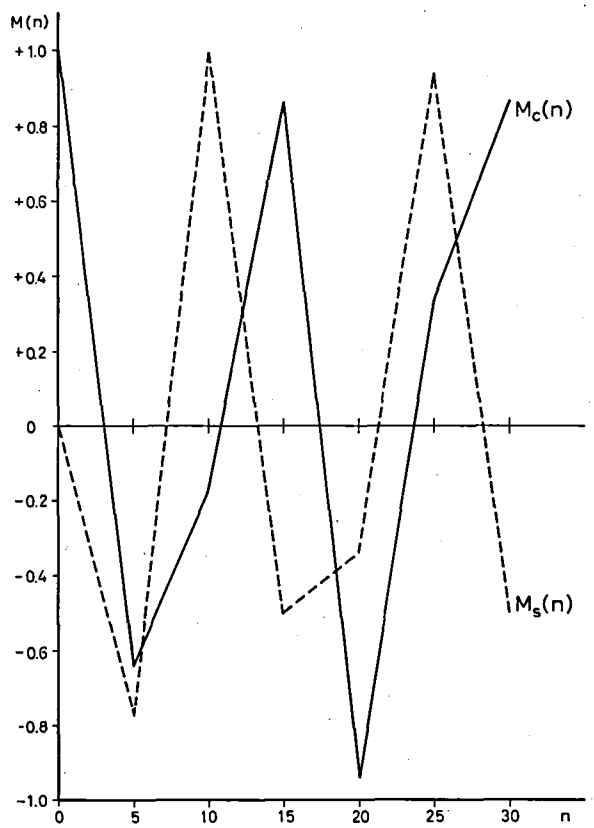

Fig. 24. $M_c(n)$ and $M_s(n)$ for a powder consisting of infinitely long columns where 5 unit cells separate stacking faults each of which gives a phase difference of $+130°$.

added to give the curves for the powder, peaks and depressions will tend increasingly to cancel each other out, the higher the value of n. If z varies, $|\langle\exp(-2\pi iz)\rangle|$ will become less than one, and the maxima and minima will be less pronounced.

In order to explain the experimental data, $|M(t)|$ and $M_s(t)$ have been calculated for a number of models which were different with regard to size and distribution of stacking faults. All the models, however, have been given up apart from one in which three stacking faults occur as a triplet. Within the triplet the stacking faults are separated by w cells, the triplets being separated by W cells, $W > 2w$. By counting on the model it can be determined with which frequency 1, 2 or 3 stacking faults will occur within a length of n cells. (32B) can then be written:

For $n \leq w$:

$$M(t) = \frac{P(p)[p - n]}{N_q[W + 2w]}[[W + 2w - 3n] + 3n\langle\exp(-2\pi iz)\rangle].$$

For $w \leq n \leq 2w$:

$$M(t) = \frac{P(p)[p - n]}{N_q[W + 2w]}[[W - n] + [4w - n]\langle\exp(-2\pi iz)\rangle + 2[n - w]\langle\exp(-2\pi i2z)\rangle].$$

For $2w \leq n \leq W$:

$$M(t) = \frac{P(p)[p - n]}{N_q[W + 2w]}[[W - n] + 2w\langle\exp(-2\pi iz)\rangle + 2w\langle\exp(-2\pi i2z)\rangle + [n - 2w]\langle\exp(-2\pi i3z)\rangle].$$

etc.

Fig. 25 corresponds to this model. $|M(n)|$ and $M_s(n)$ have been calculated for two values of z, namely 0.347 and 0.847. W and w have been chosen in accordance with the lengths of the normals to $\{10\bar{1}0\}$ (see fig. 23, b). One third of the volume is assumed to be made up of infinitely long columns without stacking faults. Two thirds of the volume is assumed to be made up of infinitely long columns containing the above-mentioned triplets of stacking faults, with $w = 5$ and $W = 25$. Below $n = 25$ the curves for $z = 0.347$ have much in common with the experimental curves for the $\{10\bar{1}0\}$ reflection. The curves for $z = 0.847$ show some analogy to the experimental curves for the $\{10\bar{1}1\}$ reflection. It seems therefore probable that μ_{22} and μ_{23} are close to 0.35 and 0.5

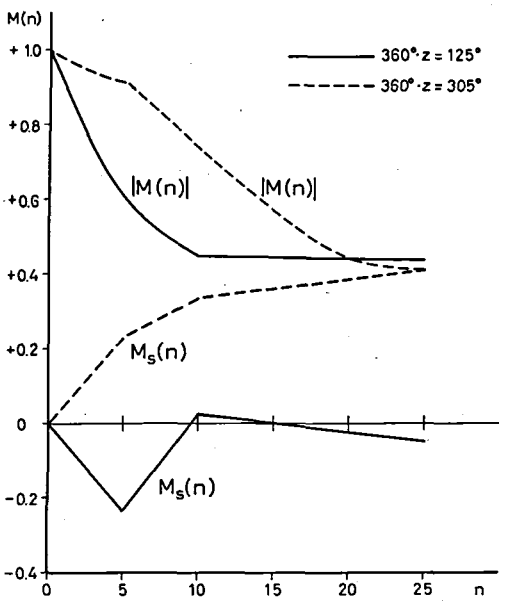

Fig. 25. $|M(n)|$ and $M_s(n)$ for two $\{h0\bar{h}l\}$ reflections. $\frac{2}{3}$ of the columns contain triplets of stacking faults with $w = 5$ and $W = 25$. $\frac{1}{3}$ of the columns have no stacking faults. All the columns are treated as infinitely long.

respectively, and the model seems to be close enough to nature to make possible detailed calculations of z, w, and W. For this purpose a computer program in GIER algol III has been worked out for $n \leq 2W + 4w$ with the kind help of ANDERS BJERRE, cand. polyt. The program gives $|M(0)| = 0.94$ in an attempt to account for the volume of quartz being $\leq 95\%$ (see p. 343). The calculations were carried out on the GIER computer of the Astronomical Observatory of the University of Copenhagen.

Determination of the lattice faults in dark flint

In flint the triplet of stacking fault planes must be parallel to $(\bar{1}2\bar{1}0)$ as shown by electron microscopy (see p. 319). Initially it is assumed that the columnar lengths determined by means of $\{10\bar{1}0\}$ (table 5) are largely correct. A model is then obtained of the quartz grains in flint, much like the one given by fig. 22, b but with stacking faults instead of grain boundaries. In accordance with (19), p. 328, $M_c(t)$ and $M_s(t)$ are calculated for a powder by adding up the contributions from each kind of column. These contributions are calculated separately, taking into account the orientation of the face normals as shown in fig. 23, b.

In the first calculations, it was assumed that z was a constant and had the same value for reflections from $(\bar{1}100)$ and $(01\bar{1}0)$, i.e. $\mu_{21} = 0$ and $\mu_{22} = z$. p was assumed to be 250 cells, corresponding to a length of ca. 100 nm. On these assumptions the M(t) curves were calculated for the $\{10\bar{1}0\}$ reflection for different values of w, W, and of μ_{22}, the latter varying from 0.3 to 0.5. By comparison with the experimental data the following values were found to give the best approximation:

$\mu_{22} = 0.37 \pm 0.02$, $w = 6 \pm 2$ cells, and $W = 33$–56 cells with a mean value of 43 cells.

The variations in w and W, which are necessary to suppress strong maxima at $n > 35$, have been taken into account by use of 18 different combinations of w and W in each calculation of M(t).

The M(t) curves calculated from the above figures were now improved by making $\mu_{21} \neq 0$. The z values for $(\bar{1}100)$ and $(01\bar{1}0)$ were now different. Their mean value is $\mu_{22} - \frac{1}{2}\mu_{21}$ and turned out to be 0.35. The following values gave the best fit between the calculated and the experimental M(t) curves:

$$\mu_{21} = 0.10 \pm 0.04 \quad \text{and} \quad \mu_{22} = 0.40 \pm 0.03.$$

Another set of values gives the same results as the above set, namely $\mu_{21} = -0.10$ and $\mu_{22} = 0.30$. These two displacement vectors cannot be distinguished in the calculations due to the orientation of the fault plane being $(\bar{1}2\bar{1}0)$. The former vector is used in the following as it corresponds to the detailed structures shown in fig. 31.

These values were now used in the calculation of the M(t) curves for $\{10\bar{1}1\}$ after changing w and W according to the new orientation of the face normals. μ_{23} was allowed to vary from 0 to $+\frac{1}{2}$. The sign of μ_{23} cannot be determined

since $\{10\bar{1}1\}$ comprises faces with both positive and negative values of l. The result became $\mu_{23} = \pm 0.35 \pm 0.02$, giving a displacement vector of

$$\vec{\mu}_2 = 0.10\vec{a} + 0.40\vec{b} \pm 0.35\vec{c}.$$

The M(t) curves were then calculated for the other reflections, taking into account as far as possible the influence of the shape of the crystals on w and W. The results, however, were not convincing, even allowing for deviations due to the probable occurrence of a stacking fault on (0001) and deviations due to the unknown termination of the domains in the direction of the a*-axis. To improve the calculated M(t) curves it was now taken into consideration that the observed lattice faults might not be genuine stacking faults but faults where a parallel displacement is accompanied by a twinning of the lattice. M. J. BUERGER (1960) used the term stacking fault twins with reference to close packed structures where a stacking fault implies twinning. In quartz, a stacking fault does not imply formation of a twin, and the author will therefore use the term "twin fault". Twinning implies that two $(\bar{1}2\bar{1}0)$ faces are adjacent at every second twin fault while two $(1\bar{2}10)$ faces are adjacent at the interjacent twin faults. The low symmetry of quartz makes $(\bar{1}2\bar{1}0)$ and $(1\bar{2}10)$ different, making the twinning possible. The structure of quartz thus implies that the structural details of an $(\bar{1}2\bar{1}0)$ interface must be different from those of an $(1\bar{2}10)$ interface, and the displacement vectors connected with the two interfaces are therefore likely to be different. The two different, alternating vectors will be called

$$\vec{\mu}_{+2} = \mu_{+21}\vec{a} + \mu_{+22}\vec{b} + \mu_{+23}\vec{c}, \quad \text{and}$$
$$\vec{\mu}_{-2} = \mu_{-21}\vec{a} + \mu_{-22}\vec{b} + \mu_{-23}\vec{c}.$$

The above-determined vector is close to the mean value of $\vec{\mu}_{+2}$ and $\vec{\mu}_{-2}$. The calculations have been carried out by using independent variations of $(\mu_{+2j} - \mu_{-2j})$ and of $(\mu_{+2j} + \mu_{-2j})$, j = 1 to 3. The calculations soon showed that the results were not improved by making $(\mu_{+22} - \mu_{-22}) \neq 0$, or by making $(\mu_{+23} - \mu_{-23}) \neq 0$, but the results are not very sensitive to variations in these differences. μ_{+22} and μ_{+23} are therefore not bound to be identical to μ_{-22} and μ_{-23} respectively. On the contrary, a value of ± 0.22 for $(\mu_{+21} - \mu_{-21})$ improves the fit between the calculated and the experimental $M_s(t)$ curves for $\{10\bar{1}0\}$ (see fig. 28). The calculations were repeated a few times to improve the accuracy by successive approximations. The final results were:

$$\vec{\mu}_{+2} = 0.02\vec{a} + 0.415\vec{b} \pm 0.37\vec{c} \quad \text{for } (\bar{1}2\bar{1}0), \quad \text{and}$$
$$\vec{\mu}_{-2} = 0.24\vec{a} + 0.415\vec{b} \pm 0.37\vec{c} \quad \text{for } (1\bar{2}10).$$

Up to this point, μ_{+21} and μ_{-21} can be interchanged in the calculations, but the structural interpretation of the two vectors indicates that the above equations are the probable solution. However, if the lattice faults are twin faults, the lack of a centre of symmetry in α-quartz is to be taken into account. The zero point of a wave from a unit cell is determined by a phase angle φ given by

$$\varphi = \arctan\left(\frac{B}{A}\right),$$

where A and B are the cosine and the sine terms of the structure factor $F^2_{hkl} = A^2 + B^2$. The $\{h0\bar{h}l\}$ faces are parallel to the diad axes, and the φ values are π. Twinning will therefore produce a phase angle of 2π, which do not influence the above calculations of the M(t) curves. The $\{11\bar{2}l\}$ faces are not parallel to diad axes, and the sine terms and hence the φ values are not zero. For the $\{11\bar{2}0\}$ reflections φ becomes $(1 - 0.075)\pi$ for $(\bar{1}2\bar{1}0)$, $(2\bar{1}\bar{1}0)$ and $(\bar{1}\bar{1}20)$, but $(1 + 0.075)\pi$ for the three opposite faces $(1\bar{2}10)$, $(\bar{2}110)$ and $(11\bar{2}0)$. A hypothetical rotation twin boundary, which gives no displacement of the lattice, will make the normal to $(\bar{1}2\bar{1}0)$ parallel to the normal to $(1\bar{2}10)$ and will thus give a phase change of $2(+0.075\pi) = +0.15\pi$. Continuing in the same direction the next twin boundary will give a phase change of -0.15π. This means that phase changes of $+0.15\pi$ and -0.15π alternately will be produced by the twin boundaries when we regard a $\{11\bar{2}0\}$ reflection. For the $\{11\bar{2}2\}$ reflections the phase changes at the twin boundaries are $+0.11\pi$ and -0.11π. These phase changes are to be added to the phase changes laid down by the displacement vectors of the twin faults which have been determined by the $\{h0\bar{h}l\}$ reflections. For these calculations, the GIER algol program was modified (appendix 2). However, the effects of these phase angles on the M(t) curves are very small and they neither prove nor disprove the hypothesis of twin faults.

The μ_{ij} coefficients have been determined as the values which, within an interval of ± 0.03, give the best fit of the calculated M(t) curves to the experimental curves for the $\{10\bar{1}0\}$ and $\{10\bar{1}1\}$ reflections. The kind of "fit" used here is primarily a question of correspondence between the slope of the curves and the abscissae of the points of maximum curvature. For the $M_s(t)$ curve, however, a straight line through (0,0) can be used as a background line instead of the abscissa axis, because a small shift of the X-ray diffraction peak will change the $M_s(t)$ in this way. In agreement herewith the $M_s(t)$ value for $t = 2.3$ nm has been used as a critical point for the $\{10\bar{1}0\}$ data during the calculations.

Figs. 15–20 show the M(t) curves calculated from the model for six reflections. For $\{12\bar{3}1\}$ the curves have not been calculated as this reflection will be highly influenced by the unknown termination in the direction of the a*-axis of the quartz domains. It should be noticed that the weak reflections $\{11\bar{2}0\}$, $\{20\bar{2}0\}$, and $\{20\bar{2}1\}$ are rather inapt for this detailed analysis. Furthermore, it is necessary to allow some effect of the unknown termination of the quartz domains in the directions of the c- and of the a*-axes.

The agreement between the calculated and the experimental curves is not good although the general slopes of the calculated $|M(t)|$ curves are rather similar to the slopes of the experimental curves in the range from 5 to 15 nm which is the most reliable part. Changes of the displacement vectors have not improved the fit; more often the changes have worsened the fit of the results. Also an attempt to improve the calculated curves by use of other values of w and W gave poorer results. The author therefore concludes that the model and the μ_{ij} values determined agree so well with the experimental results that they can be accepted as largely correct, but it should be stressed that the model used in the calculations does not allow a variation in the values of w and W inside one column, and the triplets may be a statistical average of clusters of twin

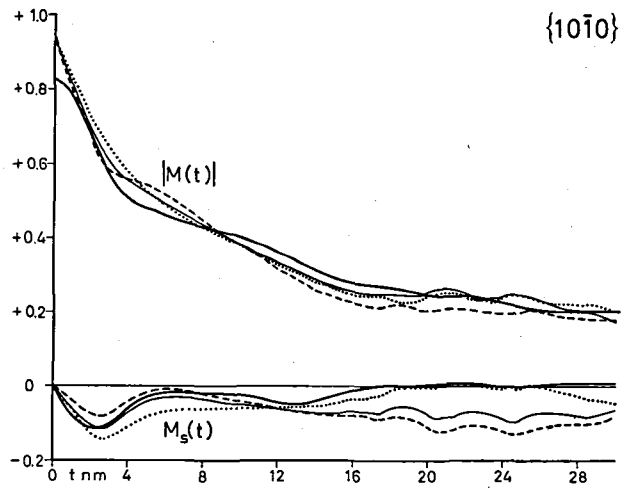

Fig. 26. Experimental M(t) curves (full, heavy lines) and calculated M(t) curves for different values of $\mu_{+22} = \mu_{-22} = \mu_{22}$. $\mu_{+21} = 0.02$, $\mu_{-21} = 0.24$, and $\mu_{+23} = \mu_{-23} = 0.37$ are constant. Dotted lines: $\mu_{22} = 0.365$. Full, thin lines: $\mu_{22} = 0.415$, the best approximation. Dashed lines: $\mu_{22} = 0.465$.

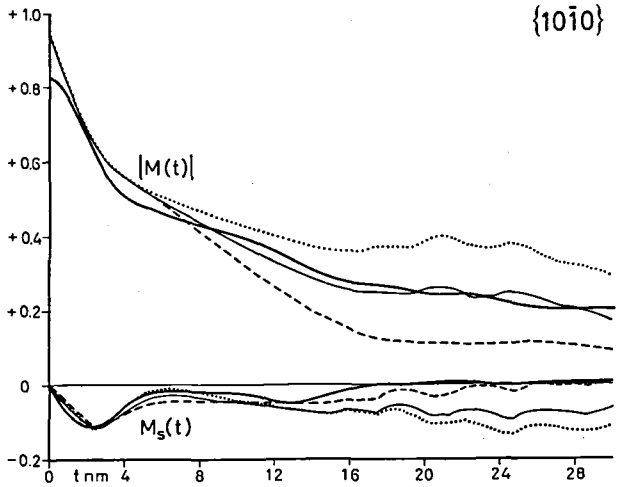

Fig. 27. Experimental M(t) curves (full, heavy lines) and calculated M(t) curves for different values of $\frac{1}{2}(\mu_{+21} + \mu_{-21})$. $(\mu_{-21} - \mu_{+21}) = 0.22$, $(\mu_{22} - \frac{1}{2}(\frac{1}{2}(\mu_{+21} + \mu_{-21}))) = 0.35$, and $\mu_{23} = 0.37$ are constant. Dotted lines: $\frac{1}{2}(\mu_{+21} + \mu_{-21}) = 0.08$. *Full, thin lines:* $\frac{1}{2}(\mu_{+21} + \mu_{-21}) = 0.13$, the best approximation. Dashed lines: $\frac{1}{2}(\mu_{+21} + \mu_{-21}) = 0.18$.

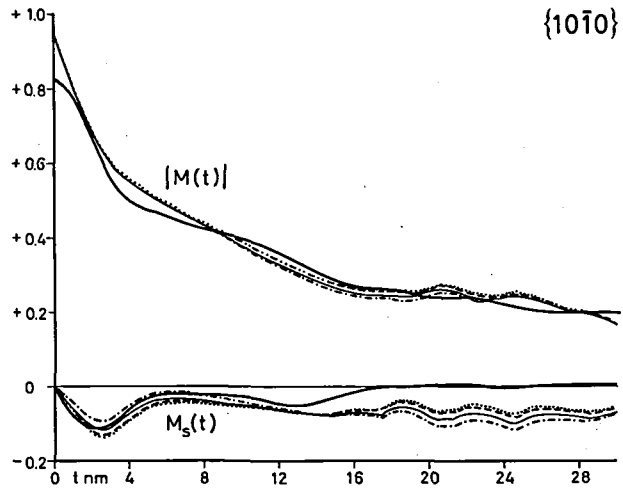

Fig. 28. Experimental M(t) curves (full, heavy lines) and calculated M(t) curves for varying values of $(\mu_{-21} - \mu_{+21})$. $\frac{1}{2}(\mu_{+21} + \mu_{-21}) = 0.13$, $\mu_{22} = 0.415$, and $\mu_{23} = 0.37$ are constant. Dotted lines: $(\mu_{-21} - \mu_{+21}) = 0.000$. Dashed lines: $(\mu_{-21} - \mu_{+21}) = 0.12$. Full, *thin* lines: $(\mu_{-21} - \mu_{+21}) = 0.22$, the best approximation. Dot and dashed lines: $(\mu_{-21} - \mu_{+21}) = 0.32$.

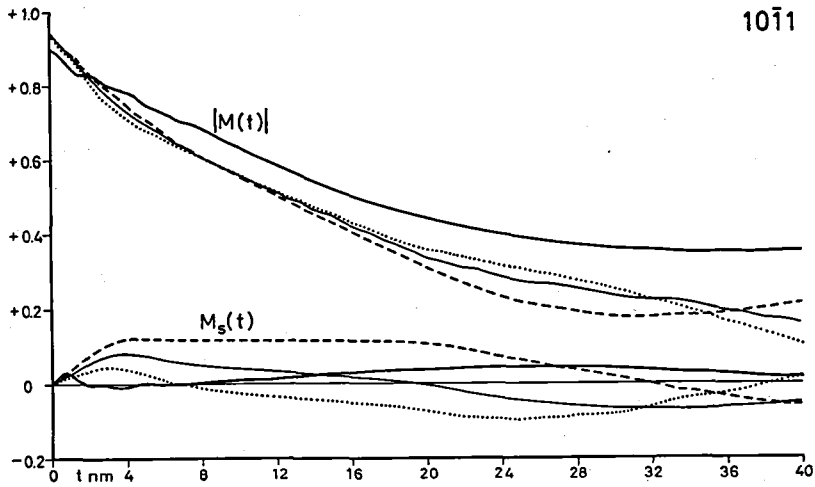

Fig. 29. Experimental M(t) curves (full, heavy lines) and calculated M(t) curves for varying values of $\mu_{+23} = \mu_{-23} = \mu_{23}$. $\mu_{+21} = 0.02$, $\mu_{-21} = 0.24$, and $\mu_{22} = 0.415$ are constant. Dotted lines: $\mu_{23} = 0.32$. Full thin lines: $\mu_{23} = 0.37$, the best approximation. Dashed lines: $\mu_{23} = 0.42$.

faults. It does seem probable that clusters of two or four twin faults exist, as the twin fault pattern of plate 12, 2 implies that the lattice fault, which is seen to end, should consist of an even number of twin faults. The $M_s(t)$ curves for groups of 2 or 4 twin faults, however, are very different from the experimental $M_s(t)$ curve for $\{10\bar{1}0\}$. The number of such groups must therefore be low compared with the number of triplets.

The limits of best fit given above are not true limits of error, but the experimental results are not considered to be sufficiently accurate to allow more detailed calculations. It is not possible to give definite limits of error, but in any case changes of the μ_{ij} values of more than ± 0.05 are not likely, as can be seen from the effects of such changes in figs. 26–29.

The significance of $(\mu_{-21} - \mu_{+21})$ is conclusive in the problem of whether the lattice faults are stacking faults or twin faults. Although the calculations seem to indicate that the difference is significant, the author has attempted to undertake a structural interpretation on the assumption that $\mu_{+21} = \mu_{-21}$, the lattice faults being a kind of stacking faults which contain Si-OH groups (see p. 359).

The influence of thermal treatment on the lattice faults of flint

A number of samples of dark flint from Stevns have been heated or autoclaved in order to see the effects of such treatment on the shape of the X-ray diffraction peaks. For most of this work the author used the approximation formula for average particle size determination of K. DRENCK (1959, p. 81); these results are shown in fig. 30. A few samples were selected for detailed Fourier transformations, the results of which are given in table 5.

Heating to temperatures below ca. 300°C has nearly no effect on the peak shape of the reflections. Prolonged heating to temperatures above ca. 450°C makes the diffraction peaks sharper corresponding to an increase of the average particle size. At the same time the asymmetry of the $\{10\bar{1}0\}$ peak disappears. This means that the lattice faults in the natural flint are annealed at high temperatures.

Autoclaving at low vapour pressures produces the same results as heating in dry air. Autoclaving at high vapour pressures produces much greater effects than heating in air at the same temperature and for the same period. However, a sample of flint was heated to 650°C during the day and allowed to cool during the night, and this was repeated 80 times; this sample gives results which are very similar to those obtained on a sample which had been autoclaved at 510°C and 2200 bars water pressure for 20 days (see table 5). One effect of the high vapour pressure thus seems to be that it increases the mobility of the lattice defects, as also shown by G. DONNAY, J. WYART, and G. SABATIER (1959). Another effect of the high vapour pressure is that the OH groups of the flint do not disappear. The OH content of a flint sample, autoclaved at 2500 bars H_2O at 540°C for 20 days, corresponds to a monolayer with an area of 126 m^2/cm^3 (see p. 301). The area of {0001} is assumed to be 34 m^2/cm^3, and the remaining 92 m^2/cm^3 is probably the area of the prism faces. The area of the prism faces can also be determined by the $\{10\bar{1}0\}$ reflection, giving 67 m^2/cm^3 corresponding to a volume of 88% quartz. The volume of the quartz is 98% –

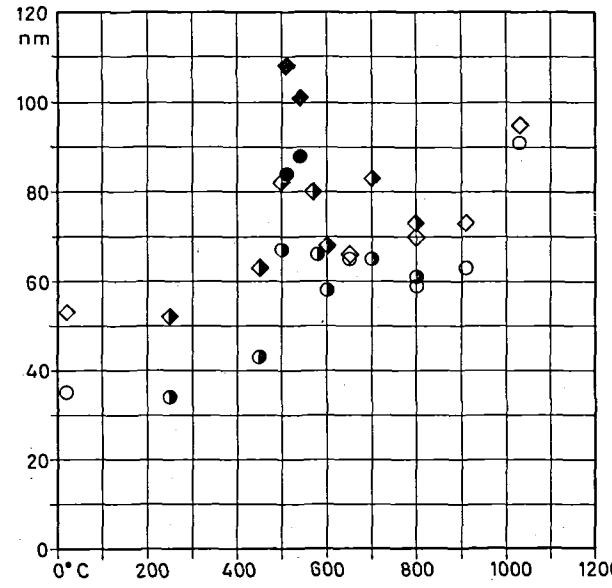

Fig. 30. Average particle sizes of dark flint from Stevns after treatment at various temperatures under the following conditions. Open squares and circles: heating in air. One half black: autoclaving at low vapour pressures (<300 bars H_2O). Black: autoclaving at high vapour pressures (2000–3000 bars H_2O). Circles indicate average particle sizes measured with $\{10\bar{1}0\}$. Squares indicate average particle sizes measured with $\{10\bar{1}1\}$.

as can be derived from the chemical analysis. The corresponding surface area is $67 \cdot 98/88 = 75\ m^2/cm^3$. The geometrical approximation used for the determination of the surface area, p. 333, is rather inaccurate, and, within the limits of error, the 75 m^2/cm^3 and the 92 m^2/cm^3 may be identical. This means that the monolayer of OH groups is likely to be found on the surface of the quartz grains formed by the autoclaving.

The conclusion from these experiments is that the lattice faults of flint can be annealed at temperatures below 650°C, and that the annealing process unifies neighbouring quartz domains in the directions parallel to {0001}. This change shows that the neighbouring quartz domains cannot form reflection twins, as reflection twinning would imply that right-handed quartz should change into left-handed quartz during the treatment. The structural transition from right- to left-handed quartz involves a rather complete destruction and reconstruction of the lattice and is not likely to occur in the dry, solid state below 900°C (G. DONNAY, J. WYART and G. SABATIER, 1959). Consequently, if the lattice faults inside the quartz plates are twin faults, the twinning law must be the Dauphiné law according to which individuals of one kind of quartz are turned 180° about the c-axis.

At temperatures above ca. 500°C the α-quartz of flint will change into β-quartz, and the twin faults will thereby change into a kind of stacking faults.

Even then, the annealing cannot be imagined as a result of conservative motion of dislocations (A. H. COTTRELL, 1964), because the original twin fault zones contain a surplus number of silicon atoms. The catalytic effect of high vapour pressures on the annealing thus seems to be connected with the capability of supercritical water to transport silicon, as shown on p. 313.

Conclusions on the results obtained by X-ray diffraction

The results of the X-ray diffraction work are:

1) The dark flint from Stevns consists of α-quartz.
2) The flint grains are oriented at random.
3) The X-ray diffraction peaks show broadenings, which cannot be explained as being due to small grains, but in the main they can be explained as effects of lattice faults parallel to $(\bar{1}2\bar{1}0)$.
4) The mean size of the displacement vectors at the lattice faults is $[0.13\vec{a}, 0.415\vec{b}, 0.37\vec{c}]$, but two different lattice faults are likely to alternate. The displacement vectors of these two faults are: $\vec{\mu}_{+2} = [0.02\vec{a}, 0.415\vec{b}, 0.37\vec{c}]$ and $\vec{\mu}_{-2} = [0.24\vec{a}, 0.415\vec{b}, 0.37\vec{c}]$.
5) The lattice faults occur as triplets in which the single faults are separated by a mean distance of 2.2 nm, the triplets being separated by a mean distance of ca. 15.7 nm. The period of repeat of the triplets is $2.2 + 2.2 + 15.7 \simeq 20$ nm, in agreement with the value determined by electron microscopy.
6) The mean distance between the lattice faults is $6.7 \simeq 7$ nm. The corresponding mean distance determined from the area occupied by Si-OH groups is 13.4 nm. Within the limits of accuracy, this implies that the number of Si-OH groups present is only one half of the number of groups needed to form a full monolayer on each surface of the faults. It might be supposed that every second lattice fault contained all the Si-OH groups. This supposition, however, does not agree with the fact that the lengths of the two displacement vectors are so close to each other – namely 2.8 and 2.7 Å respectively. The two different lattice faults are therefore likely to contain the same amount of Si-OH groups, each lattice fault containing a number of Si-OH groups corresponding to one full monolayer. The remaining half of the electrostatic charges in the surfaces must be balanced by Si^{4+}.
7) When the difference between the displacement vectors of two lattice faults is significant, then the lattice faults are likely to be twin faults. The thermal treatments show that the twin law is the Dauphiné law and that the annealing of the lattice faults is not a mere removal of OH-groups.

The structures of the Dauphiné twin boundaries

In order to elucidate the problem of stacking faults contra twin faults, the author has tried to draw the detailed structures of such boundaries. The quartz structure has been drawn according to the coordinates given by P.-H. WEI (1935), and one side of the structure has been displaced according to the displacement vectors determined.

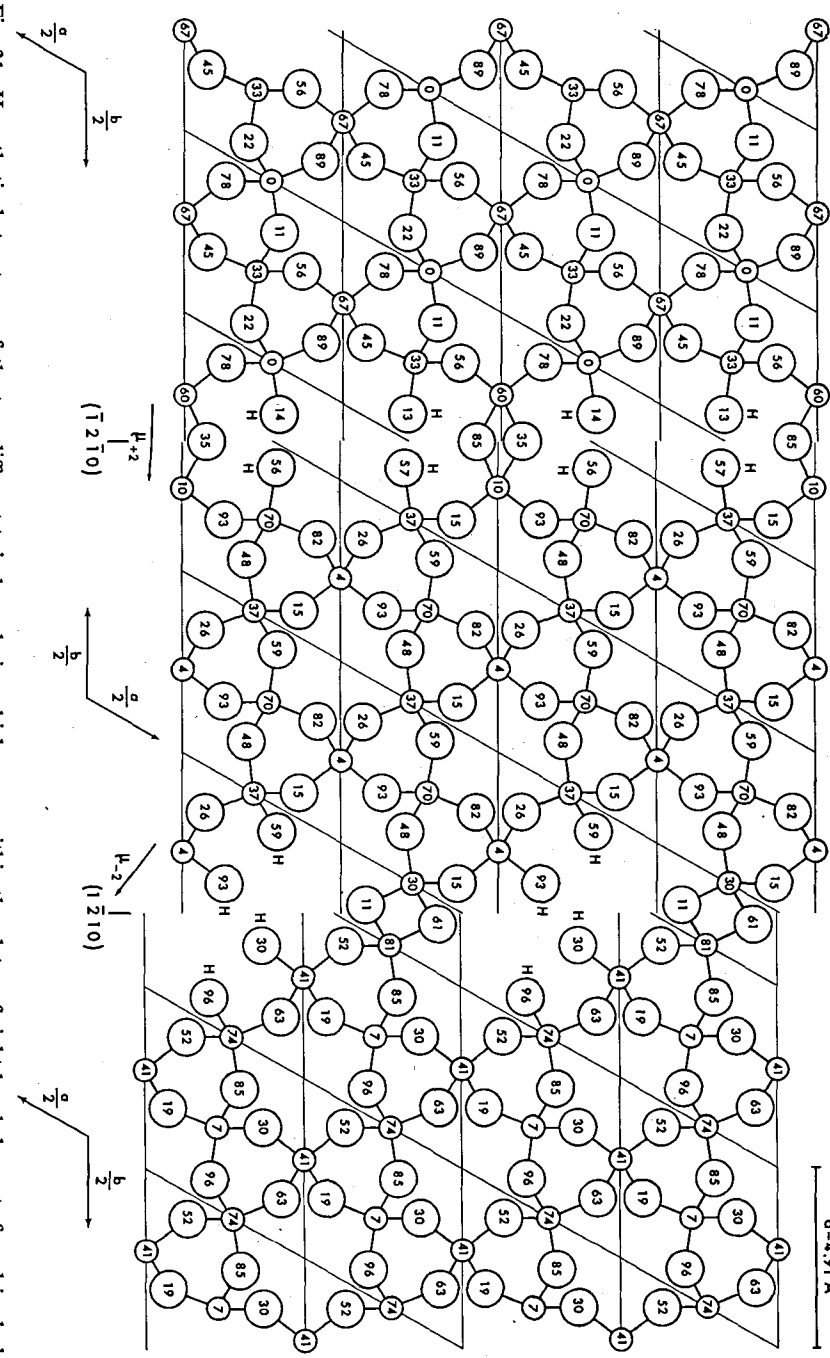

Fig. 31. Hypothetical structures of the two different twin boundaries which occur within the plates of right-handed quartz found in dark flint from Stevns.

The effect of a hypothetical stacking fault with a displacement vector of $\vec{\mu}_2 = 0.13\vec{a} + 0.415\vec{b} + 0.37\vec{c}$ is that no set of 4 oxygen atoms can form a tetrahedron in which a silicon atom can be placed. The smallest of the coordination polyhedra formed by 4 oxygen atoms is roughly a distorted tetrahedron but only three of the Si-O distances can be close to 1.6 Å, the fourth distance being 2.8 Å. Another coordination polyhedron is even more distorted and gives Si-O distances of 1.7, 2.3, 2.3 and 2.9 Å. Actually, as far as can be seen from a drawing of surface structures, both surfaces would probably be covered by complete monolayers of Si-OH groups if the lattice faults were true stacking faults. The hypothesis that the lattice faults in flint should be stacking faults is therefore abandoned.

At first sight, the structures of two different twin faults seem to be difficult to determine as the calculations do not show whether the displacement between two $(\bar{1}2\bar{1}0)$ faces is described by $\vec{\mu}_{+2}$ or by $\vec{\mu}_{-2}$. A few trials, however, showed that the $\vec{\mu}_{+2}$ vector gives a reasonable structure for the twin boundary between two $(\bar{1}2\bar{1}0)$ faces (fig. 31, left half). Si-O-Si bridges readily explain the occurrence of only half a monolayer of OH groups on each surface. It is necessary to shift the atoms of the boundary zone a little in order to make room for them. A positive value of μ_{-23} gives smaller atomic shifts than a negative value and is accepted in the following.

The detailed structure of the twin boundary between two $(1\bar{2}10)$ faces can now be imagined on the basis of the $\vec{\mu}_{-2}$ vector (fig. 31, right half). As expected, this twin boundary is different from the above-mentioned boundary, but it contains the same Si-O-Si bonds, and the atomic shifts are of the same magnitude (≤ 0.8 Å).

It should be noted that the structures of the two interfaces change into their mirror images when the left-handed $P3_121$ quartz is considered instead of the right-handed $P3_221$ quartz. The four displacement vectors thus become:

$$\begin{aligned}
\vec{\mu}_{+2,\,\text{right}} &= +0.02\vec{a} + 0.415\vec{b} + 0.37\vec{c},\\
\vec{\mu}_{-2,\,\text{right}} &= +0.24\vec{a} + 0.415\vec{b} + 0.37\vec{c},\\
\vec{\mu}_{+2,\,\text{left}} &= -0.24\vec{a} + 0.175\vec{b} - 0.37\vec{c},\\
\vec{\mu}_{-2,\,\text{left}} &= -0.02\vec{a} + 0.395\vec{b} - 0.37\vec{c}.
\end{aligned}$$

Twin faults have thus turned out to be more likely than stacking faults both in the calculations of the M(t)-curves and in the attempt to give a structural interpretation of the lattice faults. The theory of multiple twinning according to the Dauphiné law will therefore be accepted here. This polysynthetic twinning gives the quartz plates a bulk pseudosymmetry corresponding to the crystal class 622. It has been proposed earlier, p. 307, that neighbouring quartz plates are probably twinned according to the Brazil law. This means that inside the pile of quartz plates which make up the flint grains, alternate plates should consist of left-handed or right-handed quartz. In this way the flint grains obtain a bulk pseudosymmetry corresponding to the class 6/mmm.

VI. Conclusions

Conclusions about the structure of the dark flint from Stevns can be drawn directly from only rather few of the observations given in this paper. Most of the structural details have been deduced by coordination of results obtained from independent methods of investigation; a complete picture of the structure of the dark flint can hardly be obtained directly from the experimental results. For this reason, the most important approach used in this work was a systematic trial of structural models which could be experimentally controlled. The conclusion of this work is therefore the proposal of the structural model which best accounts for the observations; this is not to say that it is definitely the correct model.

The dark flint from Stevns consists of anhedral flint grains, 2–30 μ in size with a mean of 7.5 μ. Optically, the grains seem to consist of quartz, and they have a random orientation. The intergranular fissures between the flint grains have a mean width of 4½ nm, determined on the assumption that the fissures are completely filled with water at a relative humidity of 100%.

The flint grain is built up of a pile of plates of quartz. The plates are parallel to (0001) and have a mean thickness of 59 nm. The {0001} faces are covered by monolayers of Si-OH groups, and adjacent quartz plates are joined by one single monolayer of water molecules. Every second of the Si-OH groups in the structure between the {0001} faces has no hydrogen bond, whereas the remaining Si-OH groups have hydrogen bonds to the water molecules. The presence of water molecules makes it likely that neighbouring quartz plates form twins according to the Brazil law. This means that alternate quartz plates are likely to consist of right-handed or left-handed quartz.

The quartz plates of the flint grains consist of subgrains separated by low angle boundaries. The subgrains have a size of 0.2–3 μ and are finely divided by twin faults. The twin faults are parallel to $(\bar{1}2\bar{1}0)$ and occur in threes with a mean spacing of 2.2 nm. These triplets are separated by perfect quartz over a mean distance of ca. 16 nm. The twinning corresponds to the Dauphiné law. In right-handed quartz two $(\bar{1}2\bar{1}0)$ faces are displaced $+0.02\vec{a} + 0.415\vec{b} + 0.37\vec{c}$ from each other, and two $(1\bar{2}10)$ faces are displaced $+0.24\vec{a} + 0.415\vec{b} + 37\vec{c}$ from each other. In left-handed quartz, the two displacement vectors are $-0.24\vec{a} + 0.175\vec{b} - 0.37\vec{c}$, and $-0.02\vec{a} + 0.395\vec{b} - 0.37\vec{c}$. In the twin fault zones ⅔ of the oxygen atoms form Si-OH groups and ⅓ of the oxygen atoms form Si-O-Si bonds from one side of the fault zone to the other. The bulk structure of each quartz plate has hexagonal pseudosymmetry corresponding to the class 622. This symmetry is identical to that of β-quartz – where this symmetry is also due to twinning – and it explains why the flint gives nearly no α — β inversion heat in the differential thermal analysis. The Brazil law twinning of the quartz plates gives the flint grains a bulk pseudosymmetry corresponding to the class 6/mmm.

VII. A note on the genesis of dark flint

In the introduction to this paper it was stated that lack of knowledge hinders fruitful discussion of the genesis of dark flint. The structure proposed here, however, contains so many curious details that a tentative suggestion about the genesis is felt to be necessary in order to see if the results are plausible from a geological point of view.

The dark flint from Stevns has probably been formed by some kind of recrystallization of the "subsidiary cryptocrystalline silica" found in many Danish flint types (A. TOVBORG JENSEN, C. J. WØHLK, K. DRENCK and E. KROGH ANDERSEN, 1957). This substance is probably a disordered intergrowth of cristobalite and tridymite (M. DANØ, personal communication) and gives a {111} reflection with a d-value varying from 4.07 to 4.13 Å. The lowest d-value is found in pure "subsidiary cryptocrystalline silica". The highest d-value is found in samples where the content of "subsidiary cryptocrystalline silica" is low, a large amount of fine-grained quartz being present. The diffraction peak of the "subsidiary cryptocrystalline silica" becomes more broad the higher the d-value, i.e. the higher the quartz content. This fine-grained quartz is likely to be similar to the dark flint from Stevns. The bulk symmetry of a disordered intergrowth of cristobalite and tridymite probably corresponds to the class 6/mmm – the same class as found for the pseudosymmetry of the flint grains.

The author puts forward the hypothesis that the quartz of the flint grains has epitaxially replaced the original "subsidiary cryptocrystalline silica" of the nodules.

If we use a cubic indexing of the "subsidiary cryptocrystalline silica", then a {111} face – referred to hereafter as (111) – is likely to be parallel to the (0001) of quartz, and the low symmetry then implied that the α-quartz crystallized with four different orientations as growth twins corresponding to the observed Brazil and Dauphiné laws.

An important point is the lattice spacing of "subsidiary cryptocrystalline silica" just before the formation of quartz. On (111) the other {111} planes will form a hexagonal line pattern with a spacing of $4.07/\sin((111) \wedge (\bar{1}11)) = 4.31$ Å. This means that the line spacing on (111) is only ca. 1.4% larger than that of quartz. This difference in spacing is so small that epitaxial overgrowth is possible according to J. H. VAN DER MERWE (1964). However, instead of interfacial dislocations the twin faults of flint may accommodate a large interface misfit – 0.35 d – and the period of fit and misfit between the two crystal lattices may therefore be given by $0.35/0.014 \simeq 25$ spacings of $\{10\bar{1}0\}$ of quartz. This means that 25 lattice planes $\{10\bar{1}0\}$ of quartz plus one twin fault will correspond to 25 lattice planes of "subsidiary cryptocrystalline silica" on (111) at the beginning of the crystallization of quartz. During the crystallization of quartz the spacing of the {111} of the "subsidiary cryptocrystalline silica" increases to 4.13 Å corresponding to a line spacing of 4.38 Å in the (111) plane. This spacing differs from that of $\{10\bar{1}0\}$ of quartz by 3% and corresponds to an average distance of only 11 unit cells between the twin faults in flint. In the three $\{10\bar{1}0\}$ directions the twin faults of the dark flint occur with mean dis-

tances of 18, 18 and ca. 200 unit cells. This gives an average distance of ca. 26 cells between two twin faults, i.e. virtually the same distance as predicted from the lattice spacing of the "subsidiary cryptocrystalline silica" at the beginning of the crystallization of quartz. An average distance as low as 11 unit cells between the twin faults in flint is only found in the narrow twin lamellae where the average distance is about 9 unit cells. These tentative correlations between lattice misfit and twin fault density therefore suggest that the clustering of the twin faults into triplets is produced during the development of the matrix upon which the quartz has grown. On the other hand, the development of the matrix may have been deeply influenced by the growing quartz.

The quartz plates in the flint grains have some resemblance to the piles of thin plates or rods known from the tactoids often developed in aged gels (J. F. KERRIDGE, 1964). The "subsidiary cryptocrystalline silica" has probably been a silica gel before its consolidation, and the quartz plates may be a palimpsest structure from a very early stage of the flint formation.

As very little is known about "subsidiary cryptocrystalline silica", the hypothesis outlined above, however promising it may seem, clearly must remain a hypothesis, for a number of important details cannot at present be usefully discussed, even qualitatively. A proper discussion of the genesis of the dark flint from Stevns on this basis must wait until the detailed structures of "subsidiary cryptocrystalline silica" have been elucidated.

Acknowledgments

I am deeply indebted to prof. dr. phil. ARNE NOE-NYGAARD for the tolerance and trust which allowed and encouraged six years of work in a seemingly hopeless task. I also want to thank prof. dr. phil. AKSEL TOVBORG JENSEN and cand. polyt. G. M. IDORN for their friendly interest in this work from the very beginning and for economic support. Thanks are also due to prof. dr. phil. JØRGEN KOCH who has kindly placed laboratory space at my disposal during a period of reconstruction in the Mineralogical Museum.

This work would not have been possible if a number of scientists had not unselfishly placed their time, knowledge and instruments at my disposal. I therefore owe my best thanks to cand. polyt. H. L. ANDSAGER, cand. polyt. ANDERS BJERRE, cand. real. HALDIS BOLLINGBERG, cand. polyt. HANS BOHLBRO, cand. polyt. et lic. techn. DANIEL HØJGAARD CHRISTENSEN, Dr. TORE DAGERHAMN, cand. polyt. MARIANNE DANØ, mag. scient. PREBEN HANSEN, R.W. HORNE, Ph. D., cand. polyt. EBBE LANGER, cand. polyt. MARIE LOUISE MOURITZEN, mag. scient. BJARNE SVEJGAARD, and cand. polyt. et lic. techn. IB SØRENSEN.

I wish to thank C. PULVERTAFT, B. A., G. HENDERSON, B. Sc., cand. polyt. et mag. scient. OLE LARSEN, Dr. GWYNETH NORD and MARIANE MICHEELSEN for correction and improvement of my English manuscript. Furthermore I should like to thank all those who have assisted me in the practical work, E. BØGGILD, M. GRUMLØSE, V. HAARUP, H. HELBÆK, H. NEBEL, G. KRAUL JENSEN, RAGNA LARSEN and AGNETE SØRENSEN.

DANSK RESUMÉ

Den mørke flint fra skrivekridtet i Stevns klint er blevet undersøgt ved en række forskellige metoder, hvis resultater gennemgående har måttet kombineres for at kunne tolkes. Blandt de vigtigste undersøgelser og deres resultater skal nævnes følgende: Størrelsen af de optisk kohærente områder såvel som deres lysbrydning, dobbeltbrydning og orientering er bestemt ved lysoptisk mikroskopi. Ved isoterm dehydrering, termogravimetrisk analyse og infrarød-absorptionsspektroskopi har det været muligt at bestemme mængden af vandmoleculer og Si-OH-grupper, hvorefter størrelsen af de indre overflader er beregnet. En kemisk analyse viser, at flinten næsten udelukkende består af SiO_2 og H_2O. Flintens gitterfejl må derfor være knyttet til OH-grupperne, således at gitterfejlenes antal og tæthed kan bestemmes og korreleres med flintens indre overflader. Elektronmikroskopi har vist, at gitterfejlene er parallelle med $(\bar{1}2\bar{1}0)$ og (0001). På grundlag af resultaterne fra de nævnte undersøgelser har det været muligt at tolke røntgen-diffraktionsliniernes forbredninger, hvad der førte frem til en mere detaljeret beskrivelse af gitterfejlene og deres fordeling i krystallerne.

Det har ikke været muligt at udlede flintens struktur direkte fra måleresultaterne, men efter en del forsøg er det lykkedes at finde frem til en strukturmodel, som ser ud til at stemme overens med samtlige observationer:

Den mørke flint fra Stevns består af anhedrale »flintkorn«, der i størrelse varierer fra 2 til 30 μ og er tilfældigt orienteret. Flintkornene har samme lysoptiske egenskaber som kvarts. De består af plader af kvarts, der er parallelle med (0001) og i middel 59 nm tykke. {0001} fladerne er dækket af monolag af Si-OH-grupper, og mellem to af disse monolag findes et enkelt monolag af vandmoleculer. Tilstedeværelsen af vandmoleculer sandsynliggør, at kvartspladerne danner polysyntetiske tvillinger efter Brazil-loven; det vil sige, at pladerne skiftevis skulle bestå af højre- og af venstre-kvarts. Kvartspladerne kan indeholde lav-vinkel korngrænser, der deler flintkornene op i underkorn af størrelsen 0.2–3 μ, men fremfor alt er kvartspladerne gennemsat af et stort antal gitterfejl, der er parallelle med $(\bar{1}2\bar{1}0)$. Hver gitterfejl består af 3 tvillinggrænser, der kun er adskilt af nogle få enhedsceller af kvarts (2.2 nm i middel). Mellem disse grupper af tvillinggrænser findes bredere lameller af kvarts (i middel ca. 16 nm brede). Tvillingdannelsen følger Dauphinéloven. Tvillinggrænserne er ikke blot steder, hvor en symmetrioperation finder sted, men de er også ledsaget af parallelforskydninger af gitteret. For højre-kvarts gælder således, at forskydningsvektoren mellem to $(\bar{1}2\bar{1}0)$ flader, der på grund af tvillingoperationen vender mod hinanden, er $0.02\vec{a} + 0.415\vec{b} + 0.37\vec{c}$, medens forskydningsvektoren mellem de tilsvarende to $(1\bar{2}10)$ flader er $0.24\vec{a} + 0.415\vec{b} + 0.37\vec{c}$. På grund af tvillinggrænserne vil en del oxygen-atomer ikke være knyttet til siliciumatomer på samme måde som i kvartsen. To trediedele af disse oxygen-atomer indgår i Si-OH-grupper, medens den sidste trediedel indgår i Si-O-Si bindinger tværs over tvillinggrænserne.

Den mørke flint fra Stevns er opbygget af den trigonale α-kvarts, men den polysyntetiske tvillingdannelse efter Dauphiné-loven bevirker, at hver enkelt plade får en pseudosymmetri svarende til krystalklassen 622. Hvis kvartspladerne, som ovenfor nævnt, danner tvillinger efter Brazil-loven, får flintkornene en pseudosymmetri svarende til klassen 6/mmm. På grundlag af disse betragtninger over pseudosymmetri fremsættes den hypotese, at flinten er dannet ved epitaksisk replacering af en ældre, »opalagtig« substans, den såkaldte »subsidiære kryptokrystallinske kiselsyre«, som forekommer almindeligt i en del danske flinttyper.

APPENDIX 1

```
Program in GIER algol III for calculating |M(t)|and Ms(t) for flint
begin
integer p;
begin
integer fl, tp,tq,m,SCAFA;
real c,BAG,d,h,n1,n2;

procedure TRYK(P);
array P;
begin
integer m,k;
for m:= 0 step 1 until 8 do begin
for k:= 0 step 1 until 9 do
output(¢ndddd¢,P[m×10+k]); outcr;
for k:= 0 step 1 until 9 do
output(¢ndddd¢,P[-(m×10+k)]); outcr; outcrend;
output(¢ndddd¢,P[90],outcr,P[-90],outcr)
end TRYK;

procedure PWSPC(f,M,N,P,a,b);
value M,N,P; array f,a,b; integer M,N,P;
begin integer m,n,p;
real c,k,u1,u2,v1,v2,w,theta;

real procedure ARC(x,y);
value x,y; real x,y;
begin
ARC:= if x=0∧y=0 then 0 else
      if abs(x)≥abs(y)
      then arctan(y/x)+ (if x<0 then 3.14159265 else
                                if y≥0 then 0 else 6.28318531)
      else arctan(-x/y)+(if y≥0 then 1.57079633 else 4.71238898)
end;

k:= 2/M; theta:= 3.14159265×k;
for p:= 0 step 1 until P do
begin
v2:= v1:= u2:= u1:= 0; c:= cos(p×theta)↑2;
for n:= N step -1 until 1 do begin
w:= (f[-n]+f[n])×0.5+c×u1-u2;
u2:= u1; u1:= w;
w:= (f[n]-f[-n])×0.5+c×v1-v2;
v2:= v1; v1:= w end;
w:= (f[0]+0.5×c×u1-u2)×k;
v1:= sin(p×theta)×v1×k;
a[p]:= sqrt(w↑2+v1↑2);
b[p]:= ARC(w,v1)
end
end PWSPC;
outcopy(¢<<[]¢);
Input(p,c,d,SCAFA); h:= c×d;

begin array Q[-90:90], rq,phiq[-2:p+2];
outtext(¢<<SCAFA=¢);output(¢-ndddd¢,SCAFA);outcr;outtext(¢<<

Kvarts
¢); Input(Q);
for m:=-90 step 1 until 90 do
Q[m]:=Q[m]+ Q[m]↑2×SCAFA×10.5₁₀-6;
BAG:=Q[-90];
for m:=-90 step 1 until 90 do
Q[m]:=Q[m]-BAG+(BAG-Q[90])×(m+90)/180;TRYK(Q);outcr;

PWSPC(Q,360,90,p,rq,phiq);
tq:= drum place; to drum(rq); to drum(phiq)
end;
tp:= drum place;
flint:
begin array P[-90:90],rp,phip[-2:p+2];
outtext(¢<<
Flint

¢); fl:=1n one; if fl=0 then goto ud;
outtext(¢<<fl:=¢);output(¢nddd¢,fl);outcr;
Input(P);
for m:=-90 step 1 until 90 do
P[m]:= P[m]+P[m]↑2×SCAFA×10.5₁₀-6;
BAG:=P[-90];
for m:=-90 step 1 until 90 do
P[m]:=P[m]-BAG+(BAG-P[90])×(m+90)/180;TRYK(P);outcr;
drum place:= tp;
PWSPC(P,360,90,p,rp,phip);
to drum(rp); to drum(phip)
end;
begin
array F,S,rq,phiq[-2:p+2]; real dif,f;
drum place:= tq;
from drum(rq); from drum(phiq); from drum(F); from drum(S);outcr;
outtext(¢<<c = ¢); output(¢-n.ddddd¢,c,outtext(¢<<  d = ¢), d);
outcr;
outtext(¢<<
mmmmmFmmmmSmmmmPHImmmmnmmmmmt
¢);
for m:= 0 step 1 until p do begin
f:= F[m]/rq[m]×1000; dif:= (S[m]-phiq[m])×57.29578;
dif:= dif-entier(dif/360)×360;
if dif>180 then dif:= dif -360;
output(¢-ndddd¢,m,f,f×sin(dif/57.29578));
output(¢-nddd.d¢,dif,m×c,m×h); outcrend
end;
goto flint

;ud:end end  end;
```

APPENDIX 2

```
program in GIER algol III for calculating IM(t)Iand Ms(t) for
a triplet of twin or stacking faults

2 different stacking faults alternate

begin
integer q,n,Q,N;
real X,Y,Z,x,y,z,d,t,A,B,D,E,U;
integer array h[1:Q], k[1:Q],l[1:Q],w[1:Q],W[1:Q],p[1:Q];
real array  a[1:6,1:Q],  b[1:6,1:Q],C[0:N],S[0:N],F[0:N];

Input(Q,N,X,Y,Z,x,y,z,U);

for q:=1 step 1 until Q do begin

Input (h[q], k[q],l[q],  w[q], W[q], p[q]);
A:=6.28319×(h[q]×(X+x) +k[q]×(Y+y) + l[q]×(Z+z));
B:=6.28319×(h[q]×(X-x) + k[q]×(Y-y) + l[q]×(Z-z));
D:=6.28319×(h[q]×(X+x) + k[q]×(Y+y) - l[q]×(Z+z));
E:=6.28139×(h[q]×(X-x) + k[q]×(Y-y) - l[q]×(Z-z));
A:=A+U×(2×k[q]-3); B:=B-U×(2×k[q]-3)  ; D:=D+U×(k[q]×2-3); E:=E-U×(2×k[q]-3);
a[1,q]:=(cos(A)+cos(D) +cos(B) +cos(E))/4;
a[2,q]:=(cos(A+B) +cos(D+E))/2;
a[3,q]:=(cos(2×A+B) + cos(A+2×B) + cos(2×D+E) + cos(2×E+D))/4;
a[4,q]:=(cos(2×(A+B)) + cos(2×(D+E)))/2;
a[5,q]:=(cos(3×A+2×B)  + cos(2×A+3×B) + cos(3×D+2×E)+ cos(2×D+3×E))/4;
a[6,q]:=(cos(3×(A+B)) + cos(3×(D+E)))/2;

b[1,q]:=(sin(A)+sin(B)+sin(D)+sin(E))/4;
b[2,q]:= (sin(A+B) + sin(D+E))/2;
b[3,q]:=(sin(2×A+B) + sin(A+2×B) + sin(2×D+E) + sin(D+2×E))/4;
b[4,q]:=(sin(2×(A+B)) + sin(2×(D+E)))/2;
b[5,q]:=(sin(3×A+2×B) + sin(2×A+3×B) + sin(3×D+2×E) + sin(2×D+3×E))/4;
b[6,q]:=(sin(3×(A+B)) + sin(3×(D+E)))/2;

end;

d:=(4×(h[1]↑2 +h[1]×k[1] + k[1]↑2)/(3×0.4912↑2) + l[1]↑2/0.5400↑2)↑(-1/2);

outtext(‡< model af triplet af stablingsfejl i flint›); outcr;outcr;
outtext(‡<< 2 different stacking faults alternate ›);outcr;
outtext (‡<<X,Y,Z =›); output(‡-n.ddd›,X,Y,Z);outcr;
outtext(‡<<x,y,z,U =›); output(‡-n.ddd›,x,y,z,U);outcr;
outtext(‡<␣␣␣␣␣␣h␣␣␣␣␣k␣␣␣␣␣l␣␣␣␣␣w␣␣␣␣␣W␣␣␣␣␣p›);outcr;
for q:=1 step 1 until Q dobegin
output(‡-ndddd›,q,h[q],k[q], l[q], w[q], W[q], p[q]);outcr,
end;

for n:=0 step 1 until N do
C[n]:=S[n]:=0;
outtext(‡<␣␣␣␣n␣␣␣␣␣␣␣t␣␣␣␣C[n]␣␣␣S[n]␣␣␣F[n]›);outcr;

for q:=1 step 1 until Q do begin


for n:=0 step 1 until w[q] do begin
if n>N then goto ud;
C[n]:=C[n]+94×(p[q]-n)/(p[q]×(W[q] +2×w[q])×Q)×((W[q]+2×w[q] -3×n +3×n↑a[1,q]));
S[n]:=S[n]+94×(p[q]-n)/(Q×p[q]×(W[q]+2×w[q]))×(3×n×b[1,q]);

end;

for n:=w[q]+1 step 1 until 2×w[q] do begin
if n>N then goto ud;
C[n]:=C[n]+94×(p[q]-n)/(Q×p[q]×(W[q]+2×w[q]))×(W[q]-n+(4×w[q]-n)×a[1,q]
          +2×(n-w[q])×a[2,q]);
S[n]:=S[n]+94×(p[q]-n)/(Q×p[q]×(W[q]+2×w[q]))×((4×w[q]-n)×b[1,q]+2×(n-w[q])×b[2,q]);
end;
for n:=2×w[q]+1 step 1 until W[q] do begin
if n>N then goto ud;
C[n]:=C[n]+94×(p[q]-n)/(Q×p[q]×(W[q]+2×w[q]))×(W[q]-n+2×w[q]×(a[1,q]+a[2,q])
          +(n-2×w[q])×a[3,q]);
S[n]:=S[n]+94×(p[q]-n)/(Q×p[q]×(W[q]+2×w[q]))×(2×w[q]×(b[1,q]+b[2,q])+(n-2
          ×w[q])×b[3,q]);
end;
for n:=W[q]+1 step 1 until W[q]+w[q] do begin
if n>N then goto ud;
C[n]:=C[n]+94×(p[q]-n)/(Q×p[q]×(W[q]+2×w[q]))×(2×(W[q]+w[q]-n)×a[1,q]+(2×w[q]+n-W[q])×
          a[2,q]+(n-2×w[q])×a[3,q]);
S[n]:=S[n]+94×(p[q]-n)/(Q×p[q]×(W[q]+2×w[q]))×(2×(W[q]+w[q]-n)×b[1,q]+(2×w[q]+n-W[q])×
          b[2,q]+(n-2×w[q])×b[3,q]);
```

APPENDIX 2, continued

```
end;
for n:=W[q]+w[q]+1 step 1 until W[q]+2×w[q] do begin
  if n>N then goto ud;
C[n]:=C[n]+94×(p[q]-n)/(Q×p[q]×(W[q]+2×w[q]))×(3×(W[q]+2×w[q]-n)×a[2,q]
        +(3×n-4×w[q]-2×W[q])×a[3,q]);
S[n]:=S[n]+94×(p[q]-n)/(Q×p[q]×(W[q]+2×w[q]))×(3×(W[q]+2×w[q]-n)×b[2,q]
        +(3×n-4×w[q]-2×W[q])×b[3,q]);end;
for n:=W[q]+2×w[q]+1 step 1 until W[q]+3×w[q] do begin
if n>N then goto ud;
C[n]:=C[n]+94×(p[q]-n)/(Q×p[q]×(W[q]+2×w[q]))×((4×W[q]+8×w[q]-3×n)×a[3,q]
        +3×(n-W[q]-2×w[q])×a[4,q]);
S[n]:=S[n]+94×(p[q]-n)/(Q×p[q]×(W[q]+2×w[q]))×((4×W[q]+8×w[q]-3×n)×b[3,q]
              +3×(n-W[q]-2×w[q])×b[4,q]);

end;
for n:=W[q]+3×w[q]+1 step 1 until W[q]+4×w[q] do begin
if n>N then goto ud;
C[n]:=C[n]+94×(p[q]-n)/(Q×p[q]×(W[q]+2×w[q]))×((2×W[q]+2×w[q]-n)×a[3,q]
        +(W[q]+6×w[q]-n)×a[4,q] + 2×(n-W[q]-3×w[q])×a[5,q]);
S[n]:=S[n]+94×(p[q]-n)/(Q×p[q]×(W[q]+2×w[q]))×((2×W[q]+2×w[q]-n)×b[3,q]
        +(W[q]+6×w[q]-n)×b[4,q] + 2×(n-W[q]-3×w[q])×b[5,q]);
end;

for n:=W[q]+4×w[q]+1 step 1 until 2×W[q]+2×w[q] do begin
  if n>N then goto ud;
C[n]:=C[n]+94×(p[q]-n)/(Q×p[q]×(W[q]+2×w[q]))×((2×W[q]+2×w[q]-n)×a[3,q]
        + 2×w[q]×(a[4,q]+a[5,q] )+(n-W[q]-4×w[q])×a[6,q]);
S[n]:=S[n]+94×(p[q]-n)/(Q×p[q]×(W[q]+2×w[q]))×((2×W[q]+2×w[q]-n)×b[3,q]
        + 2×w[q]×(b[4,q]+b[5,q])+ (n- W[q]-4×w[q])×b[6,q]);
end;


for n:=2×W[q]+2×w[q]+1 step 1 until 2×W[q]+3×w[q] do begin
if n>N then goto ud;
C[n]:=C[n]+94×(p[q]-n)/(Q×p[q]×(W[q]+2×w[q]))×((4×W[q]+6×w[q]-2×n)×a[4,q]
        +(n-2×W[q])×a[5,q]+ (n-W[q]-4×w[q])×a[6,q]);
S[n]:=S[n]+94×(p[q]-n)/(Q×p[q]×(W[q]+2×w[q]))×((4×W[q]+6×w[q]-2×n)×b[4,q]
        +(n-2×W[q])×b[5,q] + (n-W[q]-4×w[q])×b[6,q]);
end;

for n:=2×W[q]+3×w[q]+1 step 1 until 2×W[q]+4×w[q] do begin
if n>N then goto ud;


C[n]:=C[n]+94×(p[q]-n)/(Q×p[q]×(W[q]+2×w[q]))×((6×W[q]+12×w[q]-3×n)×a[5,q]
              +(-5×W[q]-10×w[q]+3×n)×a[6,q]);
S[n]:=S[n]+94×(p[q]-n)/(Q×p[q]×(W[q]+2×w[q]))×((6×W[q]+12×w[q]-3×n)×b[5,q]
              +(-5×W[q]-10×w[q]+3×n)×b[6,q]);
end;     ud:
end;

for n:=0 step 1 until N do begin

F[n]:=(C[n]↑2 + S[n]↑2)↑(1/2);
output(¢-nddd.d¢, n,n×d, C[n],-S[n],F[n]);outcr;

end;
outcr;outcr;

end;
```

REFERENCES

ARNOLD, H. (1962) Die Struktur des Hochquarzes. Z. Krist., 117, 467–469.

BAYLISS, P. (1964) Effect of particle size on differential thermal analysis. Nature, London, 201, 1019.

BENESI, H. A. and A. C. JONES (1959) An infrared study of the water-silica gel system. J. Phys. Chem., 63,1, 179–182.

BRADLEY, D. E. (1954) Evaporated carbon films for use in electron microscopy. Brit. J. Appl. Phys., 5, 65–66.

BRUNAUER, S. (1943) The adsorption of gases and vapors. 1, Physical adsorption. Princeton.

— , P. H. EMMET and E. TELLER (1938) Adsorption of gases in multimolecular layers. J. Amer. Chem. Soc., 60, 309–319.

BRUNNER, G. O., H. WONDRATSCHEK und F. LAVES (1961) Ultrarotuntersuchungen über den Einbau von H in natürlichem Quarz. Z. Elektrochemie, 65, 735–750.

BUERGER, M. J. (1960) Twinning, with special regard to coherence. Instituto "Lucas Mallada", Cursillos y Conferencias, VII, 5–7.

COTTRELL, A. H. (1964) Theory of crystal dislocations. Blackie and Son, London.

DANA, E. S./W. E. FORD (1932) A textbook of mineralogy. J. Wiley and Sons.

DONNAY, G., J. WYART and G. SABATIER (1959) Structural mechanism of thermal and compositional transformations in silicates. Z. Krist., 112, 161–168.

DRENCK, K. (1959) X-ray particle size determination and its application to flint. X-ray and Crystal Structure Laboratory, The Pennsylvania State University, U.S.A.

EWALD, P. P. (1921) Das "reziproke Gitter" in der Strukturtheorie. Z. Krist., 56, 129–156.

FOLK, R. L. and C. E. WEAVER (1950) Surface features of chert as studied by the electron microscope. Abstr. 31st. Ann. Meeting, Min. Soc. Amer., p. 10.

— and C. E. WEAVER (1952) A study of the texture and composition of chert. Amer. J. Sci., 250, 498–510.

GILL, A. C. (1894) Beiträge zur Kenntniss des Quarzes. P. Groth, Z. Kryst. Min., XXII, 97–128, 2 pl.

GREENBERG, S. A. (1956) The chemisorption of calcium hydroxide by silica. J. Phys. Chem., 60, 325–330.

GRY, H. og B. SØNDERGAARD (1958) Flintforekomster i Danmark. The occurring of flint in Denmark. Com. Alkali Reactions in Concrete, Copenhagen, Progress Rep. D 2, 63 pp.

HACKERMAN, N. and A. C. HALL (1958) The adsorption of water vapor on quartz and calcite. J. Phys. Chem., 62, 1212–1214.

Handbook of Physics and Chemistry (1949) Chemical Rubber Publishing Co., Cleveland, Ohio.

HILLEBRAND, W. F. and G. E. F. LUNDELL (1944) Applied inorganic analysis. J. Wiley and Sons, New York.

JENSEN, A. TOVBORG, C. J. WØHLK, K. DRENCK, and E. KROGH ANDERSEN (1957) A classification of Danish flints etc. based on X-ray diffractometry. Com. Alkali Reactions in Concrete, Copenhagen, Progress Rep. D 1, 37 pp.

JENSEN, E. and H. MØLLER HANSEN (1961) An elutriator for particle-size fractionation in the sub-sieve range. Soil Sci., 92, 94–99.

JUDD, J. W. (1887) On the unmaking of flints. Proc. Geol. Assoc., London, 10, 217–226.

KERRIDGE, J. F. (1964) On the investigation of tactoids by means of transmission electron microscopy. Proc. 3rd. European Regional Conf. Electron Microscopy, Prague, A, 355–356.

MAMPEL, K. L. (1940) Zeitumsatzformeln für heterogene Reaktionen an Phasengrenzen fester Körper. 2. Die Zeitumsatzformeln für ein Pulver aus kugelförmigen Teilchen. Z. Phys. Chem., A, 187, 235–249.

MARTINEZ, E. (1961) The effect of particle size on the thermal properties of serpentine minerals. Amer. Min., 46, 901–912.

MCDONALD, R. S. (1958) Surface functionality of amorphous silica by infrared spectroscopy. J. Phys. Chem., 62, 1168–1178.

MEGAW, H. D. (1961) Order and disorder. I. Theory of stacking faults and diffraction maxima. Proc. Royal Soc. London, Ser. A, 259, 59–78.
MERWE, J. H. VAN DER (1964) Interfacial misfit and bonding between oriented films and their substrates. *in* Single-Crystal Films, 139–163. Edited by M. H. FRANCOMBE and H. SATO. Pergamon Press.
MICHEELSEN, H. (1957) An immersion method for exact determinations of refractive indices – the glass method. Medd. Dansk Geol. Foren., 13, 177–191.
MIDGLEY, H. G. (1951) Chalcedony and flint. Geol. Mag., 88, 179–184.
MONROE, E. A. (1964) Electron optical observations of fine-grained silica minerals. Amer. Min., 49, 339–347.
OAKLEY, K. P. (1939) The nature and origin of flint. Sci. Progr., 34, 277–286.
OTSU, H. and T. YASUDA (1964) Thermal behaviour of interlayer water in stevensite. Min. J. (Japan), 4, 91–114. [Quoted from Min. Abstr., 17, 257.]
PELTO, C. R. (1956) A study of chalcedony. Amer. J. Sci., 254, 32–50.
PINSKER, Z. G. (1953) Electron diffraction. Butterworths, London.
PITTMAN, J. S., Jr. (1959) Silica in Edwards Limestone, Travis County, Texas. Silica in Sediments (Soc. Econ. Paleon. and Mineralogists, Amer. Assoc. Petroleum Geologists, Tulsa, Oklahoma), 121–134.
POTTS, W. J., Jr. (1963) Chemical infrared spectroscopy. Vol. I: Techniques. J. Wiley and Sons.
ROSENKRANTZ, A. (1938) Kortfattet Oversigt over Danmarks Geologi. 2. udg., C. A. Reitzel, Copenhagen.
RØRDAM, K. (1897) Kridtformationen i Sjælland. Danmarks Geol. Unders., 2. Rk., Nr. 6.
SCHMALZ, R. F. (1960) Flint and the patination of flint artifacts. Proc. Prehist. Soc., XXVI, 44–49.
SMITH, E. and J. NUTTING (1956) Direct carbon replicas from metal surfaces. Brit. J. Appl. Phys., 7, 214–217.
STOKES, A. R. (1948) A numerical Fourier-analysis method for correction of widths and shapes of lines on X-ray powder photographs. Proc. Phys. Soc., 61, 382–391.
SVEHLA, R. A. (1962) Estimated viscosities and thermal conductivities of gases at high temperatures. National Aeronautics and Space Administration. Tech. Rep., R-132.
VINCIENNE, H. (1938) Sur l'altération des silex crétacés dans les sables supérieurs de la Perte du Rhône à Bellegarde. C. R. Acad. Sci. Paris, 207, 295–297.
WAHL, F. M., R. E. GRIM, and R. B. GRAF (1961) Phase transformations in silica as examined by continuous X-ray diffraction. Amer. Min., 46, 196–208.
WARREN, B. E. (1955) A generalized treatment of cold work in powder patterns. Acta Cryst., 8, 483–486.
— and E. P. WAREKOIS (1955) Stacking faults in cold worked alpha-brass. Acta Metall., 3, 473–479.
WEI, P.-H. (1935) The structure of α-quartz. Z. Krist., A, 92, 355–362.
WETZEL, O. M. (1960) Eine neue Dinoflagellaten-Gruppe aus dem baltischen Geschiebefeuerstein. Schr. Naturw. Vereins Schleswig-Holstein, 31, 81–86.
WHELAN, M. J. and P. B. HIRSCH (1957a) Electron diffraction from crystals containing stacking faults. I. Phil. Mag., 2, 1121–1142.
— and P. B. HIRSCH (1957b) Electron diffraction from crystals containing stacking faults. II. Phil. Mag., 2, 1303–1324.

PLATES

Plate 1, 1. Photomicrograph of flint grains in dark flint from Stevns. The thickness of the section is 3.1 μ. Crossed nicols.

Plate 1, 2. Photomicrograph of chalcedony in dark flint from Stevns. The thickness of the section is ca. 20 μ. Crossed nicols.

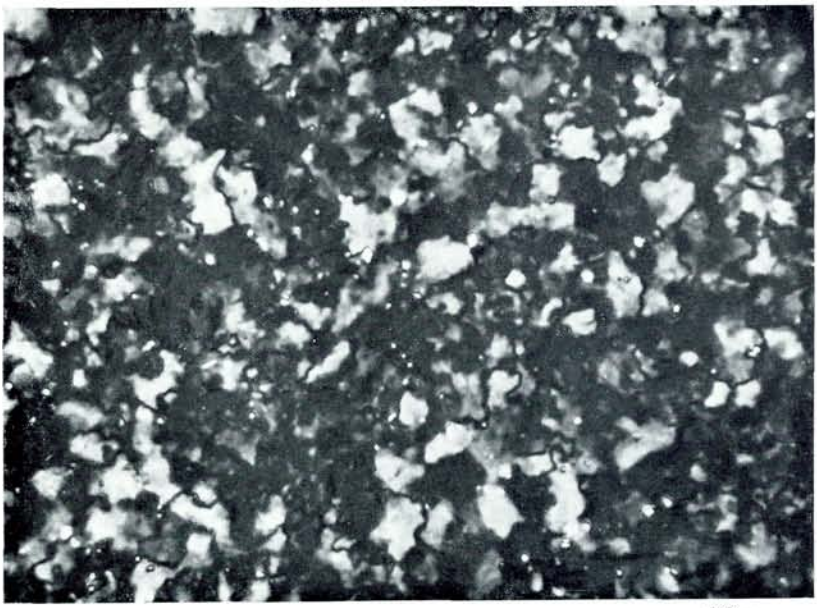

1 20 µ

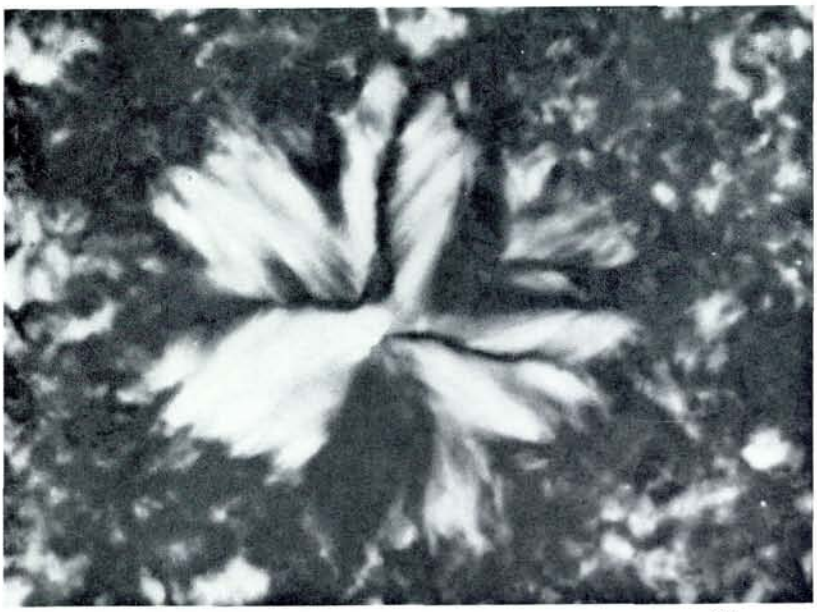

2 20 µ

Plate 2, 1. Photomicrograph of a thin section of a chip of flint which has been heated to 540°C. Plane polarized light.

The embedding plastic, which is seen in the upper part of the picture, fills the fractures which pass through the clear crust into the altered, turbid flint.

Plate 2, 2. Electron micrograph of a polished surface of dark flint from Stevns, autoclaved at 500°C and 300 bars H_2O for 48 hours. Carbon replica. E. LANGER photo.

Boundaries of flint particles are visible as ca. 0.2 μ wide fissures.

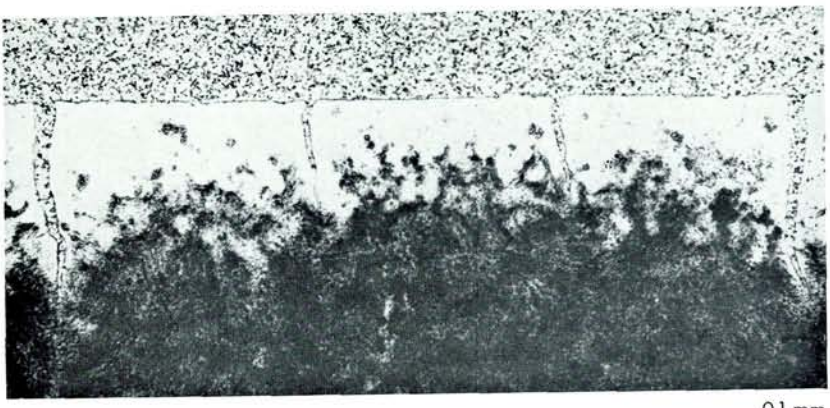

1 0.1 mm

2 10 µ

Plate 3, 1. Electron micrograph of a polished surface of dark flint from Stevns, autoclaved at 500°C and 300 bars H_2O for 48 hours. Carbon replica. E. LANGER photo.

The etching has revealed a block structure with spacings of 50 to 400 nm in the interior of a flint grain.

Plate 3, 2. Electron micrograph of a polished surface of dark flint from Stevns, autoclaved at 500°C and 300 bars H_2O for 48 hours. Carbon replica. E. LANGER photo.

The etching has revealed a laminar structure which is dipping toward N.E.

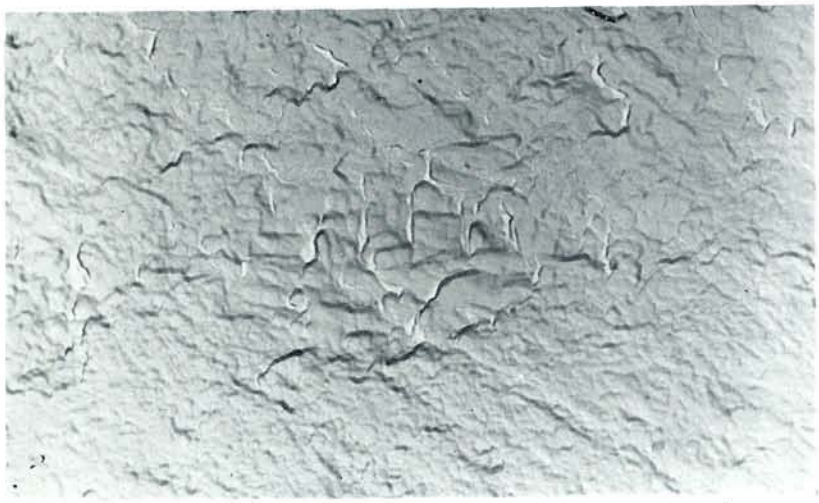

1

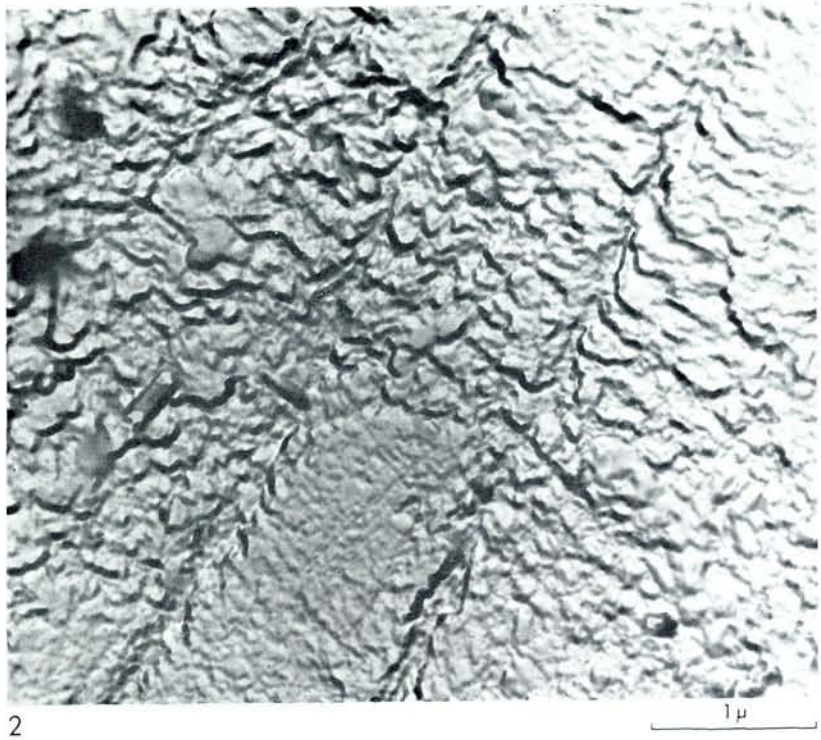

2

Plate 4. a) Electron micrograph, b) diffraction pattern, and c) dark field electron micrograph of an irregularly shaped piece of flint. Dark flint from Stevns, polished and etched with HF. R. W. HORNE photo.

The diffraction pattern is the $h0\bar{h}l$-plane of the reciprocal lattice. (Note the presence of (000l)-reflections with $l \neq 3n$). The bright spots in the dark field micrograph are the quartz particles which contribute to the $10\bar{1}1$-reflection, i.e. all the quartz particles which have the same orientation of the reciprocal lattice. The c-axis is vertical in all three pictures, and (0001) is parallel to the sharp lower edge of the grain. In the central parts of the two micrographs 30–100 nm thick plates which are parallel to (0001) can be discerned.

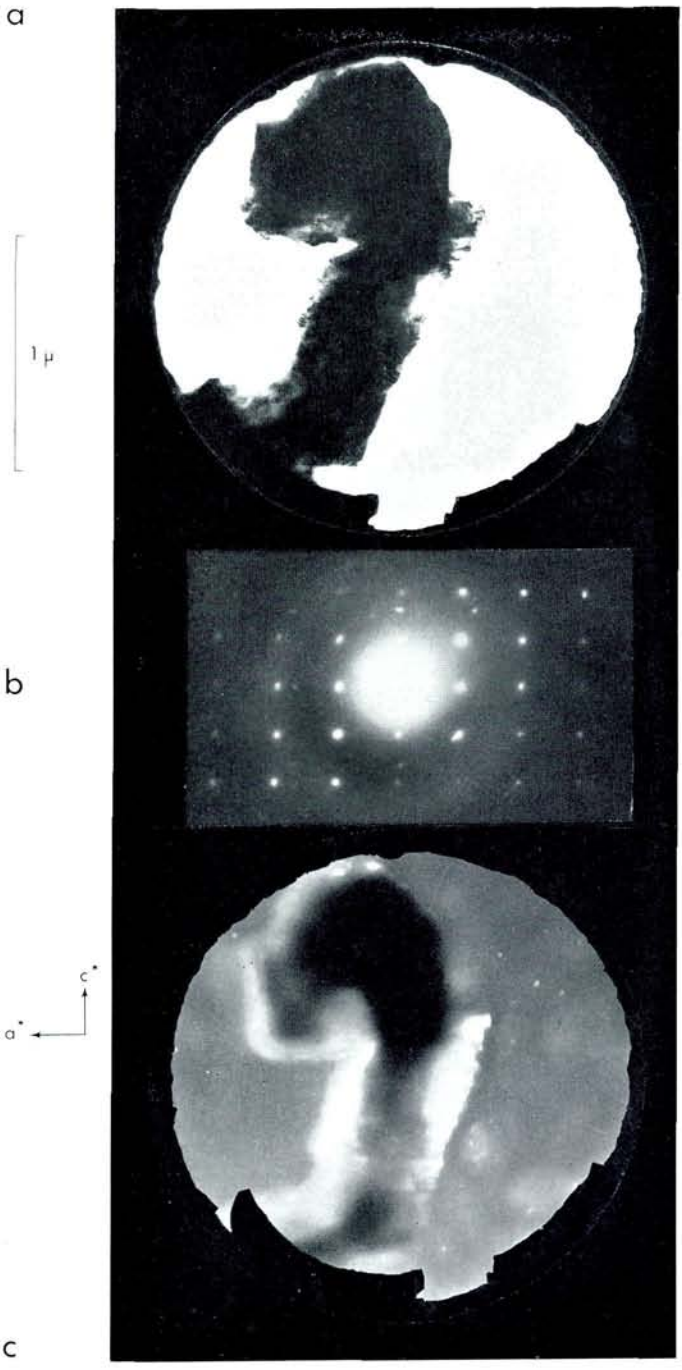
a
1 μ
b
c*
a*
c

Plate 5. a) Electron micrograph and b) diffraction pattern of a thin plate of quartz. Dark flint, Stevns, polished and etched with HF. R. W. HORNE photo.

The plate is parallel to (0001). The edges belong to ⟨100⟩ and ⟨210⟩. The edges are thought to be due to prism faces, namely $\{10\bar{1}0\}$, with the exception of the right one which is $(\bar{1}2\bar{1}0)$. The direction of the lower edge changes by a few degrees, and the lower right corner of the plate is turned a little clockwise compared with most of the plate. This is also shown by the weak additional spots in the diffraction pattern. The $\{10\bar{1}0\}$ faces are generally rough, whereas $(\bar{1}2\bar{1}0)$ is smooth. The holes in the plate are due to prolonged etching in HF.

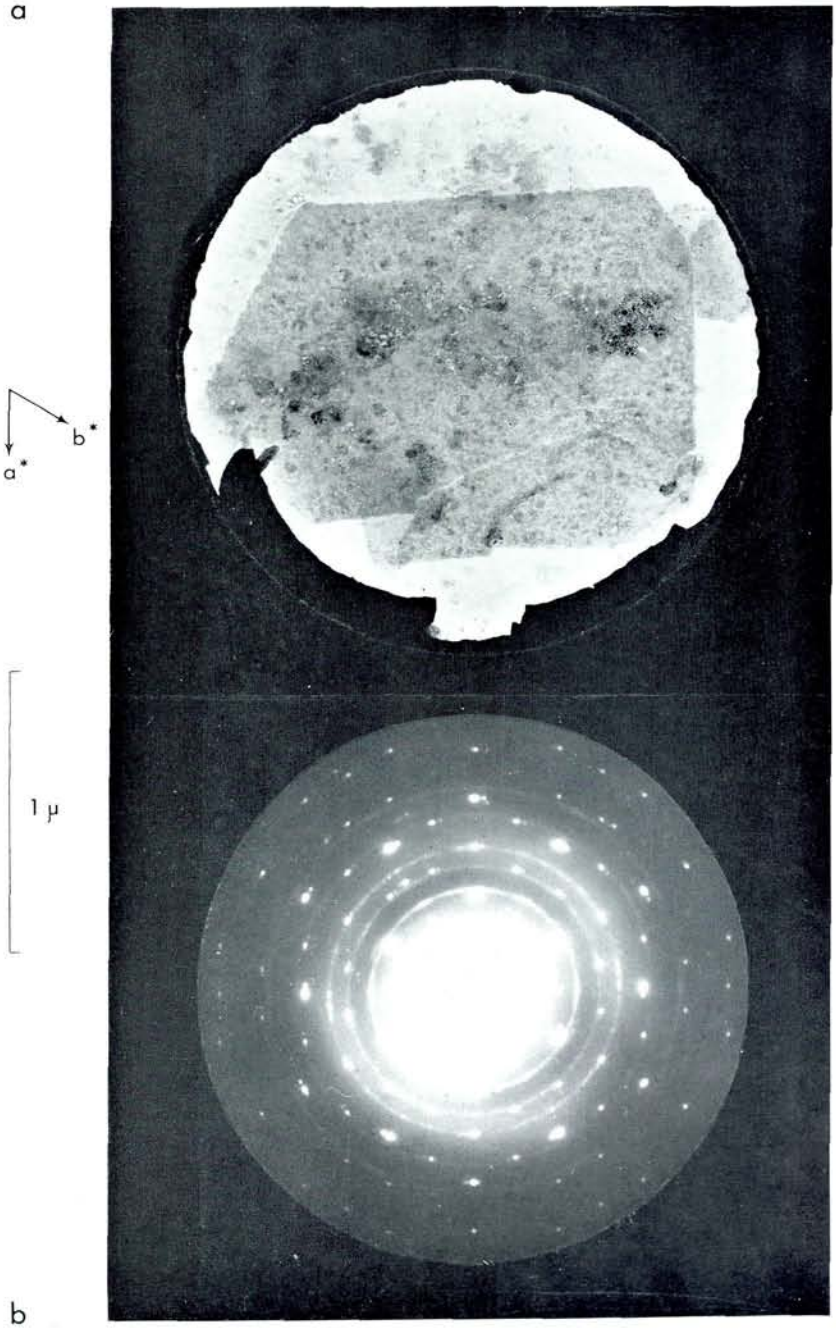
a
b*
a*
1 μ
b

Plate 6. a) Electron micrograph and b) diffraction pattern of a thin plate of quartz. Dark flint, Stevns, polished and etched by HF. R. W. HORNE photo.

The holes in the plate have been etched by HF. According to the diffraction pattern the plate is parallel to (0001) and has two orientations of the reciprocal a*-axes, being ca. 5° apart. The smooth edge in the right side of the plate is assumed to be a prism face and is indexed $(\bar{1}2\bar{1}0)$. It corresponds to the clockwise turned position of the reciprocal lattice. The other edges cannot be indexed safely, but the upper right edge seems to be $(\bar{2}110)$, corresponding to the counter-clockwise turned position of the reciprocal lattice.

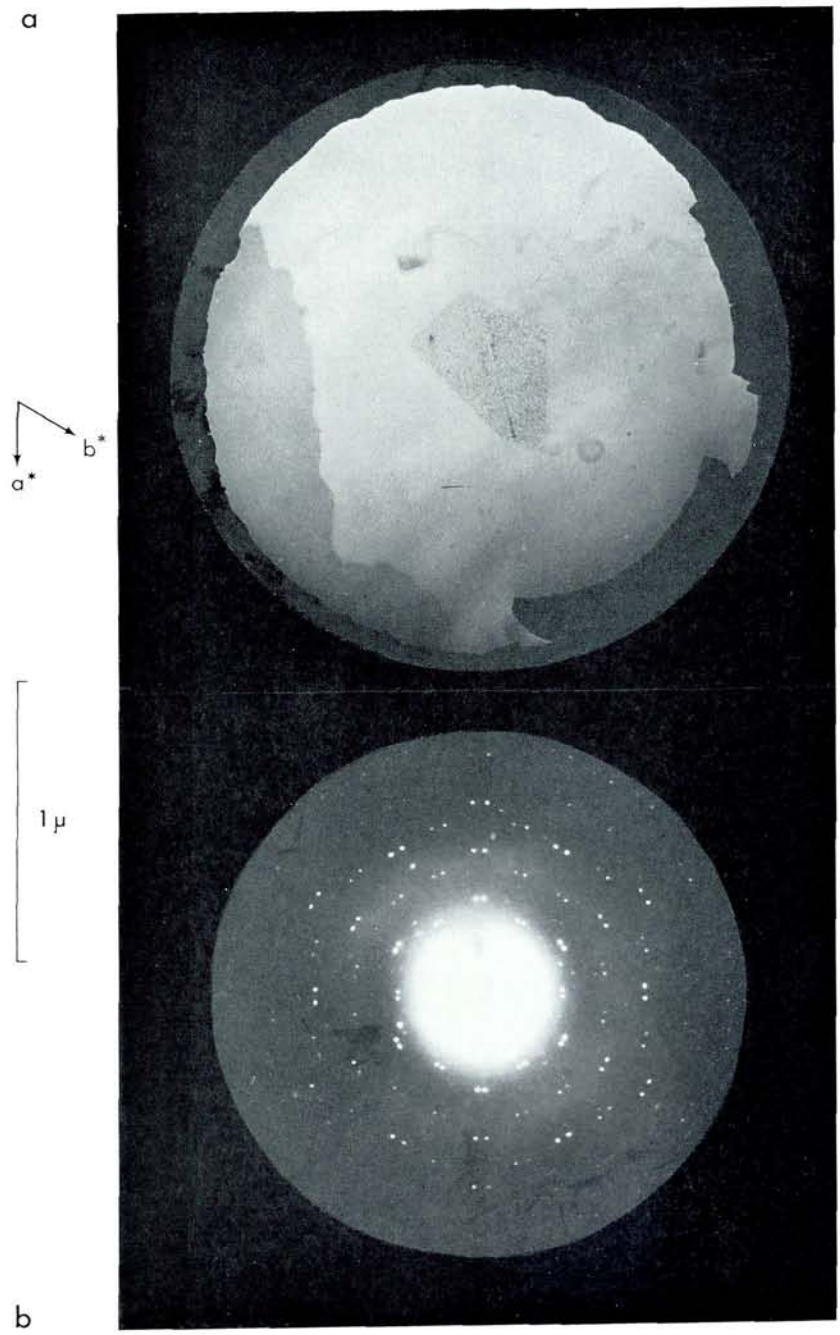
a
b*
a*
1 μ
b

Plate 7. a) Electron micrograph, b) diffraction pattern (unsharp), and c) dark field electron micrograph of a thin plate of quartz. Dark flint, Stevns, polished and etched with HF. R. W. HORNE photo.

The plate is parallel to (0001) of the quartz, which has only one orientation of the reciprocal lattice. A few extra reflections are probably due to the small grains in the field outside the plate. The lower right edge of the plate is called $(11\bar{2}0)$, the other edges correspond to $\{10\bar{1}0\}$. The dark field picture shows that quartz in all parts of the plate contributes to the $20\bar{2}0$ reflection which is used to produce the dark field picture. The plate has been strongly etched by HF during preparation of the replica, and it is therefore impossible to draw safe conclusions on the spacings of the lattice faults. The quartz domains seem to be a little oblong parallel to $(\bar{1}2\bar{1}0)$.

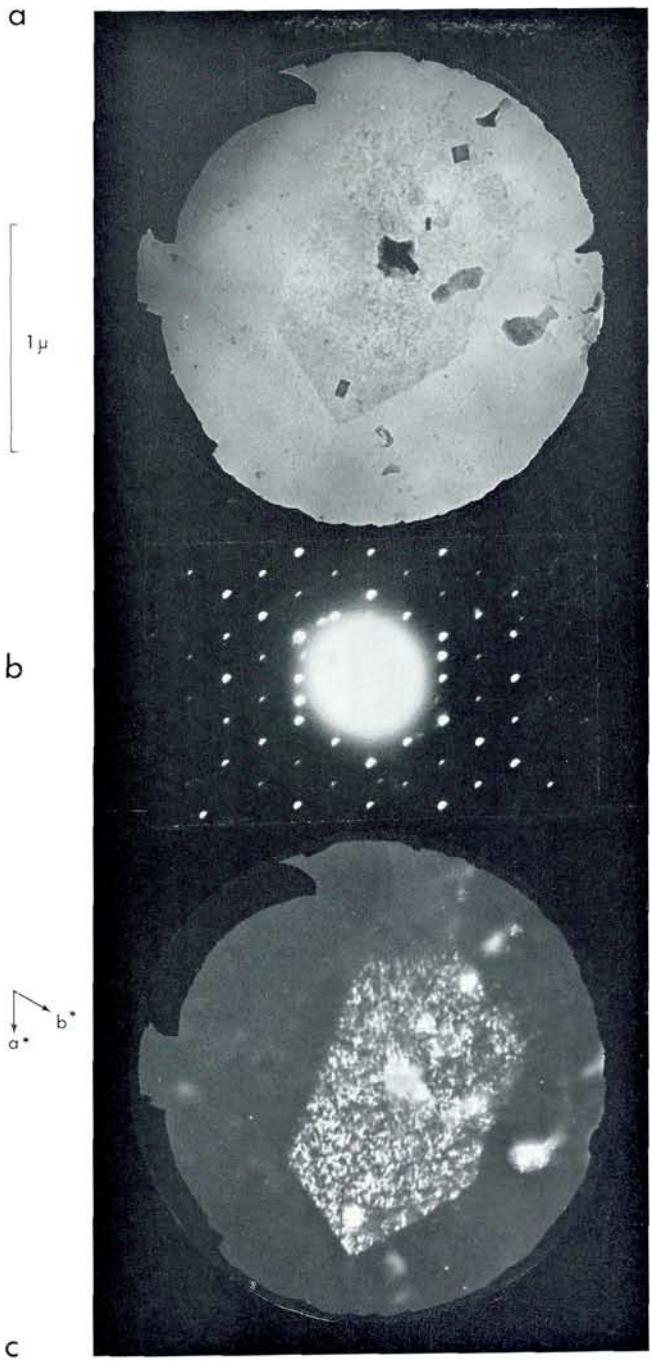
a
1 μ
b
a*
b*
c

Plate 8. a) Electron micrograph and b) dark field electron micrograph of overlapping plates of quartz. Dark flint, Stevns, polished and etched by HF. E. LANGER photo.

The plates are parallel to (0001) and give a single crystal diffraction pattern. The dark field micrograph shows that quartz from all parts of the adjacent plates has the same orientation of the reciprocal lattice. The light field micrograph shows that the intensity of the transmitted beam varies strongly. The average blackening of the picture, however, is rather uniform in the various parts of each crystal – compare with the irregularly shaped flint piece pl. 4.

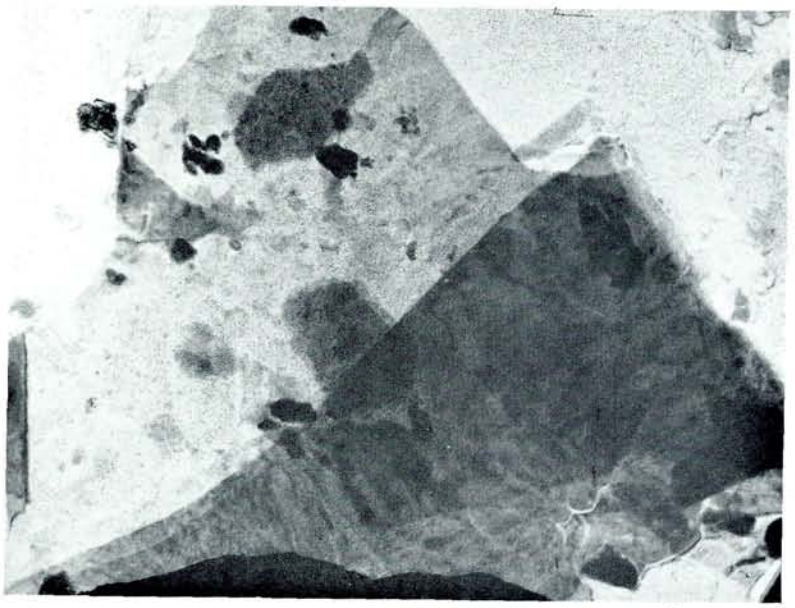

a 1 µ

b 1 µ

Plate 9. a) Dark field electron micrograph taken by the strong $11\bar{2}0$ reflection and b) electron diffraction pattern. Dark flint, Stevns, polished and etched by HF. R. W. HORNE photo.

The grain is rather irregular in shape and not uniform in thickness, but it has [001] parallel to the electron beam. The dark field photograph shows bright, irregular bands which are subparallel to $(\bar{1}2\bar{1}0)$. The direction of the bright bands varies in the same way as the direction of a* varies in the diffraction pattern. Perpendicular to $(\bar{1}2\bar{1}0)$ the spacing of the bands varies from 17 to 26 nm. The average length of the bands is estimated to be of the order 100 nm.

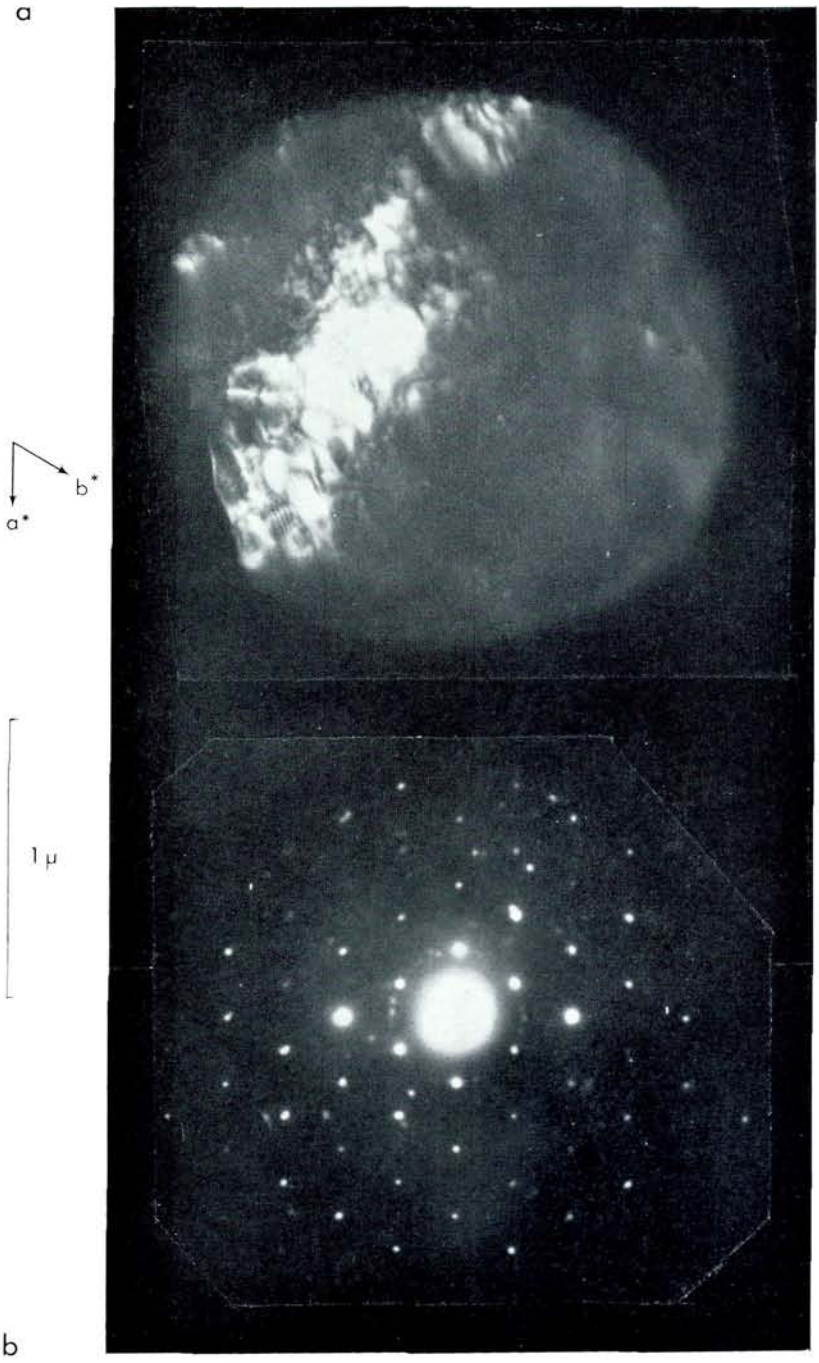
a
b*
a*
1 μ
b

Plate 10. a) Electron micrograph, b) diffraction pattern and c) dark field electron micrograph of a particle of flint. Dark flint, Stevns, polished and etched by HF. R. W. HORNE photo.

The grain has [001] parallel to the electron beam and, apart from a few randomly orientated grains, only one orientation is present. In the light field micrograph indistinct dark bands are seen in the upper part of the grain. These bands are bright in the dark field picture, which has been taken with the $11\bar{2}0$-reflection. The bands have spacings of 20–30 nm and are of the order 100 nm in length. The long direction is subparallel to $(\bar{1}2\bar{1}0)$, i.e. subparallel to a*.

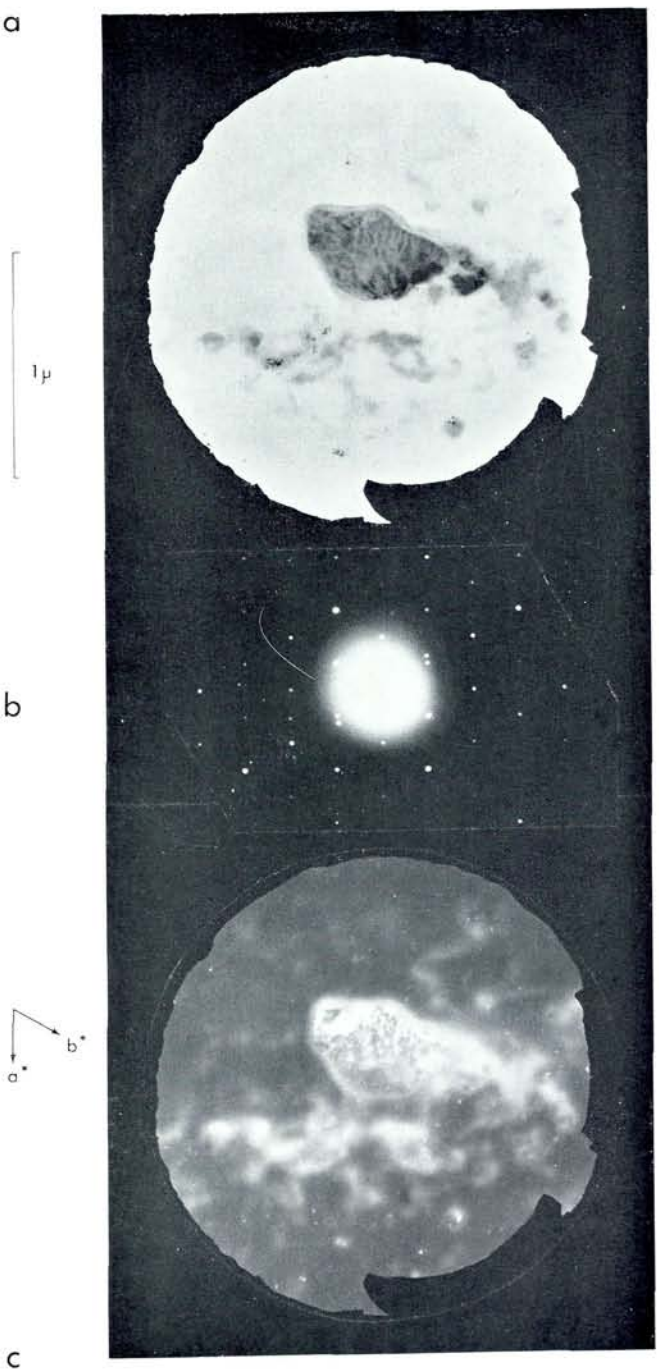
a
1μ
b
b*
a*
c

Plate 11. Electron micrograph of surface relief of dark flint from Stevns, polished and etched by HF. Carbon replica. R. W. HORNE photo.

Holes etched into the surface reveal several sets of parallel, gently bending structures with spacings between 60 and 200 nm. These structures are likely to be due to quartz plates, which are parallel to (0001). The minimum spacing of the etched lines, i.e. ca. 60 nm, should therefore be close to the thickness of the (0001) plates.

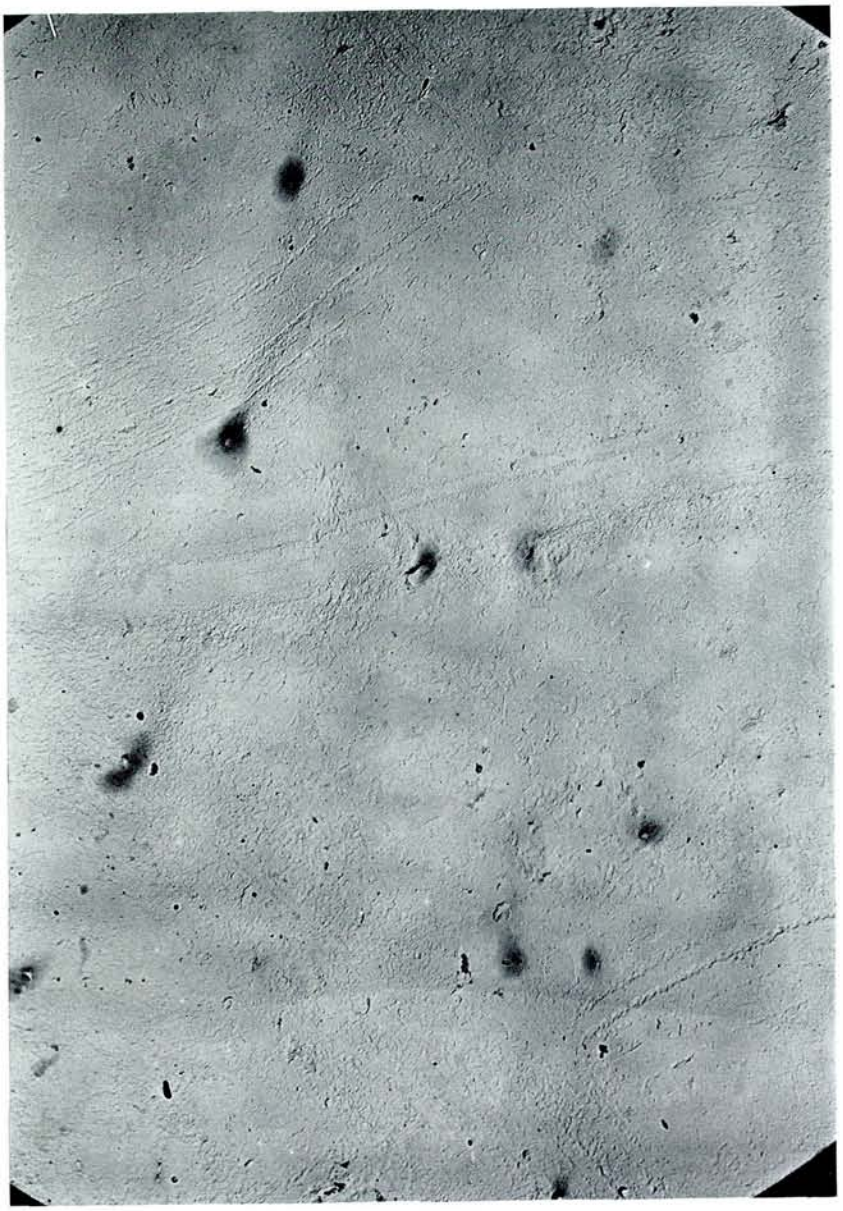
1 µ

Plate 12, 1. Electron micrograph of surface relief of dark flint from Stevns, polished and etched by HF. Carbon replica. R. W. HORNE photo.

The etched surface reveals two kinds of parallel structure. The N.E. trending rows of holes have a spacing of ca. 85 nm and are likely to occur on the trace of the {0001} faces of the quartz plates. The E.-W. running etch furrows are spaced at ca. 26 nm and are due to the lattice faults within the quartz plates (see also pl. 12, 2).

Plate 12, 2. Electron micrograph of surface relief of dark flint from Stevns, polished and etched by HF. Carbon replica. R. W. HORNE photo. Detail of pl. 12, 1 and explanatory drawing.

The bottoms of the etched furrows are indicated on the drawing; heavy lines indicate the broad furrows and thin lines indicate the faint furrows. The left part of the drawing shows the sequence of broad and faint furrows which is expected from the theory of triplets of twin faults.

0.2 µ

1

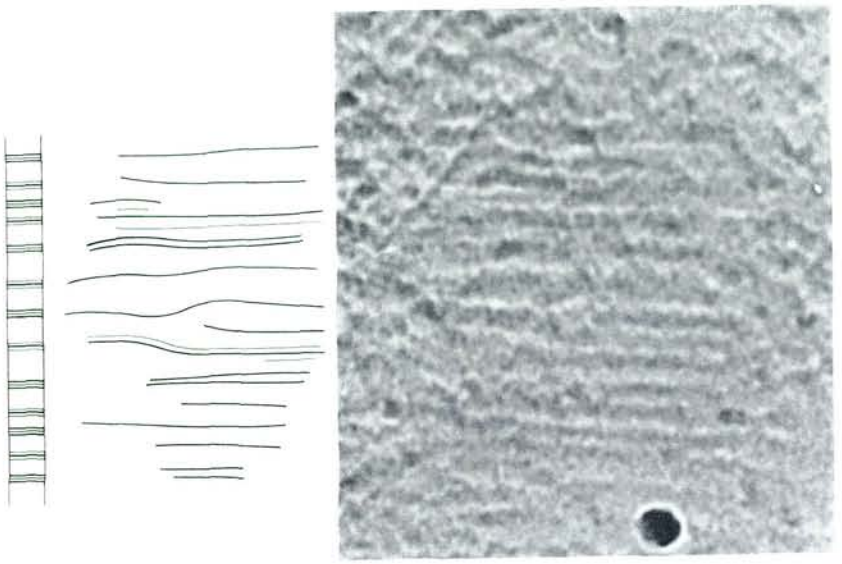

0.2 µ

2

Plate 13, 1. Electron micrograph of a fracture surface of dark flint from Stevns. Collodion replica. E. LANGER photo.

In the rough areas faint, parallel, N.E. running structures are seen. The smooth area in the centre of the picture is ca. 15 μ in diameter and probably shows the surface of a flint grain. The ridges show the fissures between the flint grains.

Plate 13, 2. Electron micrograph of a fracture surface of dark flint from Stevns. Collodion replica. E. LANGER photo.

Smooth and rough areas are seen. The ridges seen to stand out in the smooth areas show the fissures between the flint grains. At the top of the ridges their width is 10–60 nm.

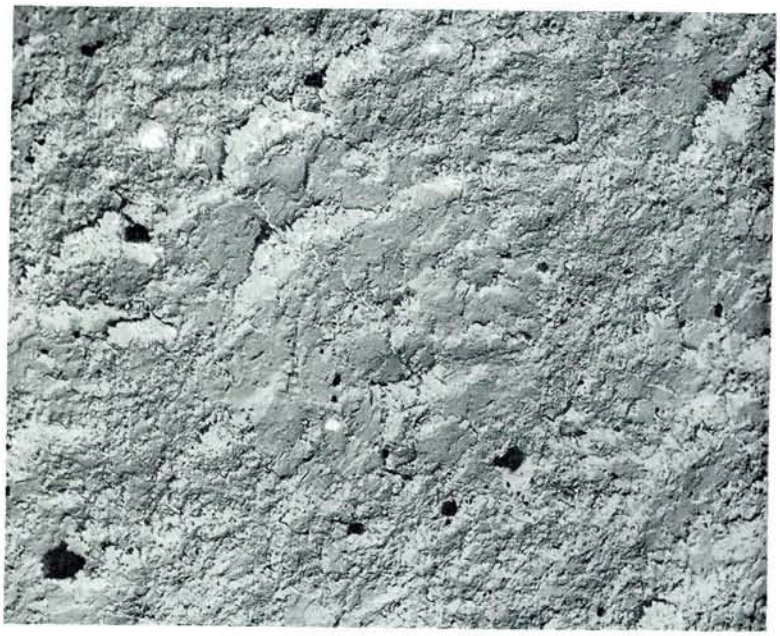

1 10 µ

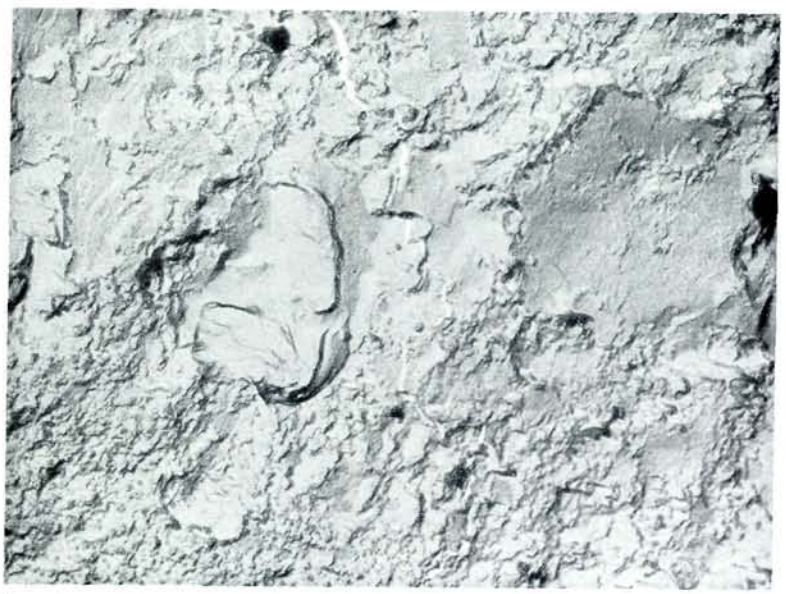

2 1 µ

Plate 14, 1. Electron micrograph of fracture surface of dark flint from Stevns. Collodion replica. E. LANGER photo.

A smooth area with small steps. The replica is shadowed by palladium which has come from N.W. of the picture. Steps directed away from the palladium source will produce a sharply defined white "shadow" in the picture. The angle of shadow-casting is between ca. 30° and ca. 60°. The height of the steps is therefore roughly equal to the widths of the white zones, when these are measured in the direction in which the shadow is cast. The height of the steps thus measured is about 40–120 nm, and the steps are therefore likely to correspond to the quartz plates, which constitute the flint grains and have an average thickness of ca. 59 nm. The smooth area is interpreted as a fracture in a flint grain, subparallel to these plates. In the lower right half of the picture faint, N.-S. running structures can be discerned in the smooth area. They have a spacing of ca. 20 nm and are probably due to the lattice faults within the plates.

Plate 14, 2. Electron micrograph of dark flint from Stevns, polished and treated with Na_2CO_3. Carbon replica. E. LANGER photo.

The polished surface has not been etched, but rounded patches have been deposited on the surface – compare with the scratch in the surface. A ridge of silica has been deposited on an intergranular fissure and it thus marks the position of the flint grain boundary.

1 1 µ

2 1 µ